

# **CRITICAL PHENOMENA IN ANTI-DE SITTER BLACK HOLES**

Thesis

submitted in partial fulfillment of the requirements for the degree of

**DOCTOR OF PHILOSOPHY**

by

**AHMED RIZWAN C.L**



**DEPARTMENT OF PHYSICS**

**NATIONAL INSTITUTE OF TECHNOLOGY KARNATAKA (NITK),**

**SURATHKAL, MANGALORE - 575 025**

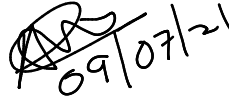
**July, 2021**



## DECLARATION

*By the Ph.D Research Scholar*

I hereby *declare* that the Research Thesis entitled “**Critical Phenomena in Anti-de Sitter Black holes**”, which is being submitted to the *National Institute of Technology Karnataka, Surathkal* in partial fulfillment of the requirements for the award of the Degree of *Doctor of Philosophy in Physics* is a *bonafide report of the research work carried out by me*. The material contained in this thesis has not been submitted to any University or Institution for the award of any degree.

Handwritten signature and date: 09/07/21

**Ahmed Rizwan C.L.**

Register No.: 138022 PH13F05

Department of Physics

National Institute of Technology Karnataka  
Surathkal.


Place: NITK - Surathkal

Date: 12 July, 2021



## CERTIFICATE

This is to *certify* that the Research Thesis entitled “**Critical Phenomena in Anti-de Sitter Black holes**”, submitted by **Ahmed Rizwan C.L** (Register Number: 138022 PH13F05) as the record of the research work carried out by him, is *accepted* as the *Research Thesis submission* in partial fulfillment of the requirements for the award of degree of *Doctor of Philosophy*.

  
13/07/21

**Dr Deepak Vaid**  
Research Guide  
Assistant Professor  
Department of Physics  
NITK Surathkal - 575025

  
15/7/21

**Chairperson - DRPC**  
(Signature with Date and Seal)



*Dedicated to*  
*my beloved mother, father, sister,*  
*my dear wife Athifa*  
*and my sweet kids Adnaan & Nawfa*





## ACKNOWLEDGEMENT

This is a befitting time to convey my wholehearted thanks to some people; without their help and support, this work would not be completed. First and foremost, I thank my research guide, Dr. Deepak Vaid, for introducing me to the exciting research field of black hole physics and supporting me in all possible ways to pursue a career in physics. I have significantly benefited from his critical thinking and wide range of interests.

I am so grateful to Dr. Ajith K.M, Associate professor and Head of the Department, Department of Physics, NITK Surathkal, for his valuable advice, support, criticism, and encouragement. I am thankful to faculties in our department, Dr. Shajahan T.K and Dr. Sreenath V, for useful discussions, feedback, and constant motivations during the research. I sincerely thank Research Progress Assessment Committee members Dr. Santhosh George, Professor, Department of Mathematical and Computational Sciences, and Dr. Partha Pratim Das, Assistant Professor, Department of Physics, for their valuable suggestions and timely interference, which have much helped me to improve the thesis.

I am thankful to my collaborators A. Naveena Kumara, Dr. Md Sabir Ali, and Kartheek Hegde for the active discussions and for sharing their knowledge, which always pushed me further in research. I want to thank my lab mates Rajani K.V, Safir T.K, and Ananthram K.S for their support and cooperation throughout the research. I would like to express my gratitude to all former and current Ph.D. scholars, MSc students of the NITK physics department, in particular to Dr. Siby Thomas, Dr. Manoj Kumar, Dr. Sreejesh M, Dr. Nimith K.M, Yadukrishnan, Mrudul M.S, Archana Sampath, Revathy B.S, Sterin N S, Ahamed Khasim, Sibesh P.P, Anupama Sebastian, Shreyas Punacha, Amrutha S.V, Achyutha, Brijesh for providing me some unforgettable experience at NITK. For the comments on the first draft of the thesis, I am thankful to Sibesh and Anupama. I remember all my teachers and mentors with gratitude, who have always made me a better and more thoughtful person. Especially, I thank the teachers of Aliya English school Paravanadukkam, Chemnad-Jamaath higher secondary school Chemnad, St.Aloysius College Mangalore, and Nehru Arts and Science College Kanhangad.

I acknowledge the financial support from the U.G.C Government of India, and NITK, Surathkal, through the UGC-NET-SRF scheme.

I am indebted to my cousin Feroz Paloth for his generous help and assistance during the hard times. Special thanks are reserved for the childhood friend and cousin Rasmiya Paloth for cheering up my childhood days. My teenage friends Salahudeen, Kamal, and Shakkir for giving memorable teenage days and connecting me to the real world. A special mention is reserved for Abdurahman M, who passed away last month, a grandfather-like figure and mentor in my life.

I would like to express my profound gratitude to my family for their unfailing support and encouragement. My parents, C.L. Raheem and Asma, parents-in-law C.L. Abdulla and Nishath V, sister Rumana, niece Fatima Zela Falak, brother-in-law Firoz P.V, my grandparents, Late C.L. Ahammed and Late C.L. Ummalimma. I am indebted for their patience, prayers, and constant encouragement that kept me going in life.

Finally, heartfelt gratitude to my soul mate Athifa Mariyam A and my sweet kids Adnaan Ahmed C.L. & Nawfa Nourin C.L. for their love and for preserving my sanity during difficult times. You have been a blessing in my life. It's your care and affection paid off in my career. Above all, I would like to express my gratitude to Almighty God Allah for all his blessing bestowed upon me, fulfilled my dreams, gave me comfort and good companions that kept me happy in my life.

Ahmed Rizwan C.L

## Statement of Contribution

---

THIS THESIS IS BASED ON THE FOLLOWING ARTICLES.

- **C.L. Ahmed Rizwan**, A. Naveena Kumara, Deepak Vaid, K.M. Ajith. “*Joule-Thomson expansion in AdS black hole with a global monopole*”. **Int. J. Mod. Phys. A** **33** (2018), **1850210**, [arXiv:1805.11053](#).
- **C.L. Ahmed Rizwan**, A. Naveena Kumara, Kartheek Hegde, Deepak Vaid. “*Coexistent Physics and Microstructure of the Regular Bardeen Black Hole in Anti-de Sitter Spacetime*”. **Annals Phys.** **422** (2020), **168320**, [arXiv:2008.06472](#).
- **C.L. Ahmed Rizwan**, A. Naveena Kumara, K.V. Rajani, Deepak Vaid, K.M. Ajith. “*Effect of Dark Energy in Geometrothermodynamics and Phase Transitions of Regular AdS black hole*” **Gen. Rel. Grav.** **51** (2019), **12**, **161**, [arXiv:1811.10838](#).
- KV Rajani, **C.L. Ahmed Rizwan**, A. Naveena Kumara, Deepak Vaid, K.M. Ajith. “*Regular Bardeen AdS black hole as a heat engine*” **Nucl. Phys. B** **960** (2020), **115166**, [arXiv:1904.06914](#).
- A. Naveena Kumara, **C.L. Ahmed Rizwan**, Deepak Vaid, K.M. Ajith. “*Critical Behaviour and Microscopic Structure of Charged AdS Black Hole with a Global Monopole in Extended and Alternate Phase Spaces*” [arXiv:1906.11550](#).

Details of other articles written by the author and are not included in the thesis are given in the list of publication section (Sec.7).



## ABSTRACT

This thesis investigates thermodynamic phase transitions in anti-de Sitter (AdS) black holes. Motivated by the inconsistency of Smarr relation and the first law of black hole thermodynamics in AdS spacetime, cosmological constant  $\Lambda$  is given a status of thermodynamic variable pressure. This modification has led to the addition of pressure-volume term in the first law of black hole thermodynamics. In this extended phase space, black hole phase behavior is found analogous to everyday physical phenomena. We have focussed our studies on the van der Waals (vdW) like phase transitions and their manifestations, including Joule-Thomson expansion and heat engine in asymptotically AdS black holes. We have chosen charged black hole with a global monopole and a regular Bardeen black hole in AdS spacetime for our study. A detailed study of thermodynamical properties through the Hawking temperature, mass, entropy, heat capacity, and Gibbs free energy is conducted. A first-order phase transition similar to the liquid-gas phase transition is observed between small black hole (SBH) and large black hole (LBH) phases. Critical exponents calculated near the critical point match those of the van der Waals fluid. Further, we investigate the effect of global monopole on the Joule-Thomson expansion (JT) of charged AdS-black holes. We have calculated an exact expression for the JT coefficient, which determines the cooling and heating in the final phase. Using the JT coefficient, we have analyzed the effect of the monopole parameter in the inversion temperature and isenthalpic curves. Similarly, we have extended our studies to regular Bardeen black holes. In another aspect of our study, a heat engine constructed using a black hole as a working substance. The heat engine efficiency is calculated via thermodynamic cycle in the  $P - V$  plane, which receives and ejects heat. It is observed that the heat engine efficiency is improved by adding a quintessence field. In the second part of the thesis, we probe the phase structure of the black hole using thermodynamic geometry. Constructing a thermodynamic metric in the phase space, we studied the critical behavior and microstructure of the black hole. Utilizing the analogy with vdW fluid, the thermodynamic geometry of a charged Bardeen AdS black hole is analyzed.

*Keywords:* Joule-Thomson effect; Heat engine; Thermodynamic geometry.



# Contents

<b>List of Figures</b>	<b>v</b>
<b>List of Tables</b>	<b>vii</b>
<b>1 Introduction</b>	<b>1</b>
1.1 Phase transitions and Critical Phenomena . . . . .	7
1.1.1 Conformal field theories and its AdS space correspondence . . . . .	8
1.1.2 AdS spacetime . . . . .	9
1.1.3 Objectives . . . . .	13
1.2 Organization of the Thesis . . . . .	14
<b>2 Introduction to Black hole thermodynamics</b>	<b>15</b>
2.1 Introduction . . . . .	15
2.1.1 Komar Integral . . . . .	23
2.1.2 Killing horizon . . . . .	29
2.2 Laws of black hole mechanics . . . . .	31
2.3 Thermodynamics in AdS space . . . . .	36
2.4 Conclusion . . . . .	42
<b>3 Phase transitions and Joule-Thomson effect in AdS black holes with a Global Monopole</b>	<b>45</b>
3.1 Introduction . . . . .	45
3.2 The charged AdS black hole with a global monopole . . . . .	47
3.3 Thermodynamics in Extended Phase Space . . . . .	50
3.4 Joule Thomson Expansion . . . . .	60

3.4.1	Joule-Thomson Effect . . . . .	60
3.4.2	van der Waals fluid . . . . .	61
3.5	Joule Thomson Expansion of Charged AdS Black Hole with Monopole Term . . . . .	64
3.6	Conclusions . . . . .	69
<b>4</b>	<b>Thermodynamics of Regular black holes in AdS Spacetime</b>	<b>71</b>
4.1	Introduction . . . . .	71
4.2	Regular Bardeen AdS Black hole . . . . .	74
4.3	Thermodynamics and phase structure . . . . .	76
4.4	Thermodynamic Geometry . . . . .	83
4.4.1	Microstructure of the Bardeen AdS Black Hole . . . . .	86
4.5	Summary and Conclusions . . . . .	90
<b>5</b>	<b>Effect of Quintessence on Phase transitions and Thermodynamic geometry of Regular black holes</b>	<b>93</b>
5.1	Introduction . . . . .	93
5.2	Thermodynamics of the black hole . . . . .	95
5.3	Quintessence and Thermodynamic Geometry . . . . .	98
5.3.1	Weinhold Geometry . . . . .	100
5.3.2	Ruppeiner Geometry . . . . .	101
5.3.3	Geometrothermodynamics . . . . .	103
5.4	Conclusion . . . . .	104
<b>6</b>	<b>Heat engine in the Regular AdS black holes sur- rounded by Quintessence</b>	<b>107</b>
6.1	Introduction . . . . .	107
6.2	Regular black hole as a Heat Engine . . . . .	108
6.3	Influence of Quintessence on efficiency . . . . .	112
6.4	Conclusions and Discussions . . . . .	117



<b>7 Summary and Future Work</b>	<b>119</b>
<b>Appendices</b>	<b>125</b>
<b>A Differential Forms</b>	<b>127</b>
<b>B Stoke's Theorem</b>	<b>131</b>
<b>C Komar Integrals in Various Notations</b>	<b>135</b>
<b>D Komar Integral for Schwarzschild Black Hole</b>	<b>137</b>
<b>E Surface Gravity and Killing Horizon</b>	<b>139</b>
<b>F Bardeen Black Hole with a Quintessence</b>	<b>141</b>
<b>Bibliography</b>	<b>143</b>
<b>List of publications</b>	<b>159</b>
<b>Curriculum Vitae</b>	<b>166</b>



# List of Figures

1.1	Representation of AdS/CFT Correspondence in 2+1 dimensions . . . . .	9
1.2	AdS spacetime as a hyperboloid embedded in a flat spacetime . . . . .	10
2.1	Figure depicting conservation of charge $Q$ between two hypersurfaces $\Sigma_1$ and $\Sigma_2$ . . . . .	20
2.2	Foliation of spacetime into space-like hypersurfaces . . . . .	22
2.3	Region $R$ with space-like hypersurface $\Sigma_1$ and $\Sigma_2$ , a timelike hypersurface $S^2$ , and a null hypersurface $\mathcal{H}$ . . . . .	27
2.4	Topology of a black hole . . . . .	28
3.1	Plots of Hawking temperature $T$ versus horizon radius $r_+$ and $T$ versus entropy $S$ for different values of charge $Q$ . . . . .	51
3.2	$P - v$ isotherms in extended phase space in presence of global monopole . . . . .	53
3.3	The swallow tail behaviour of Gibbs free energy $G$ and its variation with $\eta$ in the extended phase space . . . . .	56
3.4	Coexistent $P - T$ curve in extended phase space for different values of $\eta$ . . . . .	58
3.5	Analogy in $P - v$ isotherms between van der Waals gas and AdS black holes . . . . .	62
3.6	Inversion and isenthalpic curves for van der Waals gas . . . . .	63
3.7	Effect of monopole term $\eta$ on inversion curves . . . . .	65
3.8	Inversion curves for charged AdS black hole with global monopole parameter . . . . .	67
3.9	Crossing diagrams between inversion and isenthalpic curves for different values of $\eta$ . . . . .	68

4.1	$P - V$ isotherms and Gibbs free energy plots for regular Bardeen AdS black hole . . . . .	79
4.2	Coexistence and spinodal curves in $P - T$ and $T - V$ planes . . . . .	80
4.3	The order parameter $\Delta V_r$ as a function of reduced temperature $T_r$ . . . . .	82
4.4	The normalised curvature scalar $R_N$ is plotted against the reduced volume $V_r$ . . . . .	87
4.5	The sign-changing curve of $R_N$ along with the coexistence and spinodal curves . . . . .	89
4.6	The behaviour of scalar curvature near the critical point . . . . .	90
5.1	$P - v$ diagram and $T - S$ plot for regular Bardeen AdS black hole surrounded by quintessence . . . . .	96
5.2	Effect of quintessence on specific heat versus entropy diagram for regular Bardeen AdS black hole . . . . .	96
5.3	Specific heat for different quintessence state parameter $\omega$ . . . . .	96
5.4	Curvature divergence plots for Weinhold geometry near the critical point	101
5.5	Curvature divergence plots for Ruppeiner metric near the critical point .	101
5.6	Near critical point behaviour of curvature scalar from Weinhold, Ruppeiner and Quevedo metric . . . . .	104
6.1	Schematic diagram of a traditional heat engine . . . . .	109
6.2	The variation of efficiency $\eta$ and the ratio $\eta/\eta_c$ of the engine with regular Bardeen black hole with different variables . . . . .	111
6.3	The effect of quintessence on the efficiency $\eta$ of the engine and on the ratio $\eta/\eta_c$ with different variables . . . . .	114
6.4	Effect of quintessence parameters $a$ and $\omega$ on the efficiency $\eta$ of the engine . . . . .	116

# List of Tables

5.1	The ratio $\frac{P_{cvc}}{T_c}$ is calculated for quintessence state parameter $\omega = -1, -2/3, -1/3$ . . . . .	97
6.1	Deviation in heat engine efficiency $\eta$ , with variation of quintessence equation of state parameter $\omega_q$ and strength parameter $a$ . . . . .	117



# Chapter 1

## Introduction

---

*“Imagination is more important than knowledge. Knowledge is limited, whereas imagination embraces the entire world, stimulating progress, giving birth to evolution” - Albert Einstein*

---

The word Physics means ‘knowledge of nature’ in Greek. Physics deals with understanding different phenomena occurring in nature, from subatomic particles to hypergiant stars and galaxies. Behind these events, we can see four types of fundamental forces classified as *Weak*, *Strong*, *Electromagnetic* and *Gravitational* forces. Of these, the weak and strong forces act at distances of the order of the size of atomic nuclei and are responsible for the decay processes and nuclear binding; they find applications in nuclear power plants to the medical diagnosis. The electromagnetic force deals with the interaction between charged particles; finds application in telecommunication equipments to home appliances. The gravitational force acts universally on everything and keeps us on earth. Out of these four interactions, the gravitational force is the oldest one formulated in Isaac Newton’s *Philosophiæ Naturalis Principia Mathematica* which describes gravity as a universal force of attraction between two bodies ([Newton 1687](#)). The range and time scale of these forces are distinct; weak and strong interactions act around femtometers, whereas the electromagnetic and gravitational forces interact over an infinite range. Though four interactions are distinct in their properties, there were

attempts to cast these interactions as a unified one by exploiting underlying symmetries.

The golden age of physics was the late-18th and early 19th century. In the late 18th century, studying the statistics behind the black body spectrum led to quantum mechanics. Quantum mechanics restricted one to determine position and momentum simultaneously and precisely in the microscopic world. I.e., a certain amount of uncertainty is involved when we measure two conjugate quantities like position-momentum or energy-time. In the early 19th century, incompatibility between Galilean mechanics and electromagnetism led to a new theory by Albert Einstein called the *special theory of relativity*. By that time, due to Maxwell's work, there was a strong notion that it is not the force but the field which is fundamental in physics. On the other hand, Newton's law for gravitation to a great extent was a success, which even led to the theoretical prediction of an unknown planet Neptune. The prediction came as an outcome of the discrepancies in Mercury and Uranus's orbits, which, when combined with the sun becomes a three-body problem. The three-body problem itself does not have a closed-form solution, but is amenable to perturbative analysis. On the other hand, the precession of the perihelion of Mercury's orbit explained by Newton's theory showed deviation from the actual rate by 43 arcseconds per century.

Einstein, in his special theory, postulated that no signal could travel faster than light, prohibiting *action at a distance*. Thus if the sun is removed from the solar system, the earth will take at least 8 minutes to feel the effect. In search of a relativistic theory for gravity, Einstein formulated a geometric theory for gravity called the *general theory of relativity* in 1915 ([Einstein 1915b](#)). General relativity has been extremely successful in explaining many phenomena happening on a large distance scale from the solar system to cosmological scales. Eddington's historic solar eclipse expedition in May 1919 provided observational confirmation of the deflection of light predicted by the general theory of relativity. Einstein's theory was also accurate in explaining various astrophysical phenomena such as the perihelion precession of Mercury ([Einstein 1915a](#)), gravitational redshift ([Einstein 1911](#)) and gravitational lensing ([Link 1936](#), [Einstein 1936](#)).

The core idea behind the general theory of relativity is the principle of equivalence, which states that, one cannot distinguish between the motion of a freely falling body in



a uniform gravitational field and the motion of the same body in a uniformly accelerated frame in small enough regions of spacetime. This equivalence implies that gravity is not a force but a manifestation of spacetime itself. The crux of Einstein’s theory can be summarized by John Wheeler’s statement “*spacetime tells matter how to move; matter tells spacetime how to curve*”.

Gravity is all about the curvature of spacetime caused by matter. The information about geometry is encoded in a metric tensor  $g_{\mu\nu}$ , which measures the distance between two points in spacetime. Einstein’s field equations relate the dynamics of the metric tensor with the energy-momentum tensor of the matter,

$$R_{\mu\nu} - \frac{1}{2}g_{\mu\nu}R = \frac{8\pi G}{c^4}T_{\mu\nu}, \quad (1.1)$$

where  $g_{\mu\nu}$  is the metric,  $R_{\mu\nu}$  is the Ricci tensor built out of the 2nd derivative of the metric.  $T_{\mu\nu}$  is the energy-momentum tensor, which describes the density and flux of energy-momentum in any given region of spacetime. Within few months from Einstein’s proposal of general relativity, a German physicist, Karl Schwarzschild, came up with a solution to the Einsteins equation. It was during world war II while he was serving as a lieutenant on the Russian front. The solution was for the static spherically symmetric gravitational field in the space surrounding massive spherical objects such as a star ([Schwarzschild 1916](#)),

$$ds^2 = -c^2 \left(1 - \frac{2GM}{c^2 r}\right) dt^2 + \left(1 - \frac{2GM}{c^2 r}\right)^{-1} dr^2 + r^2 (\sin^2 \theta d\theta^2 + d\phi^2), \quad (1.2)$$

where  $r = \frac{2GM}{c^2}$  is the event horizon of the black holes. After a few years, a static solution was calculated for Einstein-Maxwell’s action, a charged black hole solution, known as Reissner–Nordström (RN) metric ([Reissner 1916](#), [Nordström 1918](#)). However, John Archibald Wheeler was the one to use the word “black hole” for the first time in 1958. In the same year, David Finkelstein gave physical interpretation to the Schwarzschild solution by discussing photon trajectories around the Schwarzschild radius ([Finkelstein 1958](#)). Observation of quasars(quasi-stellar) in the luminous galaxies in 1958 sped up the research in black hole physics. In 1963, Roy Kerr ([Kerr 1963](#)) extended the

Schwarzschild solution to a rotating black hole called the Kerr black hole. In the next few years, Ezra Newman found a charged-rotating Kerr-Newman black hole ([Newman et al. 1965](#), [Newman and Janis 1965](#)). Apart from these solutions, there has been a large class of black holes in different scenarios.

However, combining Einstein's theory of relativity with the well-established single-particle quantum mechanics was hit with particle number conservation problem. As in the case of  $\beta$ -decay, single-particle approaches failed to explain various decay processes. A relativistic particle possesses enough energy to create particles. So naturally, relativistic quantum mechanics makes way to a theory with infinite degrees of freedom. The first work in this direction was to find a relativistic quantum theory for classical electrodynamics. In 1927, P.A.M. Dirac came up with *quantum electrodynamics* ([Dirac 1927](#)), which was successful in explaining the fine structure of the hydrogen atom spectra. Nevertheless, this early success didn't last long, as it faced many infinities in theory due to the "self energies."

In 1950s, Richard Feynman ([Feynman 1950](#)), Julian Schwinger ([Schwinger 1948](#)), Shinichiro Tomonaga ([Tomonaga 1946](#)) and Freeman Dyson ([Dyson 1949](#)) found a way to extract useful information from those infinities known as the *renormalisation theory*. Feynman reframed the theory into a more elegant version of *Path integral formalism*, a much simpler way for calculating probability amplitude using *Feynman diagrams*. Having a complete theoretical structure, there were attempts to put the other three interactions also into this framework. The problem of non-renormalisability of weak and strong interactions was solved by casting the theory into the gauge theory perspective. The works of 't Hooft and Veltman on Yang-Mills theory in this regard initiated the gauge theory revolution (['t Hooft and Veltman 1972](#)). Based on the Glashow-Salam-Weinberg model ([Glashow 1961](#), [Weinberg 1967](#), [Salam 1968](#)) with  $SU(2) \times U(1)$  symmetric Yang-Mills field, the electromagnetic and weak interactions were unified into an electro-weak theory. For strong interactions, with  $SU(3)$  color symmetric Yang-Mills field, it was called as *quantum chromodynamics* (QCD). The success of the gauge theory and quantum field theory (QFT) is captured in the standard model for particle physics, where electro-weak and QCD theories are tied together with  $U(1) \times SU(2) \times SU(3)$

symmetry. Except for few things like baryon asymmetry, dark matter particle, and neutrino mass, the standard model has a striking experimental confirmation in particle physics.

Another way of unification is called the Grand Unified Theory (GUT), which unifies three particle interactions at high energies of order  $10^{15}$  GeV. But the situation is markedly different in gravitational interactions, as there is no successful renormalizable gauge theory for gravity. However, a quantum gravity theory has a great role to play at these high grand unification energy scales. Given its significance, research has progressed to find a right candidate for the quantum gravity. The String theory and loop quantum gravity are popular among various other options such as asymptotic safety, causal set theory, and group field theory. String theory sees particles as an excitation of a string field, whereas loop quantum gravity focuses on quantizing spacetime geometry.

Even though we are still waiting for a complete theory of quantum gravity, our understanding of black holes has improved over the past two decades. The black holes, being a macroscopic quantum mechanical system, are ideal for exploring the intrinsic features of quantum gravity. Thus, during the past five decades, a large amount of research has been conducted in the physics of black holes. One among them is black hole thermodynamics, a field that emerged after the seminal work of Jacob Bekenstein and Stephen Hawking in the early seventies. Bekenstein's proposal that the black hole entropy should be proportional to the horizon area and semi-classical calculations of Hawking to find a surface gravity dependent black hole radiation paved the way for *black hole thermodynamics*. Unexpected connection between fundamental theories, general relativity, quantum field theory, and thermodynamics has led to a surge of interest in black hole thermodynamics ([Hawking 1975](#), [Bekenstein 1972, 1973, 1974](#)). With the temperature and entropy for a black hole defined, it is natural for it to obey the laws of thermodynamics ([Wald 2001](#)). Realizing the thermodynamics of black holes, the four laws of black hole mechanics were obtained by Bardeen, Carter, and Hawking in parallel to four laws in classical thermodynamics ([Bardeen et al. 1973a](#)).

The significance of black hole thermodynamics in anti-de Sitter (AdS) space was realized from the result that a thermodynamically stable black holes exist only in AdS

space. This contrasts with the Minkowskian case where the black hole has a negative specific heat and disappears by radiating Hawking radiation. This happens because the boundary of AdS space acts like walls of a thermal cavity. Inside this closed box-like space, below a certain temperature, only radiation can exist, and above this temperature, the radiation becomes unstable and hence collapses, resulting in the formation of black holes. Thus, the black holes exist in two forms, the larger one with positive specific heat, which is locally stable, and a smaller one with negative specific heat that is unstable. The phase transition between these black holes and radiation at the transition temperature is termed as *Hawking Page transition* (Hawking and Page 1983, Page 2005). In high-energy physics, the topic AdS space got the attention of a larger audience after the proposal of AdS/CFT correspondence by Maldacena (Maldacena 1999). This gauge-gravity duality relates gravity theory in an AdS space to the conformal field theories at the boundary of that space.

The first progress beyond Hawking Page phase transition happened after identifying a rich phase structure isomorphic to van der Waals liquid-gas system in RN-AdS black holes (Chamblin et al. 1999a,b) and in Kerr Newman-AdS black holes (Caldarelli et al. 2000). In all black hole thermodynamic studies done, the crucial thermodynamic variable pressure and volume were absent. In 2009, David Kastor introduced the pressure term into this field through the cosmological constant  $\Lambda$  (Kastor et al. 2009). This identification rectified the inconsistency between the Smarr relation and the first law. In this approach, the conjugate quantity of cosmological constant is taken as the thermodynamic volume. Simultaneously, the expansion of phase space altered the first law of thermodynamics with a  $VdP$  term, giving a new interpretation to the mass of the black hole as enthalpy (Dolan 2011). The new perspective on mass and cosmological constant in black hole thermodynamics resulted in phenomenal consequences in this domain, enabling us to establish newer analogies to the known phenomena in classical thermodynamics. In this extended phase space, the thermodynamics of charged AdS black hole is found analogous to a van der Waals fluid system (Kubiznak and Mann 2012, Gunasekaran et al. 2012, Kubiznak et al. 2017). This has led to a new arena in black hole physics called the *black hole chemistry*. Other analogies to classical ther-

modynamics were also made like Joule Thomson expansion (Ökcü and Aydiner 2017), holographic heat engines (Johnson 2014), Clausius-Clapeyron Equation (Zhao et al. 2015) and reentrant phase transitions (Altamirano et al. 2013).

## 1.1 Phase transitions and Critical Phenomena

Phase transition is a general feature of materials in nature. Interestingly, they follow a common set of characters during the transition. The solid/liquid/gas, paramagnetic/ferromagnetic, and superconductor/normal metal transitions are common examples. Phase transition is the direct outcome of a system's struggle to minimize energy and maximize its entropy or disorder. We can define an order parameter to describe these phase transitions, which appear in one phase and disappears during the transition. Order parameter can simply be referred to as an increase or decrease in order, like in boiling of a liquid to gas, freezing liquid to a solid, and arrangements of spins during para/ferromagnetic transitions, i.e., the difference in densities in earlier case and magnetization in latter are nothing but the order parameters.

One of the signatures of a phase transition is the existence of singularities in the free energy or their derivatives with respect to thermodynamic variables. According to Ehrenfest classification, the order parameter is the lowest derivative of free energy with respect to the variable that exhibits a discontinuity. But in the modern-day classification, a phase transition is classified into three types, first-order/discontinuous, second-order/continuous, and infinite order/topological transitions. A discontinuous change in order parameter, like density in the case liquid/gas transition is first order, and a continuous change in order parameter as magnetization in the case of ferromagnetic transition is the second-order. An infinite order transition does not possess singularities in free energy derivatives; nevertheless, the free energy itself contains singularities. The order parameter shows an exponential behavior near the transition point. Of which second-order phase transition is of special interest because of its distinct characteristics. These characteristic features are known as *critical phenomena*. The presence of large fluctuation around the critical point is one feature of the critical phenomenon. The appearance of discontinuities in response functions and divergence of the correlation length is asso-

ciated with critical phenomena. Correlation length tells how spin, density, or any other degrees of freedom are influenced by each other. Near the critical point, we can assign some exponents to specify the nature of divergence. These are four numbers  $\alpha, \beta, \gamma$  and  $\delta$  called as critical exponents. Interestingly, these critical exponents exhibit universality for phase transitions, thus forming a universality class. At their critical point, the Ising model, water, and van der Waals fluid share the same critical exponents. Hence, systems are equivalent at their critical point, and they belong to the same universality class. Another key feature near the critical point is the scale invariance, and the physics is explained by the scale-invariant theories, or, more generally, conformal field theories (CFT).

### 1.1.1 Conformal field theories and its AdS space correspondence

The conformal field theory is a quantum field theory that has a conformal symmetry. Conformal transformation comprises of Poincare' ( $x^\mu \rightarrow \Lambda_\nu^\mu x^\nu + a^\mu$ ) and some angle preserving transformations. CFT remains invariant under the following transformations,

$$\text{Translation : } x'^\mu \rightarrow x^\mu + a^\mu,$$

$$\text{Lorentz transformations : } x'^\mu \rightarrow \Lambda_\nu^\mu x^\nu,$$

$$\text{Dilations : } x'^\mu \rightarrow \lambda x^\mu,$$

$$\text{Special Conformal transformation : } x'^\mu \rightarrow \frac{x^\mu + a^\mu x^2}{1 + 2x^\mu a_\nu + a^2 x^2},$$

where  $a^\mu$  is the acceleration. In  $d$ -dimensions, the conformal symmetry group is  $SO(d, 2)$  with  $\frac{(d+1)(d+2)}{2}$  generators. Owing to AdS/CFT correspondence, conformal field theories are essential in understanding quantum gravity. The AdS/CFT correspondence tells us that a CFT on a  $d$ -dimensional spacetime is equivalent to a theory of quantum gravity in a  $d + 1$  dimensional asymptotically AdS spacetime, i.e.,  $\mathcal{N} = 4$  supersymmetric Yang-Mills theory is dual to a type II B string theory in  $AdS_5 \times S^5$ . The importance of AdS/CFT correspondence lies in the fact that it converts a result in classical gravity to a scale-invariant condensed matter system. This has an interesting consequence in strongly correlated field theories, where we have a significantly less an-

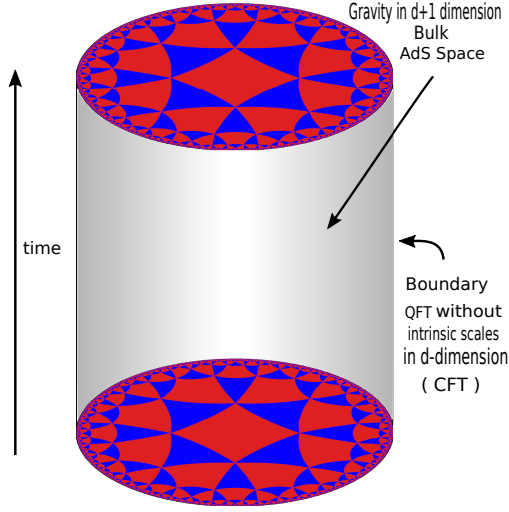


Figure 1.1: The AdS/CFT correspondence: Duality between a theory of gravity in asymptotic anti-de Sitter space in  $d = 2 + 1$  dimensions with a conformal field theory (CFT) residing on the boundary  $d = 2$  dimensions.

analytic method to study its physics. This tool is very efficient due to strong/weak duality. The main ingredient in this duality is AdS space geometry and Conformal field theory.

### 1.1.2 AdS spacetime

Anti-de Sitter spacetime abbreviated as AdS is the maximally symmetric hyperbolic space with constant negative curvature. We can represent  $d$ -dimensional AdS spacetime as a hyperboloid embedded in a  $d + 1$  dimension flat Minkowski spacetime (eqn.1.2). These are  $\mathcal{R}^{2,d-1}$  space having two timelike directions. A hyperboloid can be represented by constraint equation,

$$-X_0^2 - X_1^2 + X_2^2 + \dots + X_d^2 = -L^2,$$

where  $L$  is the radius of curvature of hyperboloid in the  $d + 1$  flat spacetime with metric,

$$ds^2 = -dX_0^2 - dX_1^2 + dX_2^2 + \dots + dX_d^2.$$

The space has a Lorentz symmetry  $SO(2, d - 1)$ . We can parametrize AdS spacetime

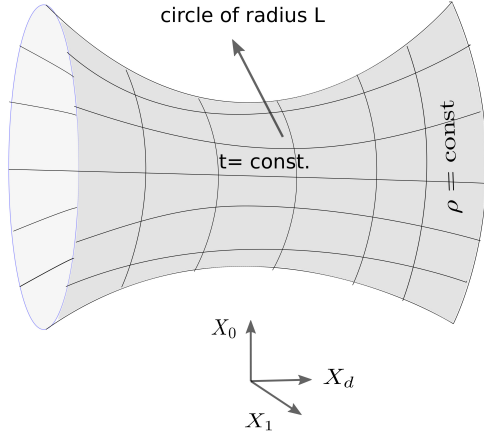


Figure 1.2: The anti-de Sitter spacetime as a hyperboloid embedded in a flat spacetime with two time-like coordinates  $X_0$  and  $X_1$ .

in 4–dimensions ( $AdS_4$ ) by intrinsic coordinates  $(t, \rho, \theta, \phi)$ ,

$$\begin{aligned}
 X_0 &= L \sin t \cosh \rho, \\
 X_1 &= L \cos t \cosh \rho, \\
 X_2 &= L \sinh \rho \cos \theta, \\
 X_3 &= L \sinh \rho \sin \theta \cos \phi, \\
 X_4 &= L \sinh \rho \sin \theta \sin \phi.
 \end{aligned}$$

Now, the metric takes the form,

$$ds^2 = L^2 (-\cosh^2 \rho dt^2 + d\rho^2 + \sinh^2 \rho d\Omega_2^2), \quad (1.3)$$

where  $d\Omega^2 = d\theta^2 + \sin^2 \theta d\phi^2$  is 2-sphere.  $AdS_4$  is  $SO(2, 3)$  invariant. The coordinates  $(t, \rho, \theta, \phi)$  cover entire space ( $\rho \geq 0, 0 \leq t \leq 2\pi$ ), hence called the global coordinates. It has a topology  $S^1 \times R^3$ . As time-like coordinate  $t$  is  $2\pi$  periodic, it allows close time-like curves. This pathology is an artifact of chosen coordinate and can be removed in *universal cover*, where  $t$  ranges from  $(-\infty, +\infty)$ . Conformally compactifying the space



by defining,  $\tan \chi := \sinh \rho$  or,  $\cosh \rho := \frac{1}{\cos \chi}$ , metric (eqn.1.3) becomes,

$$ds^2 = \frac{L^2}{\cos^2 \chi} (-dt^2 + d\chi^2 + \sin^2 \chi d\Omega_2^2), \quad (1.4)$$

where  $0 \leq \chi \leq \frac{\pi}{2}$  and  $-\infty < t < +\infty$ . Conformal boundary is located at  $\theta = \pm \frac{\pi}{2}$  which corresponds to  $\rho \rightarrow +\infty$  (spatial infinity) in the global coordinates. It is important to note that the conformal boundary of AdS spacetime is the place for the dual fields. The metric (eqn.1.4) is conformal to one-half of the Einstein static universe spacetime represented by  $d\tilde{s}^2 = (-dt^2 + d\theta^2 + \sin^2 \theta d\Omega_2^2)$ ,

$$ds^2 = \frac{L^2}{\cos^2 \chi} d\tilde{s}^2,$$

$$\text{ie, } g_{\mu\nu} = \Omega^2(\chi) \tilde{g}_{\mu\nu}.$$

Conformal boundary of  $AdS_d$  spacetime ( $\chi = \frac{\pi}{2}$ ) i.e.,  $\mathcal{R} \times S^{d-2}$  is same as that of conformally compactified Minkowski space in one lesser dimension  $\mathcal{R}^{1,d-1}$ . In simple words, anti-de Sitter spacetime is conformally flat. That is the core of AdS/CFT correspondence. AdS spacetime is written in different coordinate chart like Poincare' and static coordinates. Popular one is in static coordinates which is obtained by setting,  $r = L \sinh \rho$ ,

$$ds^2 = - \left(1 + \frac{r^2}{L^2}\right) dt^2 + \left(1 + \frac{r^2}{L^2}\right)^{-1} dr^2 + r^2 d\Omega_2^2.$$

Any spacetime which approaches this metric in the asymptotic limit is said to be asymptotically AdS spacetime. To be more precise, any spacetime which can be conformally compactified to match the conformal structure of AdS is called asymptotically AdS spacetime.

The homogeneity and isotropy of a manifold imply that space should be maximally symmetric. In that case, the curvature is the same everywhere, and the Riemann tensor can be constructed from metric in a unique way. In  $d$ -dimensional manifold, Riemann

tensor is given by,

$$R_{\mu\nu\rho\delta} = \kappa (g_{\mu\rho}g_{\nu\delta} - g_{\mu\delta}g_{\nu\rho}),$$

where,  $\kappa = \frac{R}{d(d-1)}$ . Consider Einstein equations in vacuum with a cosmological constant  $\Lambda$ ,

$$R_{\mu\nu} - \frac{1}{2}g_{\mu\nu}R + \Lambda g_{\mu\nu} = 0.$$

Here, the Ricci scalar  $R$  can be written in terms of cosmological constant  $\Lambda$  as,

$$R = \frac{2d}{d-2}\Lambda.$$

From the nature of cosmological constant  $\Lambda$ , there are three maximally symmetric spacetimes; Minkowski with  $\Lambda = 0$ , de Sitter(dS)  $\Lambda > 0$ , and anti-de Sitter(AdS)  $\Lambda < 0$ . In the case of AdS space in 4-dimensions, Ricci scalar  $R$  is equal to  $-\frac{6}{L^2}$  and cosmological constant  $\Lambda = -\frac{3}{L^2}$ . In terms of cosmological constant, the AdS metric would read as,

$$ds^2 = -\left(1 + \frac{\Lambda r^2}{3}\right) dt^2 + \left(1 + \frac{\Lambda r^2}{3}\right)^{-1} dr^2 + r^2 d\Omega_2^2.$$

In the spirit of AdS/CFT correspondence, there has been a massive amount of research on AdS black holes, in particular, black hole thermodynamics of AdS black holes.

### 1.1.3 Objectives

The main objective of this thesis is the study of “Critical phenomena in anti-de sitter black holes”. The work specifically focuses on:

- Study the phase transitions in the charged AdS black with a global monopole by analyzing Hawking temperature, mass, entropy, heat capacity, and Gibbs free energy in the extended phase space.
- Explore the effect of magnetic monopole parameter on the Joule-Thomson effect of charged AdS black hole through the inversion temperature and isenthalpic curves.
- Investigation of thermodynamics in regular Bardeen black holes and the influence of quintessence parameters in the phase transition.
- Study the heat engine constructed out of regular Bardeen black holes and analyse the effect of quintessence on the efficiency of the engine.
- Study the thermodynamic geometry of regular Bardeen AdS black hole and the effect of quintessence through Ruppeiner, Weinhold, and Quevedo approaches.
- Investigation of the interaction in the microstructure of regular Bardeen AdS black holes via novel Ruppeiner geometry approach.

## 1.2 Organization of the Thesis

The thesis is organized as follows:

**Chapter 1** gives a brief introduction of anti-de sitter black holes, phase transitions, AdS/CFT correspondence, critical phenomenon, and black hole thermodynamics. The scope and objectives of the present research work together with the organization of the thesis are also included at the end of this chapter.

**Chapter 2** presents a brief introduction to symmetries and conserved charges in general relativity. Killing vector field and Komar integral are introduced to derive laws of black hole thermodynamics. Smarr relation and variation of the cosmological constant is discussed via modified Komar integrals. A brief introduction to *black hole chemistry* is also presented.

In **Chapter 3**, thermodynamics in AdS black holes with a global monopole is discussed. Hawking temperature,  $P - V$  criticality, swallowtail behavior in Gibbs free energy, specific heat, and critical exponents are investigated. Joule-Thomson expansion in AdS black hole with global monopole is explained. Using the Joule-Thomson coefficient, the inversion and isenthalpic curves are discussed.

In **Chapter 4**, the phase structure and the microscopic interactions in regular Bardeen AdS black holes are studied. The stable and metastable phases are analyzed through coexistence and spinodal curves using numerical methods. Using the novel Ruppeiner geometry approach, the microscopic interaction in the black hole is investigated.

In **Chapter 5**, thermodynamics of regular Bardeen black hole and effect of quintessence is investigated. The effect of magnetic charge and quintessence parameter is discussed. The final part is dedicated to the thermodynamic geometry of regular Bardeen black holes.

In **Chapter 6**, a heat engine is constructed from regular black holes, and efficiency is increased by adding a quintessence field. The efficiency of the heat engine is calculated and compared with the traditional Carnot engine. The dependency of efficiency with respect to magnetic charge and quintessence parameter is studied in detail.

**Chapter 7** summarize the critical findings of the present research work by highlighting the remarkable results of the thesis along with conclusions.

# Chapter 2

## Introduction to Black hole thermodynamics

Summary

---

*This chapter presents a brief introduction to the black hole thermodynamics. Beginning with symmetries and charge conservation in gravity, we introduce Komar integrals and conserved quantities. Using the concept of Killing horizon, we review the laws of black hole thermodynamics. In the final section, we discuss the thermodynamics in the AdS black holes.*

---

### 2.1 Introduction

The symmetries and conservations play a key role in physics. They are related to each other through *Noether's theorem*, which states that for every continuous symmetry of the action, there is a conserved *Noether charge*. When it comes to gravity, symmetries are very significant due to the non-linear nature of Einstein's equations. We can observe certain symmetries in the metric tensor  $g_{\mu\nu}$  called isometries, i.e., the geometry is invariant under certain transformations. In the case of the Minkowski metric, isometries can be easily observed from translations and Lorentz transformations. The translational invariance is apparent from the metric as its components are independent of some coordinates. In general, any *diffeomorphism*  $\phi : M \rightarrow M$  is an isometry, if  $\phi^*g = g$ , i.e., physics of set  $(M, g_{\mu\nu})$  and its pullback  $(M, \phi^*g_{\mu\nu})$  remains invariant under general coordinate transformations. It is a fancy way of telling a coordinate invariance in the

geometry, or naively there does not exist a preferred coordinate system. This is the message conveyed when we call a theory generally covariant or diffeomorphism invariant.

## Killing vector fields

The isometries are generated by a *Killing vector field*, named after the German mathematician Wilhelm Killing. Defining a Killing vector is a systematic procedure to find the symmetries in the geometry. For example, time-translation and rotational symmetry of the Schwarzschild metric in  $(t, r, \theta, \phi)$  coordinates is defined by the Killing vector,

$$\xi_0^\mu = \partial_t^\mu = (1, 0, 0, 0), \quad (2.1)$$

$$K_1^\mu = \partial_\phi^\mu = (0, 0, 0, 1), \quad (2.2)$$

$$K_2^\mu = -\cos\phi\partial_\theta^\mu + \sin\phi\cot\theta\partial_\phi^\mu = (0, 0, -\cos\phi, \sin\phi\cot\theta), \quad (2.3)$$

$$K_3^\mu = \sin\phi\partial_\theta^\mu + \cos\phi\cot\theta\partial_\phi^\mu = (0, 0, \sin\phi, \cos\phi\cot\theta), \quad (2.4)$$

where  $\xi$  and  $K$  generates time-translations and rotational invariance respectively in the static and spherically symmetric spacetime. In covariant form, Killing vector is written as,

$$\xi_{0\mu} = g_{\mu\nu}\xi^\nu = \left(-\left(1 - \frac{2M}{r}\right), 0, 0, 0\right), \quad K_{1\mu} = (0, 0, 0, r^2 \sin^2\theta). \quad (2.5)$$

An useful property of Killing vector is the linear superposition, i.e., the linear combination of two Killing vectors is also a Killing vector. In addition, the Killing vectors satisfy the condition,

$$\nabla_\mu \xi_\nu + \nabla_\nu \xi_\mu = \nabla_{(\mu} \xi_{\nu)} = 0. \quad (2.6)$$

This equation is called the Killing equation. We can explain the Killing equation using the concept of Lie derivative introduced by the Norwegian mathematician Sophus Lie. The Lie derivative is just another way of comparing the tensor fields at two different points like a covariant derivative. Using the local diffeomorphism, the tensor field at different points can be brought together. The Lie derivative describes the change of a tensor field as we move along a vector field (diffeomorphism). It can be visualized as a function describing fluctuations in thermometer reading of a sailor whose boat is driven

by wind in a vast ocean. The Lie-derivative of vector field is normally expressed in the Lie-bracket between two vectors. The Lie-derivative of a vector  $V$  along a vector field  $\xi$  is defined as a Lie-bracket,

$$\mathcal{L}_\xi V^\mu := [\xi, V]^\mu = \xi^\nu \partial_\nu V^\mu - V^\nu \partial_\nu \xi^\mu. \quad (2.7)$$

The Lie derivative of a tensor  $T^{\mu_1 \mu_2 \dots \mu_k}_{\nu_1 \nu_2 \dots \nu_l}$  along a vector field  $V$  is defined as,

$$\begin{aligned} \mathcal{L}_V T^{\mu_1 \mu_2 \dots \mu_k}_{\nu_1 \nu_2 \dots \nu_l} &= V^\sigma \nabla_\sigma T^{\mu_1 \mu_2 \dots \mu_k}_{\nu_1 \nu_2 \dots \nu_l} \\ &\quad - (\nabla_\lambda V^{\mu_1}) T^{\lambda \mu_2 \dots \mu_k}_{\nu_1 \nu_2 \dots \nu_l} \\ &\quad - (\nabla_\lambda V^{\mu_2}) T^{\mu_1 \lambda \dots \mu_k}_{\nu_1 \nu_2 \dots \nu_l} - \dots \\ &\quad + (\nabla_{\nu_1} V^\lambda) T^{\mu_1 \mu_2 \dots \mu_k}_{\lambda \nu_2 \dots \nu_l} \\ &\quad + (\nabla_{\nu_2} V^\lambda) T^{\mu_1 \mu_2 \dots \mu_k}_{\nu_1 \lambda \dots \nu_l} + \dots \end{aligned} \quad (2.8)$$

For the metric tensor  $g_{\mu\nu}$ , Lie derivative along a vector field  $V$  would read,

$$\begin{aligned} \mathcal{L}_V g_{\mu\nu} &= V^\sigma \nabla_\sigma g_{\mu\nu} + (\nabla_\mu V^\lambda) g_{\lambda\nu} + (\nabla_\nu V^\lambda) g_{\mu\lambda}, \\ &= \nabla_\mu V_\nu + \nabla_\nu V_\mu, \\ &= 2\nabla_{(\mu} V_{\nu)}. \end{aligned}$$

As the Killing vector field  $\xi^\mu(x)$  generates one-parameter family of isometries, the Lie derivative of a metric along the flow generated by the Killing vector  $\xi^\mu$  is zero,

$$\mathcal{L}_\xi g_{\mu\nu} = 0. \quad (2.9)$$

Using the definition of Lie derivative and Killing vector, we get back the Killing equation (eqn.2.6),

$$i.e., \nabla_\mu \xi_\nu + \nabla_\nu \xi_\mu = \nabla_{(\mu} \xi_{\nu)} = 0. \quad (2.10)$$

Along a geodesic the Killing vector gives us a conserved quantity, which is the product of the Killing vector and the four-momentum  $P_\mu$ . The Killing equation (eqn.2.6) can also be written in terms of  $P_\mu$  as,

$$P^\mu \nabla_\mu (\xi_\nu P^\nu) = 0. \quad (2.11)$$

In the case of an arbitrary geodesic, the conserved quantities are energy  $E$  and angular momentum  $J$ . Moreover, by Noether's theorem each symmetry will produce a conserved quantity. In defining the conserved charge through *Komar integrals*, the Killing vector plays pivotal role. In addition, the derivatives of Killing vectors are related to Riemann tensor  $R^\rho{}_{\sigma\mu\nu}$  and Ricci tensor  $R_{\sigma\nu}$  respectively as,

$$\nabla_\mu \nabla_\sigma \xi^\rho = R^\rho{}_{\sigma\mu\nu} \xi^\nu \quad ; \quad \nabla_\mu \nabla_\sigma \xi^\mu = R_{\sigma\nu} \xi^\nu. \quad (2.12)$$

And using Bianchi identity and the Killing equation, (eqn.2.12) is written in terms of Ricci scalar as,

$$\xi^\mu \nabla_\mu R = 0. \quad (2.13)$$

This shows that Ricci scalars are not changing along the Killing vector field. That means the geometry is invariant along  $\xi^\mu$ . Thus the Killing vectors are a beneficial entity to depict isometries of a spacetime.

## Conservation laws and charges

The Noether's theorem paves way to the continuity equation which tells that behind every conserved current  $J$  there is a conserved charge  $Q$ ,

$$\nabla_\mu J^\mu = 0, \quad Q = \int d^3x J^0. \quad (2.14)$$

This definition of charge can be proved using Stoke's theorem,

$$\int_M \nabla \cdot F dV = \oint_{\partial M} F \cdot dA. \quad (2.15)$$



Taking time-derivative of eqn.2.14, we obtain

$$\partial_t Q = \int d^3x \partial_t J^0 = - \int d^3x \partial_i J^i = \oint dA_i J^i = 0. \quad (2.16)$$

These conservation equations are not restricted to flat spacetime  $M = R \times R$ , but exists in any  $n$ -dimensional manifold  $M$  as well. Stokes's theorem can be generically written with  $n$ -forms as,

$$\int_M d\omega = \int_{\partial M} \omega. \quad (2.17)$$

where  $\omega$  is an  $(p-1)$  form and  $d\omega$  its exterior derivative which turns out to be a  $p$ -form. And  $M$  is an  $n$ -dimensional manifold and  $\partial M$  is its  $n-1$  dimensional boundary. Thus Stokes's theorem relates a quantity on the boundary with its exterior derivative in the bulk. Using the vector identities and notations as given in the appendix (Appx.A), Stoke's theorem takes the form,

$$\int_M d^n x \partial_\nu (\sqrt{|g|} V^\nu) = \int_{\partial M} d^{n-1} y \sqrt{|\gamma|} n_\nu V^\nu, \quad (2.18)$$

where  $y$  is the coordinate on the boundary  $\partial M$ ,  $\gamma$  is the determinant of the induced metric and  $n^\nu$  is the unit normal to  $\partial M$ . The integral in this form takes care of diffeomorphism invariance and remains same in every coordinate system. We will use Stoke's theorem to show that a conserved current defines a conserved charge. Given a space-like hypersurface  $\Sigma$  of constant time and conserved current  $J^\nu$ , we can get a conserved charge  $Q_\Sigma$ ,

$$Q_\Sigma = - \int_\Sigma *J = - \int_\Sigma d^{n-1} y \sqrt{|\gamma|} n_\nu J^\nu. \quad (2.19)$$

The current obtained here represents total charge throughout the spacetime at a particular time. The negative sign in front of the integral assures a positive total charge by compensating negative sign coming from lowering the index of time component of unit normal  $n^\nu$  ( $n^\nu n_\nu = -1$ ). Now consider a region  $R$  enclosed between two space-like hypersurface  $\Sigma_1$  and  $\Sigma_2$  connected through a surface  $\Lambda$  at infinity as shown in the figure (Fig.2.1). The boundary  $\Sigma_2$  lies in the future of the  $\Sigma_1$  and hence future directed unit normal  $n^\mu$  pointing outward to the space-like hypersurface is positive for  $\Sigma_2$  and nega-

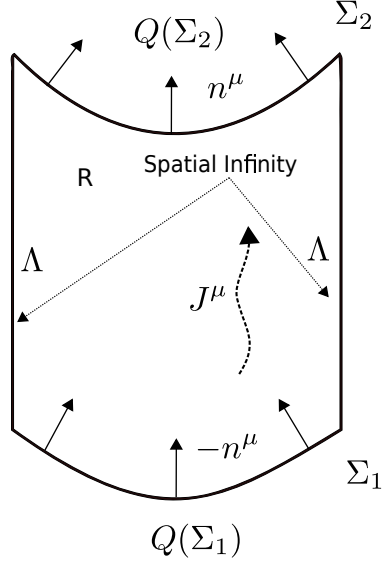


Figure 2.1: Region  $R$  is enclosed between boundaries  $\Lambda$  at spatial infinity and two space like hypersurface  $\Sigma_1$  and  $\Sigma_2$ . The hypersurface  $\Sigma_2$  is the time translation of  $\Sigma_1$ .  $Q(\Sigma_1)$ ,  $Q(\Sigma_2)$  and  $J^\mu$  are the charge and current density.

tive for  $\Sigma_1$ . We can apply the Stoke's theorem to Maxwell's field. Recall the Maxwell's equations, which can be summarised in two equations,

$$F = dA,$$

$$d * F = 4\pi * J \text{ or } d(*J) = 0.$$

Using the Stokes theorem (eqn.2.17), we can find total charge  $Q$  enclosed in the region  $R$  as,

$$\begin{aligned} \int_R d(*J) &= \int_{\partial R} *J, \\ \int_R d^n x \sqrt{|g|} \nabla_\mu J^\mu &= \int_{\Sigma_1 + \Sigma_2 + \Lambda} d^{n-1} y \sqrt{|\gamma|} n_\mu J^\mu & (2.20) \\ &= \int_{\Sigma_2} d^{n-1} y \sqrt{|\gamma|} n_\mu J^\mu + \int_{\Sigma_2} d^{n-1} y \sqrt{|\gamma|} (-n_\mu) J^\mu + \int_{\Lambda} d^{n-1} y \sqrt{|\gamma|} n_\mu J^\mu \\ &= Q_{\Sigma_2} - Q_{\Sigma_1} = 0. \end{aligned}$$

This provides a proof for the statement that a conserved current  $\nabla_\mu J^\mu = 0$  leads to the conserved charge  $Q_{\Sigma_2} = Q_{\Sigma_1}$ . In the last step of eqn.2.20, we have assumed that the current through the boundary  $\Lambda$  is zero. The Stoke's theorem can be used in elec-

rodynamics for showing the electric charge conservation. Maxwell's equation is well described in terms of antisymmetric field strength tensor as,

$$\nabla_\nu F^{\mu\nu} = 4\pi J^\mu. \quad (2.21)$$

Conserved current  $J^\mu$  enables us to define a conserved charge using eqn.2.19 and eqn.2.21 in a space-like hypersurface  $\Sigma$ .

$$Q_\Sigma = - \int_\Sigma d^3x \sqrt{|\gamma|} n_\mu J^\mu, \quad (2.22)$$

$$= - \frac{1}{4\pi} \int_\Sigma d^3x \sqrt{|\gamma|} n_\mu \nabla_\nu F^{\mu\nu}. \quad (2.23)$$

In special relativity, the space-like hypersurface is defined as,

$$\Sigma_t = \{x^\mu \in \mathcal{R}^3 / \text{constant time } t\}. \quad (2.24)$$

And the induced metric,  $\gamma_{ij} = \text{diag}(1, 1, 1)$  and time-like unit normal to the hypersurface  $\Sigma_t$  is,  $n^\mu = (1, 0, 0, 0)$  and  $n_\mu = (-1, 0, 0, 0)$ . Using eqn.2.19, conserved charge read as,

$$Q_{\Sigma_t} = - \int_{\Sigma_t} d^3x \sqrt{|\gamma|} n_\mu J^\mu = - \int_{\mathbf{R}^3} d^3x n_0 J^0 = \int_{\mathbf{R}^3} d^3x \rho(x). \quad (2.25)$$

which is nothing but the total charge in the Minkowski space. This kind of conservation is common to any spacetime. Eqn.2.23 can be rewritten using Stoke's theorem as,

$$\begin{aligned} Q &= - \frac{1}{4\pi} \int_\Sigma d^3x \sqrt{|\gamma|} n_\mu \nabla_\nu F^{\mu\nu}, \\ &= - \frac{1}{4\pi} \int_{\partial\Sigma} d^2x \sqrt{|\alpha|} n_\mu \sigma_\nu F^{\mu\nu}. \end{aligned} \quad (2.26)$$

Here, the boundary of the hypersurface is located at spatial infinity denoted by  $\partial\Sigma$ .  $\alpha_{ij}$  is the induced metric on the boundary of space-like hypersurface  $\partial\Sigma$  and  $\sigma^\mu$  is the unit normal pointing outward. As an example, we can find the conserved electric charge

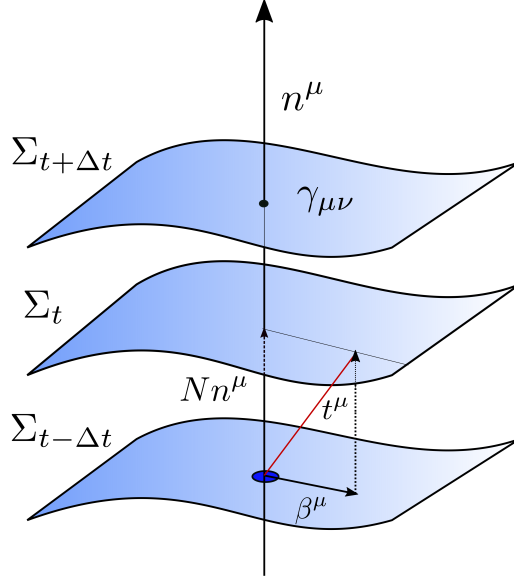


Figure 2.2: Foliation of spacetime: A spacetime  $(\mathcal{M}, g_{\mu\nu})$  can be decomposed into 3-slices (space-like hypersurfaces)  $\{\Sigma_t\}$ . A height-function  $t^\mu$  can be defined in between the hypersurface  $\Sigma_t$ ,  $t^\mu = Nn^\mu + \beta^\mu$ , where  $n^\mu$  is the unit time like normal to the hypersurface,  $N$  is the lapse function and  $\beta$  is the Shift function. .

$Q_{RN}$  for Reissner-Nordström black hole given by the metric,

$$ds^2 = -f(r)dt^2 + \frac{1}{f(r)}dr^2 + r^2d\Omega^2. \quad (2.27)$$

With  $f(r) = 1 - \frac{2M}{r} + \frac{Q^2}{r^2}$ , where  $M$  and  $Q$  are mass and charge parameters of black hole. Making use of the time-translational symmetry in the metric, we choose space-like hypersurface  $\Sigma_t$  and unit time-like normal to it as  $n^\mu$ . From the 3 + 1 foliation of spacetime,  $n^\mu$  can be found. The induced metric on the hypersurface  $\Sigma_t$  is given by  $\gamma_{\mu\nu} = g_{\mu\nu} + n_\mu n_\nu$ .

$$n^\mu = -g^{ab}\omega_b, \quad \text{and} \quad \omega_a = N\Omega_a, \quad (2.28)$$

where  $\omega$  is the normalised 1-form to the space-like hypersurface  $\Sigma_t$ ,  $\Omega$  is the unnormalised 1-form and  $N$  a lapse function measuring proper time between these hypersurface obtained by normalising  $\Omega_a$ .

$$N = \frac{1}{\sqrt{-g^{ab}\Omega_a\Omega_b}}. \quad (2.29)$$

Here in the case of Reissner-Nordström black holes,  $\Omega_a = (1, 0, 0, 0)$  and  $N = \frac{1}{\sqrt{f(r)}}$ . Hence the unit normal  $n^\mu$  is obtained as

$$n^\mu = \left( \frac{1}{\sqrt{f(r)}}, 0, 0, 0 \right), \text{ and } n_\mu = g^{\mu\nu} n_\nu = \left( -\sqrt{f(r)}, 0, 0, 0 \right). \quad (2.30)$$

The boundary  $\partial\Sigma$  is assumed as a 2-sphere with infinite radius described by the metric,

$$\alpha_{ij} = r^2 (d\theta^2 + \sin^2 \theta d\phi^2). \quad (2.31)$$

The unit normal to the  $\partial\Sigma$  is given by  $\sigma^\mu$  which satisfies  $\sigma_\mu \sigma^\mu = +1$ ,

$$\sigma^\mu = \left( 0, \sqrt{f(r)}, 0, 0 \right) \text{ and } \sigma_\mu = \left( 0, \frac{1}{\sqrt{f(r)}}, 0, 0 \right). \quad (2.32)$$

Putting all things together, the total charge of the RN-black hole is obtained from eqn.2.26,

$$Q_E = -\frac{1}{4\pi} \int_{\partial\Sigma} d^2x \sqrt{|\alpha|} n_\mu \sigma_\nu F^{\mu\nu} \quad (2.33)$$

$$= -\frac{1}{4\pi} \int_{\partial\Sigma} d\theta d\phi r^2 \sin \theta n_0 \sigma_r F^{tr} \quad (2.34)$$

$$= \frac{1}{4\pi} \int_{\partial\Sigma} d\theta d\phi r^2 \sin \theta \frac{q}{r^2} = q. \quad (2.35)$$

This shows that the total electrical charge in the RN-black hole is the same as in Maxwell's equation.

### 2.1.1 Komar Integral

After the electric charge, we now focus on other conserved quantities in the black hole, which are mass and angular momentum. The conservation equation in general relativity is expected to be the covariant conservation of stress-energy tensor  $T_{\mu\nu}$  like in any quantum field theory.

$$\nabla_\mu T^{\mu\nu} = 0. \quad (2.36)$$

But it is not true, we can show that  $T^{\mu\nu}$  itself is not conserved in GR and  $\nabla^\mu T_{\mu\nu} = \frac{c^4}{8\pi G} \nabla_\nu R$ . A quantity defined as  $\frac{8\pi G}{c^4} (T_{\mu\nu} - \frac{1}{2} g_{\mu\nu} T)$  which is equal to  $R_{\mu\nu}$  is the right

choice for the covariant conservation equation. This happens because divergence of Ricci tensor do not vanishes and becomes equal to Ricci scalar.

$$\nabla_{\mu}R^{\mu\nu} = \frac{1}{2}\nabla^{\nu}R. \quad (2.37)$$

In asymptotically flat stationary spacetime having a time-like killing vector  $\xi^{\mu}$ , we can define a conserved current  $J^{\mu}$  from  $T^{\mu\nu}$ ,

$$J^{\mu} = \xi_{\mu}T^{\mu\nu}. \quad (2.38)$$

Using the Stoke's theorem (eqn.2.23) integrating over spatial hypersurface  $\Sigma_t$ , we can find the total conserved energy  $E$ ,

$$E = - \int_{\Sigma} d^3x \sqrt{|\gamma|} n_{\mu} J^{\mu}. \quad (2.39)$$

Here our definition of current leads to subtlety that the total energy becomes zero due to the vanishing of  $T^{\mu\nu}$ . And this is indeed not true. Again as mentioned above, a right choice will be  $R_{\mu\nu}$ ,

$$J^{\nu} = \xi_{\mu}R^{\mu\nu}, \quad (2.40)$$

$$= 8\pi G \xi_{\mu} \left( T^{\mu\nu} - \frac{1}{2}g^{\mu\nu}T \right). \quad (2.41)$$

To check whether this current  $J^{\nu}$  is conserved,

$$\begin{aligned} \nabla_{\mu}J^{\mu} &= \cancel{(\nabla_{\mu}\xi_{\mu})}R^{\mu\nu} + \xi_{\mu}(\nabla_{\mu}R^{\mu\nu}), \\ &= \xi_{\mu}(\nabla_{\mu}R^{\mu\nu}) = \frac{1}{2}\xi_{\nu}\nabla^{\nu}R = 0. \end{aligned}$$

The first term vanishes due to the antisymmetric argument, and the second term is rewritten using eqn.2.37 and eqn.2.13. This shows that a new definition for the current in terms of Ricci tensor is the right choice. Now we proceed to write integral in

terms of the new definition of current (eqn.2.41),

$$\begin{aligned}
Q &= - \int_{\Sigma} d^{n-1}y \sqrt{|\gamma|} n_{\mu} J^{\mu}, \\
&= - \int_{\Sigma} d^{n-1}y \sqrt{|\gamma|} n_{\mu} \xi_{\nu} R^{\mu\nu}, \\
&= -8\pi G \int_{\Sigma} d^{n-1}y \sqrt{|\gamma|} n_{\mu} \xi_{\nu} \left( T^{\mu\nu} - \frac{1}{2} g^{\mu\nu} T \right). \tag{2.42}
\end{aligned}$$

Also, from eqn.2.12 we have,

$$\xi_{\mu} R^{\mu\nu} = \nabla_{\mu} \nabla^{\nu} \xi^{\mu}. \tag{2.43}$$

This expression (eqn.2.43) enables us to formulate the equation for the conserved charge in terms of the derivatives of the Killing vector field. This also makes it easy to apply Stoke's theorem and to rewrite it as a surface integral on the boundary of  $\Sigma$ .

$$Q = - \int_{\Sigma} d^{n-1}y \sqrt{|\gamma|} n_{\mu} \nabla_{\nu} (\nabla^{\mu} \xi^{\nu}) \tag{2.44}$$

$$= - \int_{\partial\Sigma} d^2x \sqrt{|\alpha|} n_{\mu} \sigma_{\nu} \nabla^{\mu} \xi^{\nu}. \tag{2.45}$$

This integral is called as Komar integral for a time-like Killing vector field  $\xi$ , where the  $\Sigma$  is the space-like hypersurface, and  $\partial\Sigma$  is the outer boundary of  $\Sigma$ . This is the most general version of Noether's theorem in classical physics. For example, translational and rotational invariance leads to the conserved energy and angular momentum, respectively. Komar integral is written in various forms using differential forms mentioned in appendix (Appx.C).

The total energy (mass) of an asymptotically flat stationary spacetime is given by the Komar mass formula,

$$M_{Komar} = \frac{1}{4\pi G} \int_{\partial\Sigma} d^2x \sqrt{|\alpha|} n_{\mu} \sigma_{\nu} \nabla^{\mu} \xi^{\nu}. \tag{2.46}$$

And the Komar angular momentum in an axisymmetric spacetime is given by,

$$J_{Komar} = -\frac{1}{8\pi G} \int_{\partial\Sigma} d^2x \sqrt{|\alpha|} n_{\mu} \sigma_{\nu} \nabla^{\mu} \xi^{\nu}, \tag{2.47}$$

where the normalisation appearing in front of the integral comes from the normalisation condition of Killing vector field at spatial infinity.

$$\xi_\mu \xi^\mu \rightarrow -1 \text{ at } r \rightarrow \infty. \quad (2.48)$$

Also, integrals (eqn.2.46 and eqn.2.47) should reduce to expressions of energy and momentum at the classical limit. Using the expression (eqn.2.42), we would have

$$\begin{aligned} M_{Komar} &= -\frac{8\pi G}{N_M} \int_\Sigma dV n_\mu \xi_\nu \left( T^{\mu\nu} - \frac{1}{2} g^{\mu\nu} T \right) \approx -\frac{4\pi G}{N_M} \int_\Sigma dV T^{tt} \approx -\frac{4\pi G}{N_M} M_{Newton}, \\ J_{Komar} &= -\frac{8\pi G}{N_J} \int_\Sigma dV n_\mu \xi_\nu \left( T^{\mu\nu} - \frac{1}{2} g^{\mu\nu} T \right) \approx \frac{8\pi G}{N_J} \int_\Sigma dV T^{t\phi} \approx \frac{8\pi G}{N_J} J_{Newton}. \end{aligned}$$

On simplification at the spatial infinity, we have considered only the dominant term in stress-energy tensor  $T^{\mu\nu}$ . The normalization constants  $N_M$  and  $N_J$  are fixed from the Newtonian limit as  $-4\pi G$  and  $8\pi G$  respectively.

The Komar integral result is interesting in the case of Schwarzschild spacetime, where  $R_{\mu\nu} = 0$ .

$$Q = \int_\Sigma dS_\mu R^{\mu\nu} \xi_\nu. \quad (2.49)$$

Not only for Schwarzschild solutions, but for any vacuum solutions with  $R_{\mu\nu} = 0$ , results in Komar charge  $Q = 0$ . The black hole hypersurface  $\Sigma$  has two boundaries, one at horizon  $\mathcal{H}$  and the other an infinite sphere  $S^2$  at spatial infinity. The definition of mass is obtained at spatial infinity, and hence the integral gives non zero mass regardless of the interior of the black hole. Komar mass for Schwarzschild black hole becomes equal to the mass parameter in the spacetime like that of electric charge parameter in RN case. Moreover, this definition of mass (energy) (eqn.2.46) matches with the *ADM energy* (Arnowitt, Deser and Misner) which is the total energy calculated using the Hamiltonian formulation of gravity.

For any Killing vector associated with a spacetime, the Komar integral can be defined. But the formula for mass and angular momentum holds only for asymptotically flat spacetime at asymptotic infinity. In asymptotically flat spacetime, the Komar mass obtained matches with ADM mass. But in general, Komar integral holds for any space-



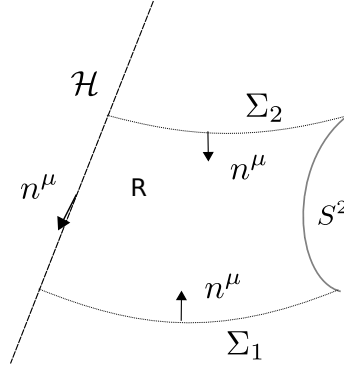


Figure 2.3: Region  $R$  with space-like hypersurface  $\Sigma_1$  and  $\Sigma_2$ , a time-like hypersurface  $S^2$ , which is a large sphere at infinity and a null hypersurface  $\mathcal{H}$ , which is the black hole horizon.

time with symmetries encoded in a conserved 'Komar charge' through an integral involving Killing vector field  $\xi_{(a)}^\mu$ .

$$Q_{\xi_{(a)}^\mu} = \frac{D-2}{8\pi G} \int_{\Sigma} dS_{\mu} R^{\mu}{}_{\nu} \xi_{(a)}^{\nu} = \frac{D-2}{8\pi G} \int_{\partial\Sigma} dS_{\mu\nu} \nabla^{\nu} \xi_{(a)}^{\mu}. \quad (2.50)$$

At asymptotic infinity, in a static, stationary and axisymmetric spacetime Komar charge calculated matches with mass  $M$  and angular momentum  $J$  parameter.

$$\lim_{r \rightarrow \infty} Q_{\xi_{(t)}} = M ; \quad \lim_{r \rightarrow \infty} Q_{\xi_{(\phi)}} = J. \quad (2.51)$$

Consider a manifold describing the black hole spacetime, which contains two boundaries on the hypersurface  $\Sigma$ . In addition to an outer boundary 2-surface  $S^2$  at infinity, there exists an inner boundary at the horizon  $\mathcal{H}$ . For any antisymmetric tensor  $X^{\mu\nu}$ , Stoke's theorem takes the form of,

$$\int_{\mathcal{V}} dS_{\mu} \nabla_{\nu} X^{\mu\nu} = \oint_{S^2} dS_{\mu\nu} X^{\mu\nu} - \oint_{\mathcal{H}} dS_{\mu\nu} X^{\mu\nu}. \quad (2.52)$$

Evaluating Komar integral at two boundaries, while taking the spacetime as static and

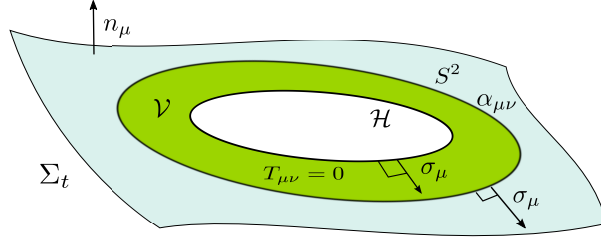


Figure 2.4: The hypersurface  $\Sigma$  consists of an inner boundary  $\mathcal{H}$  and outer boundary  $S^2$  at infinity.

stationary, we would get

$$\oint_{S^2} dS_{\mu\nu} \nabla^\mu \xi^\nu = \int_{\mathcal{V}} dS_\mu R^{\mu\nu} \xi_\nu + \oint_{\mathcal{H}} dS_{\mu\nu} \nabla^\mu \xi^\nu, \quad (2.53)$$

$$\Rightarrow M_K(s_\infty^2) = Q_{\xi_{(a)}}^{s_\infty^2} = \int_{\mathcal{V}} dS_\mu R^{\mu\nu} \xi_\nu + Q_{\xi_{(a)}}^{\mathcal{H}}. \quad (2.54)$$

On further simplification, we get Komar mass  $M_K$ ,

$$M_K = \int_{\mathcal{V}} d^3x \sqrt{|\gamma|} \left( T_{\mu\nu} - \frac{1}{2} g_{\mu\nu} T \right) n^\mu \xi^\nu + \frac{\kappa}{4\pi G} A. \quad (2.55)$$

The first term on the r.h.s is the mass contribution from matter outside the horizon to infinity and the second term gives the mass term, which is proportional to  $\kappa A$ . For the vacuum solutions, the first term vanishes, and the conservation of Komar charge turns to be,

$$Q_{\xi_{(a)}}^{s_\infty^2} = Q_{\xi_{(a)}}^{\mathcal{H}}. \quad (2.56)$$

The second term can be determined from the Killing equation,  $\xi^\mu \nabla_\mu \xi^\nu = \kappa \xi^\nu$ .

$$\frac{1}{4\pi G} \oint_{\mathcal{H}} dS_{\mu\nu} \nabla^\nu \xi_{(a)}^\mu = \frac{\kappa A}{4\pi G}. \quad (2.57)$$

From eqn.2.56, we get Smarr's relation which is very simple for the Schwarzschild black hole, as it is a vacuum solution.

$$M_K = \frac{\kappa A}{4\pi G}. \quad (2.58)$$

Smarr's formula relates the mass with other parameters of the black hole for the static

black holes (Smarr 1973). For the charged, axisymmetric spacetime, Smarr's formula includes parameters angular momentum and electric charge also.

### 2.1.2 Killing horizon

If the killing vector field  $\xi^\mu$  is normal to a null hypersurface  $\Sigma$ , then  $\Sigma$  is a Killing horizon for  $\xi^\mu$ . Note that a normal to null hypersurface is always null, e.g., light cone. Meaning  $\xi^\mu \xi_\mu = 0$ . The null hypersurface is specified by a scalar function  $\xi^0$  ( $=0$ , a constant) which does not change along the directions tangent to the hypersurface. The magnitude of  $(\xi)^2$  is constant along the horizon. Therefore the gradient,

$$g^{\mu\nu} \nabla_\nu (\xi^\alpha \xi_\alpha) = \nabla^\mu (\xi^\alpha \xi_\alpha), \quad (2.59)$$

is also normal to the null hypersurface  $\Sigma$ . On the horizon  $\Sigma$ , there exists a scalar function  $\kappa$  called the surface gravity such that,

$$\frac{1}{2} \nabla^\mu (\xi^\alpha \xi_\alpha) = -\kappa \xi^\mu. \quad (2.60)$$

Eqn.2.60 can be written using the Killing equation as,

$$\xi^\mu \nabla_\mu \xi^\nu = -\kappa \xi^\nu. \quad (2.61)$$

On simplification, we find the expressions for the surface gravity  $\kappa$  as,

$$\kappa^2 = -\frac{1}{2} (\nabla^\mu \xi^\nu) (\nabla_\mu \xi_\nu). \quad (2.62)$$

In the case of Schwarzschild black hole (calculations in Appx.D), it becomes

$$\kappa = \frac{1}{4M}. \quad (2.63)$$

It is important to note that the Killing horizon does not imply an event horizon a priori. Killing horizon can exist in flat spacetimes like Minkowski spacetime which contains no event horizon. But event horizons in some cases can be considered as a Killing horizon. Event horizon  $\mathcal{H}$  of a charged black hole is a null hypersurface, where we can have a

Killing vector field everywhere normal to the null surface. Thus a unique surface gravity  $\kappa$  can be assigned to it. In the Schwarzschild black hole, the event horizon  $\mathcal{H}$  is also the killing horizon, as the translational Killing vector field  $\xi^\mu$  is normal to the event horizon  $\mathcal{H}$ . For axisymmetric Kerr black hole, there will be an additional rotational Killing vector field  $\mathcal{R}^\mu$ . Contrary to the static case, the translational Killing vector field  $\xi^\mu$  is not normal to  $\mathcal{H}$  due to the non-vanishing  $g_{t\phi}$  component. Instead, we have the freedom to chose a local rotating frame, where the event horizon is static like in the Schwarzschild case. This enables to define a time translational Killing vector field  $\xi^\mu$  in the local frame, which rotates along with the event horizon. In a non-rotating frame, the Killing vector should take care of rotation of the frame and translational invariance as well. So the linear combination of two Killing vectors is the right choice of a Killing vector field for the Kerr black hole.

$$\xi^\mu = x^\mu + \Omega_{\mathcal{H}} R^\mu, \quad (2.64)$$

where  $\Omega_H$  is the angular velocity of particle at the horizon. For a Killing horizon  $\Sigma$ , product of Killing vector field is zero  $\xi^\mu \xi_\mu = 0$ . In the case of Kerr black holes, this condition reduces to,

$$\begin{aligned} \xi^\mu \xi_\mu &= K^\mu K_\mu + \Omega_{\mathcal{H}} K^\mu R_\mu + \Omega_{\mathcal{H}} R^\mu K_\mu + \Omega_{\mathcal{H}}^2 R^\mu R_\mu \\ &= g_{tt} + \Omega_{\mathcal{H}} g_{t\phi} + \Omega_{\mathcal{H}} g_{\phi t} + \Omega_{\mathcal{H}}^2 g_{\phi\phi} = 0. \end{aligned}$$

On the stationary surface  $g_{tt} = 0$  and, there are two solutions for the angular velocity but they becomes equal at event horizon  $r = r_+$ ,

$$\Omega_{\mathcal{H}} = \left( -\frac{g_{t\phi}}{g_{\phi\phi}} \pm \sqrt{\left(\frac{g_{t\phi}}{g_{\phi\phi}}\right)^2 - \frac{g_{\phi\phi}}{g_{tt}}} \right) \Big|_{r=r_+} \quad (2.65)$$

$$= \left( -\omega \pm \sqrt{\omega^2 - \frac{g_{tt}}{g_{\phi\phi}}} \right) \Big|_{r=r_+} = \frac{a}{r_+^2 + a^2}. \quad (2.66)$$

With the definition of Killing horizon, we can move to the laws of black hole mechanics.

## 2.2 Laws of black hole mechanics

In this section, we review the works by J. M. Bardeen, B. Carter, and S. W. Hawking in their article *The Four Laws of Black Hole Mechanics* (Bardeen et al. 1973a).

Proceeding with Smarr Formula on the space-like hypersurface  $\Sigma$  with outer boundary  $S^2$  and inner boundary  $\mathcal{H}$ , we have

$$\int_{\Sigma} dS_{\mu} R^{\mu\nu} \xi_{\nu} = \int_{S^2} dS_{\mu\nu} \nabla^{\mu} \xi^{\nu} - \int_{\mathcal{H}} dS_{\mu\nu} \nabla^{\mu} \xi^{\nu}, \quad (2.67)$$

where, r.h.s and l.h.s can be simplified as,

$$\begin{aligned} \int_{\Sigma} dS_{\mu} R^{\mu\nu} \xi_{\nu} &= 8\pi G \int_{\Sigma} d^{n-1}y \sqrt{|\gamma|} n_{\mu} \xi_{\nu} \left( T^{\mu\nu} - \frac{1}{2} g^{\mu\nu} T \right), \quad (2.68) \\ \int_{S^2} dS_{\mu\nu} \nabla^{\mu} \xi^{\nu} - \int_{\mathcal{H}} dS_{\mu\nu} \nabla^{\mu} \xi^{\nu} &= \int_{S^2} d^2x \sqrt{|\alpha|} n_{\mu} \sigma_{\nu} \nabla^{\mu} \xi^{\nu} - \int_{\mathcal{H}} \sqrt{|\alpha|} n_{\mu} \sigma_{\nu} \nabla^{\mu} \xi^{\nu}. \end{aligned} \quad (2.69)$$

Rearranging the terms, the Smarr relation becomes,

$$\int_{S^2} dA n_{\mu} \sigma_{\nu} \nabla^{\mu} \xi^{\nu} = 8\pi G \int_{\Sigma} dV n_{\mu} \xi_{\nu} \left( T^{\mu\nu} - \frac{1}{2} g^{\mu\nu} T \right) - \int_{\mathcal{H}} dA n_{\mu} \sigma_{\nu} \nabla^{\mu} \xi^{\nu}. \quad (2.70)$$

On the null hypersurface, like an event horizon, unit normal satisfies the condition that the unit normal is orthogonal to itself.

$$n_{\mu} \sigma^{\mu} = -1. \quad (2.71)$$

And also, one can identify the future-directed time-like Killing vector  $\xi^{\mu}$  with the normal to the surface  $n_{\mu}$ . For an axisymmetric rotating black hole, killing vector  $k = \partial_{\phi}$  and using the definition of Komar angular momentum  $J$ , eqn.2.70 reduces to,

$$J = \frac{1}{8\pi G} \int_{\mathcal{H}} dA \xi_{\mu} \sigma_{\nu} \nabla^{\mu} \xi^{\nu} - \int_{\Sigma} dV n_{\mu} m_{\nu} \left( T^{\mu\nu} - \frac{1}{2} g^{\mu\nu} T \right). \quad (2.72)$$

In the stationary axisymmetric black hole, using the definition of Komar mass  $M$ , we

can write

$$M = -\frac{1}{4\pi G} \int_{\mathcal{H}} dA \xi_\mu \sigma_\nu \nabla^\mu k^\nu + 2 \int_{\Sigma} dV n_\mu k_\nu \left( T^{\mu\nu} - \frac{1}{2} g^{\mu\nu} T \right). \quad (2.73)$$

Using the Killing horizon,

$$k^\mu = \xi^\mu - \Omega_H m^\mu. \quad (2.74)$$

We rewrite expression for mass  $M$  (eqn.2.73) as,

$$\begin{aligned} M &= -\frac{1}{4\pi G} \int_{\mathcal{H}} dA \xi_\mu \sigma_\nu \nabla^\mu \xi^\nu + \Omega_H \frac{1}{4\pi G} \int_{\mathcal{H}} dA \xi_\mu \sigma_\nu \nabla^\mu m^\nu \\ &\quad + 2 \int_{\Sigma} dV n_\mu \xi_\nu \left( T^{\mu\nu} - \frac{1}{2} g^{\mu\nu} T \right) - 2\Omega_H \int_{\Sigma} dV n_\mu m_\nu \left( T^{\mu\nu} - \frac{1}{2} g^{\mu\nu} T \right) \\ &= -\frac{1}{4\pi G} \int_{\mathcal{H}} dA \xi_\mu \sigma_\nu \nabla^\mu \xi^\nu + 2 \int_{\Sigma} dV n_\mu \xi_\nu \left( T^{\mu\nu} - \frac{1}{2} g^{\mu\nu} T \right) \\ &\quad + 2\Omega_H \left[ \frac{1}{8\pi G} \int_{\mathcal{H}} dA \xi_\mu \sigma_\nu \nabla^\mu m^\nu - \int_{\Sigma} dV n_\mu m_\nu \left( T^{\mu\nu} - \frac{1}{2} g^{\mu\nu} T \right) \right]. \end{aligned} \quad (2.75)$$

The last two terms inside the angular bracket is the expression for Komar angular momentum  $J$ , on substitution we arrive at the relation,

$$M = -\frac{1}{4\pi G} \int_{\mathcal{H}} dA \xi_\mu \sigma_\nu \nabla^\mu \xi^\nu + 2 \int_{\Sigma} dV n_\mu \xi_\nu \left( T^{\mu\nu} - \frac{1}{2} g^{\mu\nu} T \right) + 2\Omega_H J. \quad (2.76)$$

Further, the first term on the r.h.s of the above equation is evaluated using the surface gravity expression (eqn.2.61) and normalisation condition on the horizon ( $\sigma_\nu \xi^\nu = -1$ ),

$$\frac{1}{4\pi G} \int_{\mathcal{H}} dA \xi_\mu \sigma_\nu \nabla^\mu \xi^\nu = \frac{1}{4\pi G} \int_{\mathcal{H}} dA \kappa \sigma_\nu \xi^\nu = -\frac{\kappa}{4\pi G} A. \quad (2.77)$$

Thus the mass  $M$  is written in terms of horizon area  $A$ , surface gravity  $\kappa$ , angular velocity  $\Omega_H$  and momentum  $J$  as,

$$M = \frac{\kappa}{4\pi G} A + 2\Omega_H J + 2 \int_{\Sigma} dV n_\mu \xi_\nu \left( T^{\mu\nu} - \frac{1}{2} g^{\mu\nu} T \right). \quad (2.78)$$

This is the Smarr relation for a rotating charged black hole. In the case of a charged

rotating black hole, there is an additional term with electromagnetic potential  $\phi_H$  and charge  $Q$ . The electromagnetic potential is calculated between the event horizon and infinity. As the matter content in bulk is zero, the last term in eqn.2.78 vanishes for the vacuum Einstein equation, and Smarr relation reduces to,

$$M = \frac{\kappa}{4\pi G}A + 2\Omega_H J + \phi_H Q. \quad (2.79)$$

The small perturbation around stationary axisymmetric black hole would result in a relation for the differential mass  $dM$ . Variation of the above equation (eqn.2.79) for  $M$  leads to,

$$dM = \frac{1}{4\pi G} (Ad\kappa + \kappa dA) + 2(Jd\Omega_H + \Omega_H dJ) + (Qd\phi_H + \phi_H dQ). \quad (2.80)$$

But it can be shown using Stokes theorem and ADM formulation of gravity that,

$$dM = -\frac{1}{4\pi G}Ad\kappa - 2Jd\Omega_H \quad (2.81)$$

Adding equations (eqn.2.80) and (eqn.2.81), we obtain the *first law of black hole mechanics*,

$$dM = \frac{1}{8\pi G}\kappa dA + \Omega_H dJ. \quad (2.82)$$

This relation can be easily obtained through the scaling arguments using *Euler's theorem*, which states that if a homogeneous function  $f(x,y)$  exhibits scaling behaviour  $f(\alpha^p x, \alpha^q y) = \alpha^r f(x,y)$ , then they obey the relation,

$$rf(x,y) = p \left( \frac{\partial f}{\partial x} \right) x + q \left( \frac{\partial f}{\partial y} \right) y. \quad (2.83)$$

Due to the no-hair theorem, black hole mass is uniquely characterized by the horizon area  $A$ , angular momentum  $J$ , and charge  $Q$ . The mass  $M$  is a homogeneous function of these variables,

$$M = M(A, J, Q^2). \quad (2.84)$$

In charged Kerr solution, we see that  $M$  is a homogeneous function of degree  $\frac{1}{2}$ ,

$$M = \left( \frac{A}{16\pi} + \frac{4\pi J^2}{A} + \frac{Q^2}{2} + \frac{\pi Q^4}{A} \right)^{1/2}. \quad (2.85)$$

Applying Euler's theorem (eqn.2.83), we can write

$$\alpha M = M(\alpha^2 A, \alpha^2 J, \alpha^2 Q^2). \quad (2.86)$$

Then, their partial derivatives and function obeys the relation,

$$\begin{aligned} M &= 2A \frac{\partial M}{\partial A} + 2J \frac{\partial M}{\partial J} + 2Q^2 \frac{\partial M}{\partial Q^2}, \\ &= 2A \frac{\partial M}{\partial A} + 2J \frac{\partial M}{\partial J} + Q \frac{\partial M}{\partial Q}. \end{aligned} \quad (2.87)$$

Using the Smarr relation (eqn.2.79), mass  $M$  in the above equation is replaced,

$$\frac{\kappa}{4\pi G} A + 2\Omega_H J + \phi_H Q = 2A \frac{\partial M}{\partial A} + 2J \frac{\partial M}{\partial J} + Q \frac{\partial M}{\partial Q}. \quad (2.88)$$

Rearranging the terms from r.h.s and l.h.s of the above equation, we get

$$2A \left\{ \frac{\kappa}{8\pi G} - \frac{\partial M}{\partial A} \right\} + 2J \left\{ \Omega_H - \frac{\partial M}{\partial J} \right\} + Q \left\{ \phi_H - \frac{\partial M}{\partial Q} \right\} = 0. \quad (2.89)$$

Demanding the variables  $A$ ,  $J$  and  $Q$  to be independent and free, we get

$$\frac{\partial M}{\partial A} = \frac{\kappa}{8\pi G}; \quad \frac{\partial M}{\partial J} = \Omega_H; \quad \frac{\partial M}{\partial Q} = \phi_H. \quad (2.90)$$

From differential calculus, for a function  $M(A, J, Q)$  total differential is written as,

$$dM(A, J, Q) = \frac{\partial M}{\partial A} dA + \frac{\partial M}{\partial J} dJ + \frac{\partial M}{\partial Q} dQ. \quad (2.91)$$

Using eqn.2.90, we obtain differential mass relation,

$$dM = \frac{\kappa}{8\pi G} dA + \Omega_H dJ + \phi_H dQ. \quad (2.92)$$



This is the first law of black hole mechanics, resembles the first law of classical thermodynamics,

$$dE = TdS + \text{work terms.} \quad (2.93)$$

In black hole mechanics, the mass of the black hole  $M$ , horizon area  $A$ , and surface gravity  $\kappa$  is identified with energy  $E$ , entropy  $S$ , and temperature  $T$  in the ordinary thermodynamics. The terms  $\Omega_H J$  and  $\phi_H Q$  are work terms like that in classical thermodynamics.

$$\begin{aligned} E &\longleftrightarrow M, \\ S &\longleftrightarrow \frac{A}{4G}, \\ T &\longleftrightarrow \frac{\kappa}{2\pi}. \end{aligned}$$

But classically black hole is a perfect absorber emitting nothing, so the temperature of the black hole is constantly zero everywhere. Nevertheless, Stefan Hawking considered quantum effects on the black holes. The quantum fluctuations around the horizon lead to particle-antiparticle creation and, in effect, the ‘emission’ of particles from the horizon. This thermal radiation, called the Hawking radiation, is proportional to the surface gravity,

$$T = \frac{\kappa}{2\pi}. \quad (2.94)$$

Like the first law, there is a zeroth and a second law for black hole thermodynamics as well. We know the temperature of a black hole is given by surface gravity, which is constant over the event horizon in a stationary black hole. The *zeroth law of black hole mechanics* states that for a stationary black hole, the surface gravity  $\kappa$  is constant over the horizon. This is in parallel with the zeroth law of classical thermodynamics, which states that for a thermal body in equilibrium, the temperature is constant. The second law of thermodynamics deals with the entropy of an isolated system that will not decrease with time. The *second law of black hole* is in accordance with the area theorem which states that the area of the event horizon cannot decrease with time. On the other hand, considering quantum effects, a black hole can ‘evaporate’ completely

by vanishing the area, thereby violating the area theorem. As the matter keeps falling into the black hole, the entropy of the matter outside the black hole decreases  $\delta S < 0$ , at the same time, this increases horizon area  $\delta A > 0$ . Reverse process  $\delta S > 0$ ,  $\delta A < 0$  happens during evaporation. This has led Bekenstein to propose a *generalized second law*,

$$\delta S_{Total} = \delta (S_{stuff} + S_{bh}) \geq 0, \quad (2.95)$$

$$\text{ie, } \delta \left( S_{stuff} + \frac{A}{4G} \right) \geq 0, \quad (2.96)$$

where the total entropy  $S_{Total}$  is the sum of the entropy of stuff that fell into the black hole plus the total the entropy of the black hole. The generalized second law guarantees that the lost entropy of matter is compensated by an increase in the area of the horizon. If one assigns  $\frac{A}{4G}$  as the entropy of the black hole, then the laws of black hole mechanics are nothing more than the ordinary thermodynamics. But this encounters problems with the usual definition of entropy as the logarithm of the number of accessible microstates. The no-hair theorem puts a constraint on the number of microstates due to the fixed mass, charge, and angular momentum of the black hole. In reality, entropy for a black hole is not as small as expected from the no-hair theorem; it's huge. In any quantum gravity theory, the microscopic degrees of freedom should be  $e^{A/4}$ . Black hole thermodynamics emphasises a deep connection between gravity, quantum mechanics, and statistical mechanics. Another problem is the *information paradox*, information about anything that fell into a black hole is lost permanently as the black hole evaporates. This violates the very fundamental principle of physics. Resolution of these conflicts requires a complete quantum theory of gravity.

## 2.3 Thermodynamics in AdS space

Though Schwarzschild black hole can be treated as a thermal object, it cannot be present in thermal equilibrium. They will evaporate unless you put them in a thermal bath. This happens due to the negative specific heat of black holes. Any increase in mass or energy can reduce the black hole temperature. That makes Schwarzschild black hole thermodynamically unstable. Immersed in a thermal bath, any amount of heat absorbed

from the hot thermal bath can reduce the temperature of a black hole, contrary to a thermodynamically stable object. This leads to the cooling down of the black hole and eventually a runaway. The best way to stabilize the black hole is to put them in a finite heat bath so that any absorption of heat can cool the black hole as well as the bath. But the size of the box matters; if the bath is small, it can cool quicker than a black hole, and again old problem persists. It was noticed by Hawking that the anti-de Sitter spacetime could provide a natural box for the black hole to stabilize thermally (Hawking and Page 1983). Also, the definition of Komar integral and Smarr formula hold only for asymptotically-flat spacetimes. It does not holds same for spacetime with a cosmological constant. The action for gravity with a cosmological constant  $\Lambda$  is given by,

$$S = \int d^4x \sqrt{-g} (R - 2\Lambda). \quad (2.97)$$

For  $\Lambda \neq 0$  cases, we have to find a new Komar boundary integrand to make sure that volume integral vanishes to satisfy Komar charge  $Q = 0$ . Unlike the vacuum solutions, for  $\Lambda \neq 0$  case,  $R_{\mu\nu} = \Lambda g_{\mu\nu} \neq 0$ . As the Komar charge depends on  $R_{\mu\nu}$ , the Komar integral now depends on the integral of the cosmological constant. This can lead to the divergence of the Komar integral.

The metric for the  $AdS_4$  spacetime is given by,

$$ds^2 = -\frac{r^2}{l^2} dt^2 + \frac{l^2}{r^2} dr^2 + r^2 d\Omega_2^2. \quad (2.98)$$

where  $\Lambda = 3/l^2$ ,  $l$  is the AdS radius. We can calculate the Komar integral for this AdS spacetime,

$$Q_\xi = \frac{1}{4\pi G} \int_{\partial\Sigma} dS_{\mu\nu} \nabla^\nu \xi^\mu = \frac{1}{4\pi G} \int_{\partial\Sigma} n_\mu \sigma_\nu \nabla^\mu \xi^\nu \quad (2.99)$$

$$= \frac{1}{4\pi G} \int_{\partial\Sigma} d\theta d\phi r^2 \sin\theta n_t \sigma_r \nabla^t \xi^r = \frac{1}{4\pi G} \int_{\partial\Sigma} d\theta d\phi r^2 \sin\theta \frac{r}{l^2}. \quad (2.100)$$

As we integrate at infinite radial distance, the integral diverges. So the Komar integral relation used for arriving at Smarr formula needs to be modified. There are various ways to resolve these divergences. We follow a method using definition of a Komar

potential  $\omega^{\mu\nu}$  (Kastor et al. 2009). From the Killing equation, we write,

$$\nabla_\mu \xi^\mu = 0. \quad (2.101)$$

This enable us to define an antisymmetric potential  $\omega^{\mu\nu}$ , such that derivative of potential is same as the Killing vector  $\xi^\nu$ ,

$$\xi^\nu = \nabla_\mu \omega^{\mu\nu}. \quad (2.102)$$

The Killing potential is not unique, and we can always add a divergenceless term. So that the new potential  $\omega^{\mu\nu} = \omega^{\mu\nu} + \lambda^{\mu\nu}$  still satisfies the Killing equation. We can also add an exact term  $\lambda^{\mu\nu} = \nabla_\alpha \eta^{\alpha\mu\nu}$ , where  $\eta^{\alpha\mu\nu}$  is antisymmetric tensor. That will not change the value of the final Komar integral. With the potential term as a counter term, the Komar integral reads as,

$$Q_\xi = \frac{1}{4\pi G} \int_{\partial\Sigma} dS_{\mu\nu} (\nabla^\nu \xi^\mu + \Lambda \omega^{\mu\nu}). \quad (2.103)$$

The counter term prevents Komar integral from divergence. The divergent term from integral of  $\nabla^\nu \xi^\mu$  is thus canceled by the counter term from the Killing potential. And in the absence of a cosmological constant, one recovers the old Komar integral for asymptotically flat spacetime case.

Consider the case of Schwarzschild-AdS spacetime with metric given by,

$$ds^2 = -f(r)dt^2 + \frac{dr^2}{f(r)} + r^2 d\Omega_2^2, \quad f(r) = 1 - \frac{m}{r} - \frac{\Lambda}{3}r^2, \quad (2.104)$$

where  $m$  is the mass parameter, which is related to total mass of black hole  $M$  through the Komar integral.

$$M = \frac{(d-2)}{16\pi} \omega_{d-2} m, \quad \omega_{d-2} = \frac{2\pi^{(d-1)/2}}{\Gamma(d-1)/2}, \quad (2.105)$$

where  $\omega_{(d-2)}$  is the volume of unit  $S^{(d-2)}$  sphere. As the only Killing vector associated is  $\xi^\mu = \left(\frac{\partial}{\partial t}\right)^\mu = (1, 0, 0, 0)$ , we have to determine only  $rt$  component of Killing

potential  $\omega^{\mu\nu}$ . Using the definition of Killing potential (eqn.2.102)

$$\frac{1}{r^2} \partial_r (r^2 \omega^{rt}) = 1 \quad (2.106)$$

Integrating the above equation, we get

$$\omega^{rt} = \frac{r}{3} + \frac{C}{r^2}. \quad (2.107)$$

For the case of pure AdS spacetime,  $C = 0$ , but in Schwarzschild-AdS spacetime, there is an extra term in  $\omega^{rt}$ . Then we are left with  $\nabla_r \xi_t$  term in the Komar integral, that can be simplified for Schwarzschild-AdS metric as,

$$\nabla_r \xi_t = \frac{1}{2} \nabla_r (g_{tt} \xi^t) = -\frac{1}{2} \partial_r (f(r)). \quad (2.108)$$

Evaluating Komar integral for pure AdS spacetime, we have

$$Q_\xi = \frac{1}{4\pi G} \int_{\partial\Sigma} dS_{rt} (\nabla^r \xi^t + \Lambda \omega^{rt}) \quad (2.109)$$

$$= \frac{1}{4\pi G} \int_{\partial\Sigma} dS_{rt} \left( \frac{r}{l^2} - \frac{r}{l^2} \right) = 0. \quad (2.110)$$

The same procedure can be applied to derive Smarr relation for Schwarzschild-AdS case. As Komar charge  $Q = 0$ , we can write the enhanced Komar integral in the  $D$ -dimensional spacetime as,

$$\frac{D-2}{8\pi G} \int_{\Sigma} \left( \nabla^\mu \xi^\nu + \frac{2\Lambda}{D-2} \omega^{\mu\nu} \right) = 0. \quad (2.111)$$

Where the  $(D-1)$  hypersurface  $\Sigma$  connects the horizon and infinity, infact  $\Sigma$  is bounded by two surfaces,  $\mathcal{H}$  on the event horizon and  $S_\infty$  at the spatial infinity. Evaluating above integral at the two surfaces, we get

$$0 = \frac{D-2}{8\pi G} \left( \int_{S_\infty} dS_{\mu\nu} \left( \nabla^\mu \xi^\nu + \frac{2\Lambda}{D-2} \omega^{\mu\nu} \right) - \int_{\mathcal{H}} dS_{\mu\nu} \left( \nabla^\mu \xi^\nu + \frac{2\Lambda}{D-2} \omega^{\mu\nu} \right) \right) \quad (2.112)$$

For pure AdS case, we have showed that the component of integral vanishes at infinity.

But in the Schwarzschild-AdS spacetime integral will give a finite value, nevertheless it can be removed by infinite background subtraction as prescribed in (Magnon 1985).

Adding and subtracting  $\omega_{AdS}^{\mu\nu}$  potential will do the trick,

$$0 = \frac{D-2}{8\pi G} \int_{S_\infty} dS_{\mu\nu} \left( \left\{ \nabla^\mu \xi^\nu + \frac{2\Lambda}{D-2} \omega_{AdS}^{\mu\nu} \right\} + \frac{2\Lambda}{D-2} \omega^{\mu\nu} - \frac{2\Lambda}{D-2} \omega_{AdS}^{\mu\nu} \right) \quad (2.113)$$

$$- \frac{D-2}{8\pi G} \int_{\mathcal{H}} dS_{\mu\nu} \left( \nabla^\mu \xi^\nu + \frac{2\Lambda}{D-2} \omega^{\mu\nu} \right). \quad (2.114)$$

Rearranging the terms, we get

$$\frac{D-2}{8\pi G} \int_{S_\infty} dS_{\mu\nu} \left( \nabla^\mu \xi^\nu + \frac{2\Lambda}{D-2} \omega_{AdS}^{\mu\nu} \right) = \frac{D-2}{8\pi G} \int_{\mathcal{H}} dS_{\mu\nu} \nabla^\mu \xi^\nu \quad (2.115)$$

$$+ \frac{D-2}{8\pi G} \frac{2\Lambda}{D-2} \left( \int_{\mathcal{H}} dS_{\mu\nu} \omega^{\mu\nu} - \int_{S_\infty} dS_{\mu\nu} (\omega^{\mu\nu} - \omega_{AdS}^{\mu\nu}) \right). \quad (2.116)$$

We have already evaluated various terms in the above expression, where l.h.s is the definition of Komar mass  $M$ ,

$$\frac{D-2}{8\pi G} \int_{S_\infty} dS_{\mu\nu} \left( \nabla^\mu \xi^\nu + \frac{2\Lambda}{D-2} \omega_{AdS}^{\mu\nu} \right) = (D-3)M. \quad (2.117)$$

The integral of first term in the r.h.s is the product of surface gravity  $\kappa$  and area of event horizon,

$$\frac{D-2}{8\pi G} \int_{\mathcal{H}} dS_{\mu\nu} \nabla^\mu \xi^\nu = (D-2) \frac{\kappa A}{8\pi}. \quad (2.118)$$

The remaining terms left in eqn.2.116 are denoted by  $\Theta$ , which can be seen later as the conjugate volume,

$$\Theta = \int_{\mathcal{H}} dS_{\mu\nu} \omega^{\mu\nu} - \int_{S_\infty} dS_{\mu\nu} (\omega^{\mu\nu} - \omega_{AdS}^{\mu\nu}). \quad (2.119)$$

Combining terms together, we get the Smarr formula

$$(D-3)M = (D-2) \frac{\kappa A}{8\pi G} - 2 \frac{\Theta}{8\pi G} \Lambda. \quad (2.120)$$

In the case of 4–dimensional Schwarzschild-AdS black holes, it turns out to be,

$$M = \frac{\kappa A}{4\pi G} - 2\frac{\Theta}{8\pi G}\Lambda, \quad (2.121)$$

and

$$\Theta = -\frac{4\pi r_h^3}{3} = -V_h. \quad (2.122)$$

which is nothing but the volume of 3-sphere with a negative sign. The Smarr relation can also be obtained from scaling argument using Euler’s theorem discussed earlier in sec.2.2. The quantities mass  $M$ , area  $A$  and cosmological constant  $\Lambda$  scales as  $l^{D-3}$ ,  $l^{D-2}$  and  $l^{-2}$  respectively. Then using Euler’s theorem,

$$(D-3)M = (D-2)\left(\frac{\partial M}{\partial A}\right)A - 2\left(\frac{\partial M}{\partial \Lambda}\right)\Lambda. \quad (2.123)$$

Equating with Smarr relation, we obtain

$$(D-2)\left(\frac{\partial M}{\partial A}\right)A - 2\left(\frac{\partial M}{\partial \Lambda}\right)\Lambda = (D-2)\frac{\kappa A}{8\pi G} - 2\frac{\Theta}{8\pi G}\Lambda. \quad (2.124)$$

From the eqn.2.124, one can identify  $\frac{\partial M}{\partial A} = \frac{\kappa A}{8\pi G}$  and  $\frac{\partial M}{\partial \Lambda} = \frac{\Theta}{8\pi G}$ . Differentiation of the Smarr relation gives the first law of black hole thermodynamics in this extended phase space,

$$dM = \frac{\kappa}{8\pi G}dA + \left(\frac{\partial M}{\partial \Lambda}\right)d\Lambda. \quad (2.125)$$

The second term in the first law (eqn.2.125) and Smarr relation (eqn.2.123), fills the missing  $PV$  term in the black hole thermodynamics. The cosmological constant  $\Lambda$  is identified with thermodynamic pressure  $P$ ,

$$P = -\frac{\Lambda}{8\pi}. \quad (2.126)$$

And the conjugate quantity  $\Theta$ , we have shown that it is equal to the geometrical volume  $V_H$ . The idea of considering cosmological constant as a dynamical variable was put forward firstly by Teitelboim and Brown (Teitelboim 1985, Brown and Teitelboim 1988). Its significance and interpretation in thermodynamics were realized much later.

Also, the first term in Smarr relation (eqn.2.123) can be written in terms of Hawking temperature and entropy. The black hole emits particles with a thermal spectrum that peaking at a temperature called Hawking temperature  $T_H$ , which is related to surface gravity  $\kappa$ .

$$T_H = \frac{\hbar\kappa}{2\pi}. \quad (2.127)$$

And the entropy of a black hole  $S_{BH}$ ,

$$S_{BH} = \frac{A}{4\hbar G}. \quad (2.128)$$

Utilizing the above identifications, we can write

$$(D-3)M = (D-2)TS - 2VP, \quad (2.129)$$

$$dM = TdS + VdP. \quad (2.130)$$

In the charged rotating black hole, extra terms corresponding to the charge and rotating parameter will be added in Smarr relation and first law.

$$M = 2(TS + \Omega J - VP) + \phi Q, \quad (2.131)$$

$$dM = TdS + VdP + \phi dQ + \Omega dJ. \quad (2.132)$$

where  $J$  and its conjugate  $\Omega$  are angular momenta and angular velocity, respectively. Similarly,  $Q$  and its conjugate quantity  $\phi$  are electromagnetic charge and potential, respectively.

## 2.4 Conclusion

In the first part of this chapter, we established the Smarr relation for asymptotically flat black holes using two methods, a geometrical method via Komar integrals and then by scaling arguments via Euler theorem. In the subsequent sections, we have illustrated the failure of these methods in asymptotically AdS black holes. The failure of Smarr relation for the AdS black holes led to the extended version of thermodynamics with the cosmological constant  $\Lambda$  being interpreted as the thermodynamic pressure  $P$ . The Smarr



relation involving the  $PV$  term in the extended space is obtained from the modified Komar integrals. Mainly, we have reviewed the works of Kastor, Ray, and Traschen to derive the modified Komar integral with a counter Killing potential term. Since then, there has been a huge amount of interest in studying the thermodynamics of black holes in this extended phase space. An immediate implication of this extension led to van der Waals fluid-like phase structure in the AdS black holes ([Kubiznak and Mann 2012](#)). We will review the works of Kubiznak and Robert Mann in the coming chapters.



# Chapter 3

## Phase transitions and Joule-Thomson effect in AdS black holes with a Global Monopole

Summary

---

*This chapter is an edited version of our article (Naveena Kumara et al. 2019, Ahmed Rizwan et al. 2019a). A detailed discussion on phase transitions and the Joule–Thomson effects of charged AdS black hole with a global monopole is presented. In the analysis of critical behavior, the classical van der Waals analogy is drawn from isotherms, which is followed by Gibbs free energy study, coexistence curves, and critical exponents. We study the effect of the global monopole parameter  $\eta$  on the inversion temperature and isenthalpic curves. The obtained result is compared with Joule-Thomson expansion of van der Waals fluid, and the similarities were noted.*

---

### 3.1 Introduction

Black hole physics has changed from mere theoretical importance to experimental aspects due to the observational advances like gravitational waves and black hole imaging. However, the theoretical developments are far ahead of experiments due to their importance in several directions like quantum mechanics, quantum gravity, and string theory. Black hole thermodynamics began with a quest for incorporating quantum mechanical nature to a black hole, which had purely classical origin in general relativity. Since the

pioneering work in this regard by Hawking and Bekenstein, black hole thermodynamics remains as an exciting topic in contemporary research.

In this chapter, we concentrate on the thermodynamics of AdS black hole with a global monopole. Monopoles are one among the defects like textures, domain walls, and cosmic strings, which are formed during the cooling phase of the early universe (Kibble 1976, Vilenkin 1985). These topological defects are the consequence of a non-uniform spontaneous symmetry breaking. Geometrically these defects are the result of the impossibility of shrinking the vacuum manifold into a single point. Global monopoles are formed during the symmetry breaking of a self coupled triplet scalar field of  $SO(3)$  gauge symmetry spontaneously broken into  $U(1)$  gauge. The energy density of these global monopoles has a functional dependence on radial distance as  $1/r^2$  and exhibits a solid angle deficit of  $8\pi^2\eta^2$  (where  $\eta$  is the scale of gauge symmetry breaking). The static black hole solution with a global monopole was first obtained by Barriola and Vilenkin (Barriola and Vilenkin 1989), the topological structure of which is distinct from the Schwarzschild black hole solution. The physical properties of this black hole solution with monopole are studied extensively (Shi and Li 1991, Banerjee et al. 1996, Chen and Jing 2013, Jusufi et al. 2017). The solid angle deficit possessed by this solution is analogous to the conical deficits due to cosmic strings.

Recently the thermodynamics of black holes with conical defects has been investigated in the context of accelerating black holes (Appels et al. 2016, 2017). The effect of global monopole in superconductor/normal metal phase transition was first investigated by Chen et.al. (Chen et al. 2010). Later, in the spacetime of this monopole black hole, the thermodynamics and phase transitions were investigated (Deng et al. 2018). In all these studies, the global monopole showed its presence by affecting the phenomena under consideration significantly. Motivated by these results, in this chapter, we study the thermodynamics of charged AdS black hole with a global monopole.

The motivation for this research is to find the possible change in critical behavior and the Joule-Thomson effect of the charged AdS black hole due to the solid angle deficit induced by the global monopole. It is interesting because a similar solid angle deficit is exhibited in Skyrme black hole (Flores-Alfonso and Quevedo 2019) and

conical defect in accelerating black hole (Appels et al. 2017) has a great effect in their thermodynamics.

This chapter is organized as follows. In section 3.2 we present a brief overview of the charged AdS black hole with a global monopole. This is followed by the study of thermodynamics in extended space in section 3.3. In sections 3.4 and 3.5, we discuss the Joule-Thomson effect in van der Waals fluid and charged AdS black holes, respectively. The chapter ends with section 3.6 where we discuss our observations and results.

## 3.2 The charged AdS black hole with a global monopole

We begin this section by reviewing the details of charged AdS black hole with a global monopole. The Lagrangian density that characterises the simplest model with a global monopole is given by (Barriola and Vilenkin 1989),

$$\mathcal{L}_{gm} = \frac{1}{2} \partial_\mu \Phi^j \partial^\mu \Phi^{*j} - \frac{\gamma}{4} \left( \Phi^j \Phi^{*j} - \eta_0^2 \right)^2, \quad (3.1)$$

where  $\Phi^j$  is self coupled scalar field triplet,  $\gamma$  is a self interaction term and  $\eta_0$  is the energy scale of gauge symmetry breaking. The field configuration for the scalar triplet which describe the monopole is,

$$\Phi^j = \eta_0 h(r) \frac{x^j}{r}, \quad (3.2)$$

where  $x^j = \{r \sin \theta \cos \phi, r \sin \theta \sin \phi, r \cos \theta\}$  with  $x^j x^j = r^2$ . The generic metric ansatz for static spherically symmetric spacetime reads as,

$$d\tilde{s}^2 = -\tilde{f}(\tilde{r}) d\tilde{t}^2 + \tilde{f}(\tilde{r})^{-1} d\tilde{r}^2 + \tilde{r}^2 d\Omega^2 \quad (3.3)$$

where  $d\Omega^2 = d\theta^2 + \sin^2 \theta d\phi^2$ . The energy-momentum tensor can be obtained from the Lagrangian density, which is given by,

$$T_{\mu\nu} = \frac{2}{\sqrt{-g}} \frac{\partial}{\partial g^{\mu\nu}} (\mathcal{L}_{gm} \sqrt{-g}) = 2 \frac{\partial \mathcal{L}_{gm}}{\partial g^{\mu\nu}} - g_{\mu\nu} \mathcal{L}_{gm}. \quad (3.4)$$

The explicit forms of the components of  $T_{\mu\nu}$  are,

$$\begin{aligned} T_{tt} &= f(r) \left( \frac{\eta_0^2 h'^2 f(r)}{2} + \frac{\eta_0^2 h^2}{r^2} + \frac{1}{4} \gamma \eta_0^4 (h^2 - 1)^2 \right), \\ T_{rr} &= \frac{1}{f(r)} \left( -\frac{\eta_0^2 h'^2 f(r)}{2} + \frac{\eta_0^2 h^2}{r^2} + \frac{1}{4} \gamma \eta_0^4 (h^2 - 1)^2 \right), \\ T_{\theta\theta} &= r^2 \left( \frac{\eta_0^2 h'^2 f(r)}{2} + \frac{1}{4} \gamma \eta_0^4 (h^2 - 1)^2 \right), \\ T_{\phi\phi} &= r^2 \sin^2 \theta \left( \frac{\eta_0^2 h'^2 f(r)}{2} + \frac{1}{4} \gamma \eta_0^4 (h^2 - 1)^2 \right). \end{aligned}$$

We are using an approximate solution for the charged AdS black hole with a global monopole (Barriola and Vilenkin 1989). The solution for the field equation corresponding to the scalar action in curved space, and is approximated with that of flat space. This approximation is made assuming the structure of the monopole is not affected by gravity in a small range.

We obtained the field equation for the scalar action in the curved spacetime which reads as follows,

$$\tilde{f}'' h'' + \frac{2}{r} \tilde{f} h' + \tilde{f}' h' - \frac{2}{r^2} h - \lambda \eta_0^2 h (h^2 - 1) = 0. \quad (3.5)$$

In the flat spacetime this reduces to,

$$h'' + \frac{2}{r} h' - \frac{2}{r^2} h - \frac{h(h^2 - 1)}{\delta^2} = 0, \quad (3.6)$$

where  $\delta \approx (\eta_0 \sqrt{\lambda})^{-1}$  is the monopole core size in the flat space. At small distances, gravity does not substantially change the structure of the monopole for  $\eta_0 < m_p$  (where  $m_p$  is the Planck mass), so that the flat space estimation of  $\delta$  applies in curved space. The profile of  $h(r)$  in flat space can be obtained by the method of hyperbolic functions by setting  $x = r/\delta$  in eqn.3.6 as follows (Shi and Li 1991),

$$h(x) = \sum_{n=0}^{\infty} c_n \tanh^{2n+1} \frac{x}{\sqrt{2}}, \quad (3.7)$$

where  $c_n$  are the expansion coefficients.

From the profile of  $h(x)$ , it is apparent that  $h(r)$  linearly increases for  $r < (\eta_0\sqrt{\gamma})^{-1}$  and exponentially approaches to unity when  $r > (\eta_0\sqrt{\gamma})^{-1}$ . So, one can approximate  $h(r) \approx 1$  outside the monopole core (Barriola and Vilenkin 1989). This is a valid assumption in our calculation because the core is inside the black hole and thermodynamics is studied on the horizon. Secondly, outside the core, the potential corresponding to the monopole charge varies as  $1/r$ , which makes  $h(r) \approx 1$ . With this approximation, the components of energy-momentum tensors are reduced to,

$$T_t^t \approx T_r^r \approx \eta^2/r^2 \quad , \quad T_\theta^\theta \approx T_\phi^\phi \approx 0. \quad (3.8)$$

This is in agreement with the second argument presented above in terms of potential. The energy depends on the square of the field. The useful Einstein equation for the spherically symmetric static metric is,

$$f \left( \frac{1}{r^2} - \frac{1}{r} \frac{f'}{f} \right) - \frac{1}{r^2} = 8\pi G T_t^t, \quad (3.9)$$

$$f \left( \frac{1}{r^2} + \frac{1}{r} \frac{f'}{f} \right) - \frac{1}{r^2} = 8\pi G T_r^r. \quad (3.10)$$

The solution of these differential equations gives the required form of metric function  $\tilde{f}(\tilde{r})$ ,

$$\tilde{f}(\tilde{r}) = 1 - 8\pi\eta_0^2 - \frac{2\tilde{m}}{\tilde{r}}. \quad (3.11)$$

Incorporating the charge for the black hole in four dimensional AdS space, the function  $f(r)$  of the metric takes the form,

$$\tilde{f}(\tilde{r}) = 1 - 8\pi\eta_0^2 - \frac{2\tilde{m}}{\tilde{r}} + \frac{\tilde{q}^2}{\tilde{r}^2} + \frac{\tilde{r}^2}{l^2}. \quad (3.12)$$

Where  $\tilde{m}$ ,  $\tilde{q}$  and  $l$  are the mass parameter, electric charge parameter and AdS radius of the black hole respectively. Under the following coordinate transformations,

$$\tilde{t} = (1 - 8\pi\eta_0^2)^{-1/2}t \quad , \quad \tilde{r} = (1 - 8\pi\eta_0^2)^{1/2}r, \quad (3.13)$$

and introducing new parameters,

$$m = (1 - 8\pi\eta_0^2)^{-3/2}\tilde{m}, \quad q = (1 - 8\pi\eta_0^2)^{-1}\tilde{q}, \quad \eta^2 = 8\pi\eta_0^2, \quad (3.14)$$

we have the line element

$$ds^2 = -f(r)dt^2 + f(r)^{-1}dr^2 + (1 - \eta^2)r^2d\Omega^2, \quad (3.15)$$

with

$$f(r) = 1 - \frac{2m}{r} + \frac{q^2}{r^2} + \frac{r^2}{l^2}. \quad (3.16)$$

The spacetime described by the above metric exhibits a solid angle deficit, i.e., the area of the sphere is  $4\pi(1 - \eta^2)r^2$  instead of  $4\pi r^2$ . The electric charge ( $Q$ ) and the Arnowitt-Deser-Misner (ADM) mass ( $M$ ) can be expressed as,

$$Q = (1 - \eta^2)q, \quad M = (1 - \eta^2)m. \quad (3.17)$$

At the event horizon  $r = r_+$  the function  $f(r)$  vanishes. This condition can be used to determine the mass parameter. The ADM mass now has the following form,

$$M = \frac{(1 - \eta^2)r_+}{2} + \frac{Q^2}{2(1 - \eta^2)r_+} + \frac{(1 - \eta^2)r_+^3}{2l^2}. \quad (3.18)$$

### 3.3 Thermodynamics in Extended Phase Space

In the extended phase space, the first law of thermodynamics and Smarr relation reads as follows,

$$dM = TdS + \Phi dQ + VdP, \quad M = 2(TS - PV) + \Phi Q. \quad (3.19)$$

The existence of global monopole does not affect the form of the first law of thermodynamics and the Smarr relation. This can be easily verified by using Euler's homogeneous function theorem. However, global monopole will change the thermodynamics through its explicit appearance in the thermodynamical quantities (Deng et al. 2018). The crucial thermodynamic variable, to begin with, is the entropy  $S$  of the black hole,



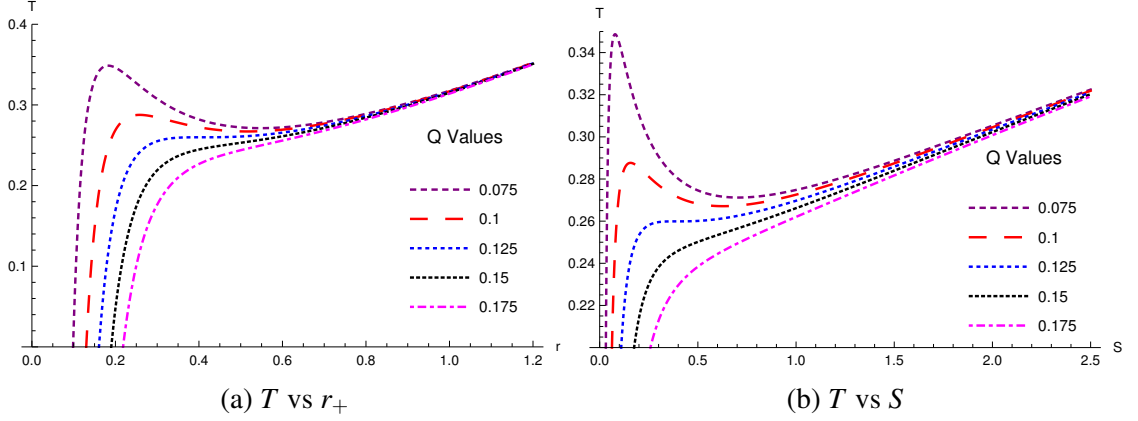


Figure 3.1: Plots of  $T$  versus  $r_+$  and  $T$  versus  $S$  for different values of  $Q$  and for  $\eta = 0.5$ . These plots show the behavior of Hawking temperature.

which is related to the area  $A_{bh}$  of the event horizon,

$$S = \frac{A_{bh}}{4} = \pi (1 - \eta^2) r_+^2. \quad (3.20)$$

The soul of extended phase space lies in the identification of cosmological constant ( $\Lambda$ ) with the thermodynamic variable pressure ( $P$ ), and association of its conjugate quantity with the thermodynamic volume ( $V$ ),

$$P = -\frac{\Lambda}{8\pi} = \frac{3}{8\pi l^2}, \quad V = \frac{4}{3}\pi (1 - \eta^2) r_+^3. \quad (3.21)$$

Using eqn.3.18 in the first law, the Hawking temperature ( $T$ ) for the black hole is an immediate result,

$$T = \left( \frac{\partial M}{\partial S} \right)_{P,Q} = \frac{1}{4\pi r_+} \left( 1 + \frac{3r_+^2}{l^2} - \frac{Q^2}{(1 - \eta^2)^2 r_+^2} \right). \quad (3.22)$$

So far all the thermodynamic variables are modified in the presence of global monopole, which has a message within it about its role in influencing the thermodynamics of the black hole. Since a charged black hole is analogous to van der Waals fluid with similar critical behavior, the tuning of  $\eta$  will enhance or suppress the phase transition (Deng et al. 2018).

As the slope of the  $T - S$  graph is related to specific heat, it's positive and negative

values are related to the stability and instability of the system with respect to fluctuations. The plots 3.1a and 5.1b show that there exists a critical point that indicates the phase transition. Plugging eqn.3.21 into eqn.3.22 eliminates the cosmological constant and the rearrangement of the remaining gives,

$$P = \frac{T}{2r_+} - \frac{1}{8\pi r_+^2} + \frac{Q^2}{8\pi(1-\eta^2)^2 r_+^4}, \quad r_+ = \left( \frac{3V}{4\pi(1-\eta^2)} \right)^{1/3}. \quad (3.23)$$

Therefore, eqn.3.23 can be seen as  $P = P(V, T)$ , which is the equation of state in the extended space. The above form is called geometric equation of state. Since, the variables are not having proper dimensions, we carry out adequate scaling as follows,

$$\tilde{P} = \frac{\hbar c}{l_P^2} P, \quad \tilde{T} = \frac{\hbar c}{k} T, \quad (3.24)$$

where  $l_P$  is the Planck length. The functional dependence of the equation of state on  $r_+$  tempts one to identify it with the van der Waals system at first sight. The comparison is complete by relating specific volume  $v$  to the horizon radius  $r_+$  as  $v = 2l_P^2 r_+$ .

Finally, we arrive at the physical equation of state,

$$P = \frac{T}{v} - \frac{1}{2\pi v^2} + \frac{2Q^2}{\pi a^2 v^4}. \quad (3.25)$$

The characteristic  $P - v$  diagram (Fig.3.2) is obtained from this eqn.3.25 which has a van der Waals like behavior. The existence of three distinct regions with alternate negative, positive and negative slopes is also a beacon of critical behavior. The negative slope regions correspond to a stable state of the system, whereas the positive regions are for unstable states since an increase in volume with pressure is physically meaningless. These unphysical regions can be handled via Maxwell construction, where the oscillating part of the isotherm is replaced by a straight line. Maxwell's equal-area law in extended phase space is,

$$\oint v dP = 0. \quad (3.26)$$

It is well-established in the literature that, in a canonical ensemble where the charge

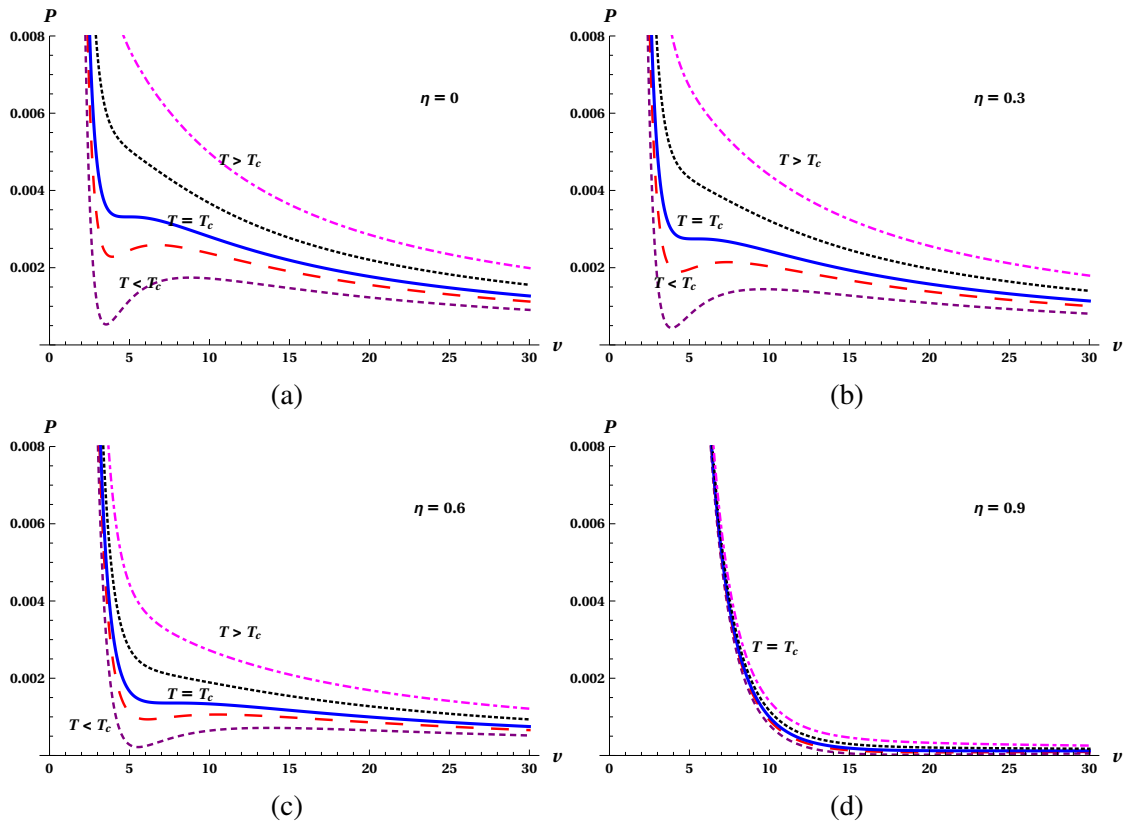


Figure 3.2:  $P - \nu$  isotherms in extended phase space. The critical behaviour is seen below a critical temperature  $T_C$ . This behaviour reduces with increase in  $\eta$ . In all these plots temperature is in decreasing order from top to bottom. (We have set  $Q = 1$  in every plot).

is fixed, the asymptotically AdS black holes show a first-order phase transition analogous to van der Waals system terminating in a second-order critical point (Chamblin et al. 1999a). The effect of monopole parameter is seen in the series of plots (Fig. 3.2), where  $\eta$  consistently suppresses the original behavior of all the isotherms and brings them closer to the critical isotherm. Also, it appears as if  $\eta$  removes the oscillating isotherms at the upper limit of its strength. This may be interpreted as the maximum value of  $\eta$  destroys the van der Waals like nature of the charged black hole. But later, we will see in Gibbs free energy plots that the inherent signature of criticality persists at least in the smaller form (Fig.3.3) even at the maximum strength of  $\eta$ . The critical parameters can be obtained by utilising the vanishing derivatives at the critical point,

$$\left(\frac{\partial P}{\partial v}\right)_T = \left(\frac{\partial^2 P}{\partial v^2}\right)_T = 0. \quad (3.27)$$

Which are,

$$P_c = \frac{(1 - \eta^2)^2}{96\pi Q^2}, \quad v_c = \frac{2\sqrt{6}Q}{(1 - \eta^2)}, \quad T_c = \frac{(1 - \eta^2)}{3\sqrt{6}\pi Q}. \quad (3.28)$$

The presence of  $\eta$  in these parameters once again validates our quest for its effect on the thermodynamics of charged black holes. Compared to the RN-AdS black hole, critical quantities  $P_c$  and  $T_c$  decreases, while  $v_c$  increases with  $\eta$ . As in classical thermodynamics, the critical behavior of a system is more effectively represented by Gibbs free energy  $G$ . This is because the thermodynamic potential  $G$  measures global stability in an equilibrium process. In extended phase space, the total Euclidean action calculated for fixed  $\Lambda$  is associated with Gibbs free energy (Kubiznak and Mann 2012). One can obtain the Gibbs free energy by the Legendre transformation  $G = M - TS$ . In our case, it is calculated as follows,

$$G(P, T) = \frac{1}{4}(1 - \eta^2)r_+ \left(1 - \frac{8\pi P r_+^2}{3}\right) + \frac{3Q^2}{4(1 - \eta^2)r_+}. \quad (3.29)$$

The behavior of Gibbs free energy in terms of  $P$  is illustrated in Fig.3.3. The  $r_+$  in eqn.3.29 is replaced with  $r_+(P, T)$  from equation of state (eqn. 3.23). For  $T > T_c$ ,  $G$  is single-valued and hence locally stable. It has a swallow tail nature below the critical temperature ( $T < T_c$ ), which is a clear indication that there is a first-order phase

transition in the system. This phase transition is between a small black hole (SBH) and a large black hole (LBH). The effect of  $\eta$  in  $G - P$  plot comes into play slowly when we increase its strength from zero to one. The swallowtail region (unstable states) persists for all values of  $\eta$ , but its presence shrinks the tail to a smaller region. It appears as if the swallowtail disappears for larger monopole strength, but a more close observation falsifies this illusion (shown in the inset of figures). The coexistence of large black hole and small black hole phases can be well depicted in a coexistence curve in  $P - T$  plane. Along the coexistence curve, the black hole undergoes a first-order phase transition. This can be achieved either from Maxwell's equal-area law or from the Clausius-Clapeyron equation directly. Another elegant way of obtaining this curve is by exploiting the fact that the temperature and Gibbs free energy coincide for SBH (with radius  $r = r_1$ ) and LBH (with radius  $r = r_2$ ) along the coexistence curve. We assert the following abbreviations for the simplification of calculation,

$$r_1 + r_2 = x, \quad r_1 r_2 = y, \quad a = (1 - \eta^2). \quad (3.30)$$

The conditions which are mentioned earlier for coexistence curve lead us to the set of three equations after some routine algebra. Equating Gibbs free energy on both sides,

$$\frac{1}{r_1} (9Q^2 + 3a^2 r_1^2 - 8\pi a^2 P r_1^4) = \frac{1}{r_2} (9Q^2 + 3a^2 r_2^2 - 8\pi a^2 P r_2^4), \quad (3.31)$$

which reduces to

$$3a^2 y - 8\pi a^2 P y(x^2 - y) - 9Q^2 = 0. \quad (3.32)$$

Since the temperature on both sides are same, from the equation of state we have,

$$T_0 = \frac{1}{4\pi r_1} \left( 1 + \frac{3r_1^2}{l^2} - \frac{Q^2}{a^2 r_1^2} \right), \quad (3.33)$$

$$T_0 = \frac{1}{4\pi r_2} \left( 1 + \frac{3r_2^2}{l^2} - \frac{Q^2}{a^2 r_2^2} \right). \quad (3.34)$$

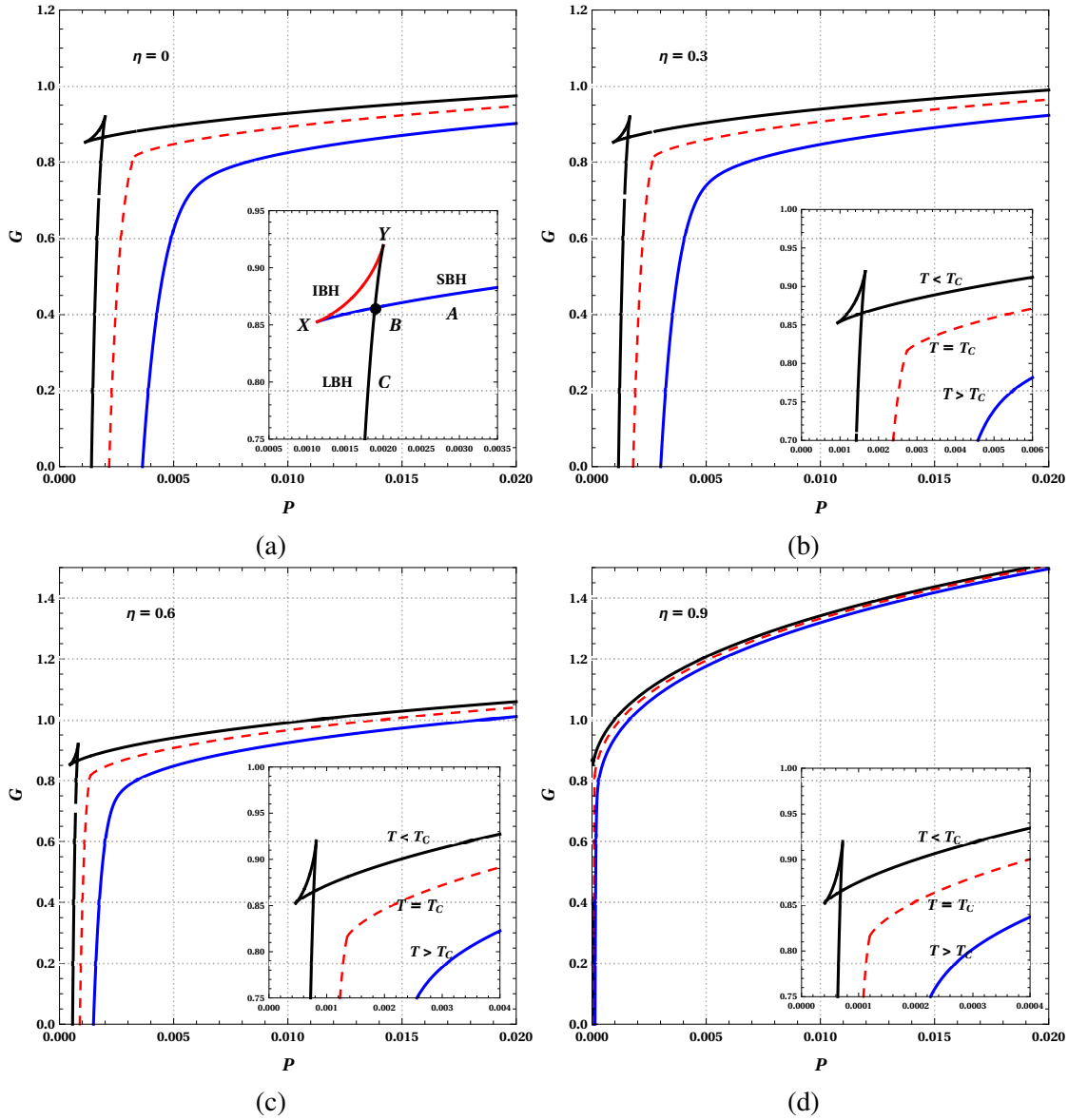


Figure 3.3: The swallow tail behaviour of Gibbs free energy and its variation with  $\eta$  in the extended phase space. The van der Waals like behaviour persists for all values of  $\eta$ . The diminishing behaviour is enlarged in inlets for close examination. We have taken  $Q = 1$ .

Equating the R.H.S of above two equations,

$$\frac{1}{r_1^3} (a^2 r_1^2 + 8\pi P a^2 r_1^4 - Q^2) = \frac{1}{r_2^3} (a^2 r_2^2 + 8\pi P a^2 r_2^4 - Q^2). \quad (3.35)$$

which simplifies to,

$$8\pi P a^2 y^3 + Q^2(x^2 - y) = a^2 y^2. \quad (3.36)$$

Adding the eqn. 3.33 and eqn. 3.34, we get

$$2T_0 = \frac{1}{4\pi a^2} \left[ \frac{a^2 r_1^2 + 8\pi P a^2 r_1^4 - Q^2}{r_1^3} + \frac{a^2 r_2^2 + 8\pi P a^2 r_2^4 - Q^2}{r_2^3} \right], \quad (3.37)$$

and simplifying,

$$8\pi T_0 a^2 y^3 = a^2 y^2 x + 8\pi P a^2 y^3 x - Q^2 x(x^2 - 3y). \quad (3.38)$$

Eqn. 3.32, eqn.3.36 and eqn.3.38 are solved for  $P - T$  plane and the result is displayed in Fig.3.4. The curve is quite similar to the van der Waals system. In the coexistence curve, an increase in  $\eta$  reduces the region for the coexistence. This is another proof for the aforementioned argument that the monopole term hinders critical behavior. This argument is based on two defining features of the coexistence curve. Firstly, crossing the curve in any way stands for a first-order phase transition. Secondly, the termination of the curve is at a second-order transition point. The lowering of termination point is related to the fact that  $P_c$  and  $T_c$  reduces with increasing  $\eta$ . A smaller region of coexistence implies a smaller range of pressure and temperature, which gives phase transition.

## Critical Exponents

Here, we compute the critical exponents  $\alpha, \beta, \gamma, \delta$  for the black hole with monopole term in the extended phase space. These universal exponents describe the behavior of response functions near the critical point. The exponent  $\alpha$  is related to the specific heat,  $\beta$  characterizes the order parameter,  $\gamma$  characterizes the isothermal compressibility, and  $\delta$  is the measure of the flatness of the critical isotherm. Firstly, we investigate the

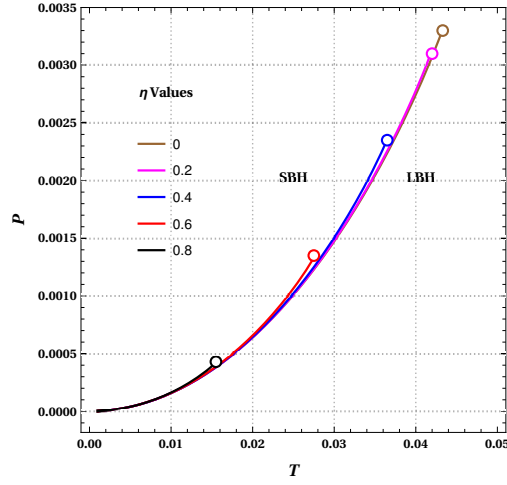


Figure 3.4: Coexistent curve in extended phase space for different values of  $\eta$ . Coexistence line separates the LBH and SBH phases. The critical point where the first order transition terminates is marked as a circle.

behavior of specific heat  $C_V$ , which can be obtained from the free energy,

$$F = G - PV = \frac{1}{2} \left( ar_+ - 2\pi Tar_+^2 + \frac{Q^2}{ar_+} \right). \quad (3.39)$$

From this entropy can be calculated as,

$$S(T, V) = - \left( \frac{\partial F}{\partial T} \right)_V = \pi ar_+^2. \quad (3.40)$$

followed by the inference that  $C_V = 0$ , since there is no dependence on temperature  $T$  in eqn.3.40. Since  $C_V \propto |t|^\alpha$  the exponent  $\alpha = 0$ .

The law of corresponding states is obtained by writing the equation of state in terms of the reduced thermodynamic variables,

$$p = \frac{P}{P_C}, \quad v = \frac{v}{v_C}, \quad \tau = \frac{T}{T_C}, \quad (3.41)$$

the relevant among them are also written in a way how much they differ from critical points as  $v = 1 + \omega$  and  $\tau = 1 + t$ . Using these and the expressions for critical values (eqn. 3.28), the equation of state (eqn. 3.25) reduces to,

$$p = \frac{8}{3} \frac{\tau}{v} - \frac{2}{v^2} + \frac{1}{3v^4}. \quad (3.42)$$



Eqn.3.42 is not altered by the presence of global monopole. Therefore, the remaining calculations on critical exponents are identical to charged AdS black hole (Kubiznak and Mann 2012). Expanding the eqn. 3.42 around the critical point, we get,

$$p = 1 + \frac{8}{3}t - \frac{8}{9}t\omega - \frac{4}{81}\omega^3 + O(t\omega^2, \omega^4). \quad (3.43)$$

Differentiating this with respect to  $\omega$  and using Maxwell's equal area law we obtain,

$$p = 1 + \frac{8}{3}t - \frac{8}{9}t\omega_l - \frac{4}{81}\omega_l^3 = 1 + \frac{8}{3}t - \frac{8}{9}t\omega_s - \frac{4}{81}\omega_s^3, \quad (3.44)$$

and

$$0 = \int_{\omega_l}^{\omega_s} \omega(6t + \omega^2)d\omega. \quad (3.45)$$

The above two equations have unique solution  $\omega_s = -\omega_l = 3\sqrt{-2t}$ . Now we can calculate,

$$\tilde{\eta} = V_C(\omega_l - \omega_s) = 2V_C\omega_l = 6V_C\sqrt{-2t}. \quad (3.46)$$

Since  $\tilde{\eta} \propto |t|^\beta$  we have  $\beta = 1/2$ . Differentiating eqn.3.43 with respect to  $V$  and inverting,

$$\left. \frac{\partial V}{\partial T} \right|_T \propto -\frac{9V_C}{8T_C} \frac{1}{t}. \quad (3.47)$$

And hence,

$$\kappa_T = -\frac{1}{V} \frac{\partial V}{\partial T} \propto \frac{1}{t}. \quad (3.48)$$

From  $\kappa_T \propto |t|^{-\gamma}$  we get  $\gamma = 1$ . The remaining critical exponent  $\delta$  is obtained by setting  $t = 0$  in eqn.3.43, which is the shape of the critical isotherm,

$$p - 1 = -\frac{4}{81}\omega^3. \quad (3.49)$$

Since  $p - 1 \propto |\omega|^\delta$ ,  $\delta = 3$ . All the critical exponents are unaffected by the presence of  $\eta$  and exactly matches with that of van der Waals system as in the case of RN-AdS black hole. The critical exponents must satisfy the universal scaling laws,

$$\alpha + 2\beta + \gamma = 2 \quad , \quad \gamma = \beta(\delta - 1). \quad (3.50)$$

These are satisfied in our case. This means that the SBH-LBH phase transition is analogous to van der Waals liquid-gas system and belongs to the same universality class.

## 3.4 Joule Thomson Expansion

### 3.4.1 Joule-Thomson Effect

Joule-Thomson effect is an irreversible adiabatic expansion of a gas when the gas is pushed through a porous plug. In this process, a non-ideal gas undergoes a continuous throttling process, leading to a temperature change in the final state. When the gas in the higher pressure side having pressure  $P_i$  and temperature  $T_i$  is made to expand through a porous plug, the gas passes through dissipative non-equilibrium states due to the friction between the gas and the plug. Usual thermodynamic coordinates cannot be used to define these non-equilibrium states, but it is found that enthalpy, which is the sum of internal energy and product of pressure-volume, remains the same in the final state (Zemansky et al. 2011). So a state function called *enthalpy*  $H = U + PV$  is defined, which remains unchanged in the end states,

$$H_i = H_f \quad (3.51)$$

It is not entitled to say that enthalpy is a constant during this process since enthalpy is not defined when gas traverses non-equilibrium states. The set of discrete points in the phase diagram initial point  $(P_i, T_i)$  and all other points  $P_f$  and  $T_f$  representing equilibrium states of some gas having the same molar enthalpy ( $h$ ) at initial and all the final equilibrium states. These discrete points corresponding to the same molar enthalpy lie on a smooth curve known as *isenthalpic curve*. To summarise, an isenthalpic curve is the locus of all points with the same molar enthalpy representing initial and final equilibrium states. A set of such curves can be obtained for different values of enthalpy.

The slope of an isenthalpic curve on  $T - P$  plane is called the *Joule Thomson coefficient*  $\mu_J$ .

$$\mu_J = \left( \frac{\partial T}{\partial P} \right)_H \quad (3.52)$$

Joule Thomson coefficient is zero at the maxima of the isenthalpic curve. The locus

of such points is called the inversion curve. The interior of the inversion curve where the gradient of isenthalps ( $\mu_J$ ) positive is called the region of cooling, and the exterior where  $\mu_J$  is negative called the region of heating. The differential of molar enthalpy is given by,

$$dh = T ds + v dP. \quad (3.53)$$

We recall the second  $TdS$  equation in classical thermodynamics (Zemansky et al. 2011),

$$TdS = C_P dT - T \left( \frac{\partial v}{\partial T} \right)_P dP. \quad (3.54)$$

Substituting eqn.3.54) in eqn.3.53, we get

$$dT = \frac{1}{C_P} \left[ T \left( \frac{\partial v}{\partial T} \right)_P - v \right] dP + \frac{1}{C_P} dh. \quad (3.55)$$

Which gives,

$$\mu_J = \left( \frac{\partial T}{\partial P} \right)_H = \frac{1}{C_P} \left[ T \left( \frac{\partial v}{\partial T} \right)_P - v \right]. \quad (3.56)$$

As  $\mu_J = 0$  defines the inversion temperature, we have,

$$T_i = v \left( \frac{\partial T}{\partial v} \right)_P. \quad (3.57)$$

### 3.4.2 van der Waals fluid

van der Waals gas is the simplest model used to explain the behavior of the real gases, which departs from the ideal gas description with richer outcomes as it includes the intermolecular interaction and the non-zero size of the molecules. The equation of state for a van der Waals gas is given by,

$$\left( P + \frac{a}{V_m^2} \right) (V_m - b) = RT. \quad (3.58)$$

Here the constants  $a$  and  $b$  parameterizes the strength of the intermolecular interaction and the volume excluded due to the finite size of the molecule. The equation of state reduces to ideal gas equation under the limit  $a$  and  $b$  both set to zero. We used  $V_m$  for

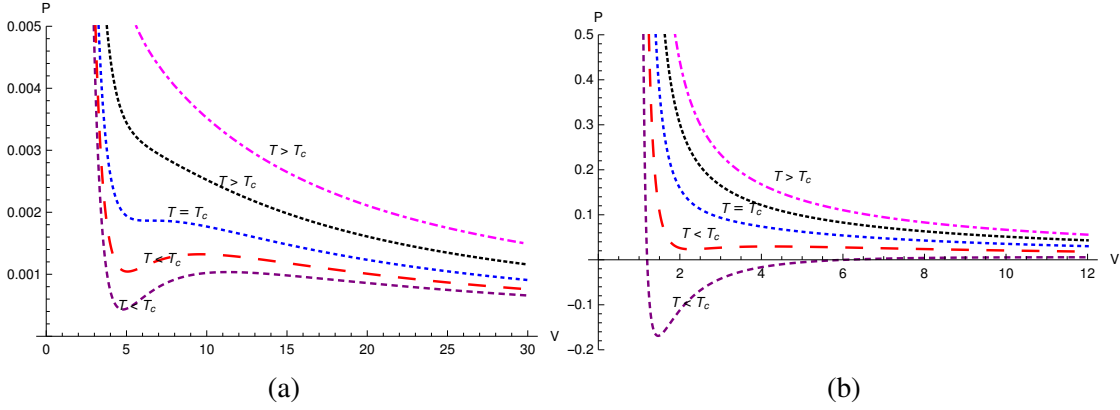


Figure 3.5: Fig. 3.5a Plotted isotherms of the van der Waals gas with temperature decreases from top to bottom. Fig. 3.5b shows  $P - v$  diagram of charged AdS black hole with global monopole where the parameters are chosen to be  $Q = 1$  and  $\eta = 0.5$ . Similar  $P - v$  diagrams can be obtained for different values of  $\eta$ . Variation of  $\eta$  does not changes the nature of the  $P - v$  diagram even though it changes the critical parameters.

molar volume, which is simply  $V$  for one mole of a substance.

To calculate the critical points namely the temperature  $T_c$ , pressure  $P_c$  and volume  $V_c$  we rearrange the equation of state (eqn. 3.58) for  $P$  as follows,

$$P = \frac{RT}{V - b} - \frac{a}{V^2}. \quad (3.59)$$

Using this equation, the  $P - v$  isotherms are plotted for van der Waals gas in Fig. 3.5a. Fig. 3.5b is the  $P - v$  diagram of the charged AdS black hole, which is obtained from eqn. 3.25. The  $P - v$  isotherm is having a typical behavior of a van der Waals fluid. In both these graphs below a certain point called the critical point, there are inflection points, and above that, a monotonic behavior is displayed. This is a general result for AdS black holes (Kubiznak and Mann 2012). At the critical point  $\left(\frac{\partial P}{\partial V}\right)_T = \left(\frac{\partial^2 P}{\partial V^2}\right)_T = 0$ , which gives

$$V_c = 3b, \quad T_c = \frac{8a}{27Rb}, \quad P_c = \frac{a}{27b^2}. \quad (3.60)$$

The internal energy of van der Waals gas is given by (Landau et al. 1980)

$$U(T, v) = \frac{3}{2}k_B T - \frac{a}{v}. \quad (3.61)$$

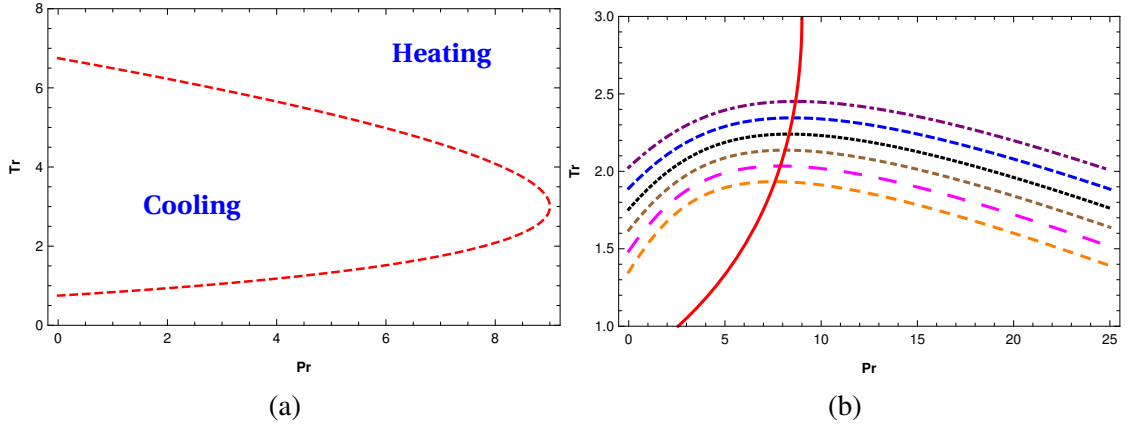


Figure 3.6: In Fig. 3.6a inversion curve separating the regions of heating and cooling are shown. In fig 3.6b isenthalpic curves for different values of enthalpy is plotted along with the lower half of inversion curve for the van der Waals gas. While plotting this, we worked with dimensionless coordinates i.e., reduced pressure  $P_r = P/P_c$  and reduced temperature  $T_r = T/T_c$ .

Making a Legendre transformation  $H = U + PV$ , we obtain the expression for enthalpy,

$$H(T, v) = \frac{3}{2}k_B T + \frac{k_B T v}{v - b} - \frac{2a}{v}. \quad (3.62)$$

The inversion temperature is calculated from eqn. 3.57 as,

$$T_i = \frac{1}{k_B} \left( P_i v - \frac{a}{v} + \frac{2ab}{v^2} \right) \quad (3.63)$$

and from equation of state (eqn. 3.58), we have

$$T_i = \frac{1}{k_B} \left( P_i v - P_i b + \frac{a}{v} - \frac{ab}{v^2} \right). \quad (3.64)$$

Eqn. 3.63 and eqn. 3.64 gives

$$P b v^2 - 2a v + 3a b = 0. \quad (3.65)$$

Solving the above equation for  $v$  and substituting in equation of state (eqn. 3.58), we obtain

$$T_i = \frac{2 \left( 5a - 3b^2 P_i \pm 4 \sqrt{a^2 - 3ab^2 P_i} \right)}{9b k_B}. \quad (3.66)$$

Using this, we plot the inversion curves (Fig. 3.6a). In Fig. 3.6b isenthalpic and inversion curves are shown together. For the sake of comparison later with the isenthalpic-inversion curve of the black hole we have taken only the lower half of  $T_i$ .

### 3.5 Joule Thomson Expansion of Charged AdS Black Hole with Monopole Term

In this section, we study the JT expansion of charged AdS black holes with monopole term. Because of the treatment of black hole mass equivalent to enthalpy in extended phase space, the isenthalpic plots are replaced by constant mass plots in this case. Recall the expression for Joule Thomson coefficient

$$\mu_J = \left( \frac{\partial T}{\partial P} \right)_M = \frac{1}{C_P} \left[ T \left( \frac{\partial V}{\partial T} \right)_P - V \right]. \quad (3.67)$$

From this, we obtain the inversion temperature

$$T_i = V \left( \frac{\partial T}{\partial V} \right)_P. \quad (3.68)$$

For this, we rewrite the equation of state in terms of  $V$  as follows

$$T = \left( \frac{(1-\eta^2)}{48\pi^2} \right)^{1/3} \frac{1}{V^{1/3}} + P \left( \frac{6}{\pi(1-\eta^2)} \right)^{1/3} V^{1/3} - \frac{Q^2}{3(1-\eta^2)} \frac{1}{V}. \quad (3.69)$$

Substituting this into eqn.3.68, we have the inversion temperature

$$\begin{aligned} T_i &= -\frac{1}{6} \left( \frac{(1-\eta^2)}{6\pi^2} \right)^{1/3} \frac{1}{V^{1/3}} + P \left( \frac{2}{9\pi(1-\eta^2)} \right)^{1/3} V^{1/3} + \frac{Q^2}{3(1-\eta^2)} \frac{1}{V} \\ &= \frac{Q^2}{4\pi r_+^3 (1-\eta^2)^2} + \frac{2}{3} P r_+ - \frac{1}{12\pi r_+}. \end{aligned} \quad (3.70)$$

From eqn.3.23, we have

$$T_i = -\frac{Q^2}{4\pi r_+^3 (1-\eta^2)^2} + 2P r_+ + \frac{1}{4\pi r_+}. \quad (3.71)$$

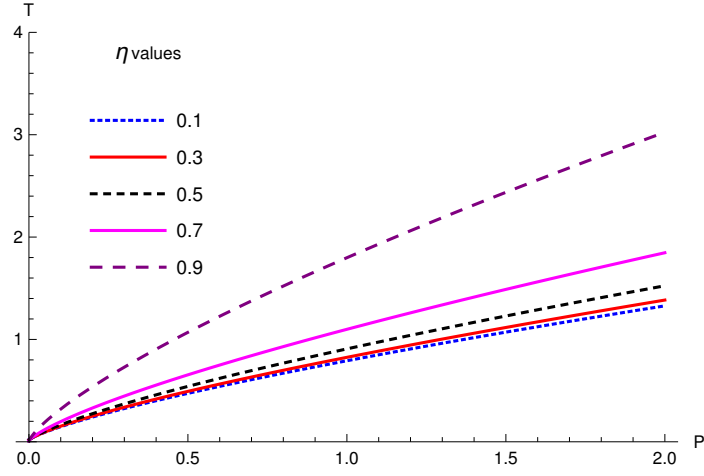


Figure 3.7: Effect of monopole term  $\eta$  on inversion curve. Here we have chosen different values of monopole ( $\eta = 0$  to  $0.9$  in steps) by keeping charge  $Q$  fixed.

From eqn.3.70 and eqn.3.71 we get,

$$8\pi(1-\eta^2)^2Pr_+^4 + 2(1-\eta^2)^2r_+^2 - 3Q^2 = 0. \quad (3.72)$$

Solving the above equation for  $r_+$  and choosing the following appropriate root:

$$r_+ = \frac{1}{2\sqrt{2\pi}} \sqrt{\frac{\sqrt{((1-\eta^2)^2 + 24\pi PQ^2)}}{(1-\eta^2)P} - \frac{1}{P}}. \quad (3.73)$$

Substituting this root into eqn.3.71, we obtain the expression for inversion temperature ( $T_i$ ) in terms of inversion pressure, charge and monopole parameter,

$$T_i = \frac{\sqrt{P_i} \left( 1 + \frac{16\pi P_i Q^2}{(1-\eta^2)^2} - \frac{\sqrt{24P_i\pi Q^2 + (1-\eta^2)^2}}{(1-\eta^2)} \right)}{\sqrt{2\pi} \left( -1 + \frac{\sqrt{24P_i\pi Q^2 + (1-\eta^2)^2}}{(1-\eta^2)} \right)^{3/2}}. \quad (3.74)$$

From this equation, the inversion curves are plotted for different values of  $\eta$  (Fig. 3.8). From the graphs, one can infer that the JT coefficient  $\mu_J$  is sensitive to  $\eta$  values, i.e.,  $\mu_J$  increases with  $\eta$ . In Fig. 3.7, this inference is depicted taking different  $\eta$  values in the

same plot for a fixed  $Q$  value. By demanding  $P_i = 0$ , we obtain  $T_i^{min}$

$$T_i^{min} = \frac{(1 - \eta^2)}{6\sqrt{6\pi}Q}. \quad (3.75)$$

Using this we calculate the ratio between  $T_i^{min}$  and  $T_c$  as

$$\frac{T_i^{min}}{T_c} = \frac{1}{2}. \quad (3.76)$$

This is an interesting result which matches with the earlier established results for the charged AdS black hole (Ökcü and Aydiner 2017, 2018). At the end of this study, we plot isenthalpic curves for various combinations of  $\eta$  and  $Q$  in the  $T - P$  plane. Inverse points  $(T_i, P_i)$  on  $T - P$  plane separates the heating phase from the cooling phase of JT expansion. Recall that the isenthalpic curve in this case is not a plot with constant enthalpy, rather constant mass. The crossing diagram between inversion and isenthalpic curve shown in Fig. 3.9 displays the sensitivity of inverse points  $(T_i, P_i)$  for the different values of  $\eta$  and  $Q$ . All our calculations and graphs show that when the global monopole parameter is zero, the results nicely reduce to the earlier studies on JT expansion of charged AdS black holes.



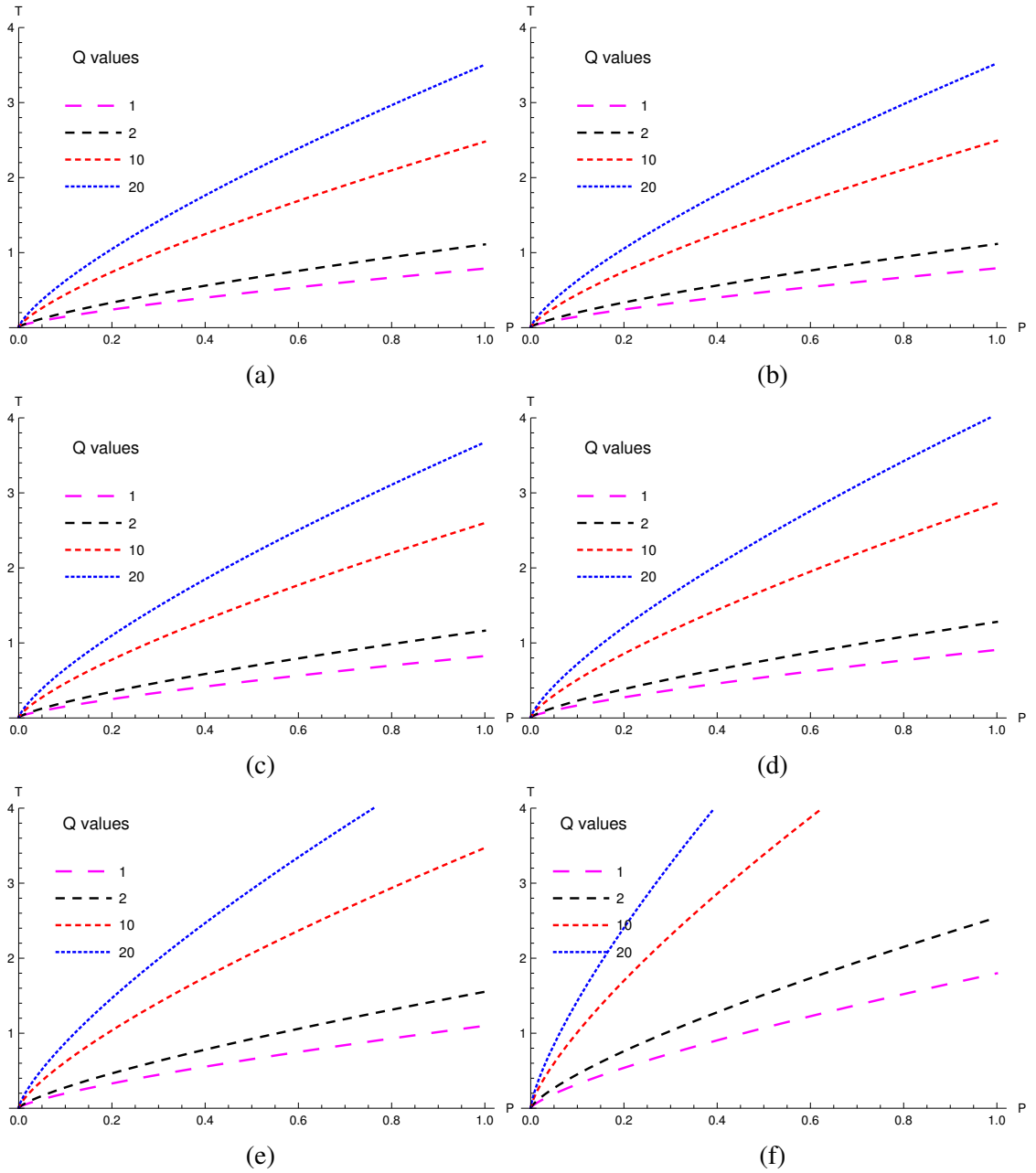


Figure 3.8: Inversion curves for charged AdS black hole with global monopole parameter  $\eta = 0, 0.1, 0.3, 0.5, 0.7, 0.9$  from top to bottom. The plots are the locus of inversion points  $(P_i, T_i)$ . Increasing  $\eta$  increases the inversion temperature for fixed pressure.

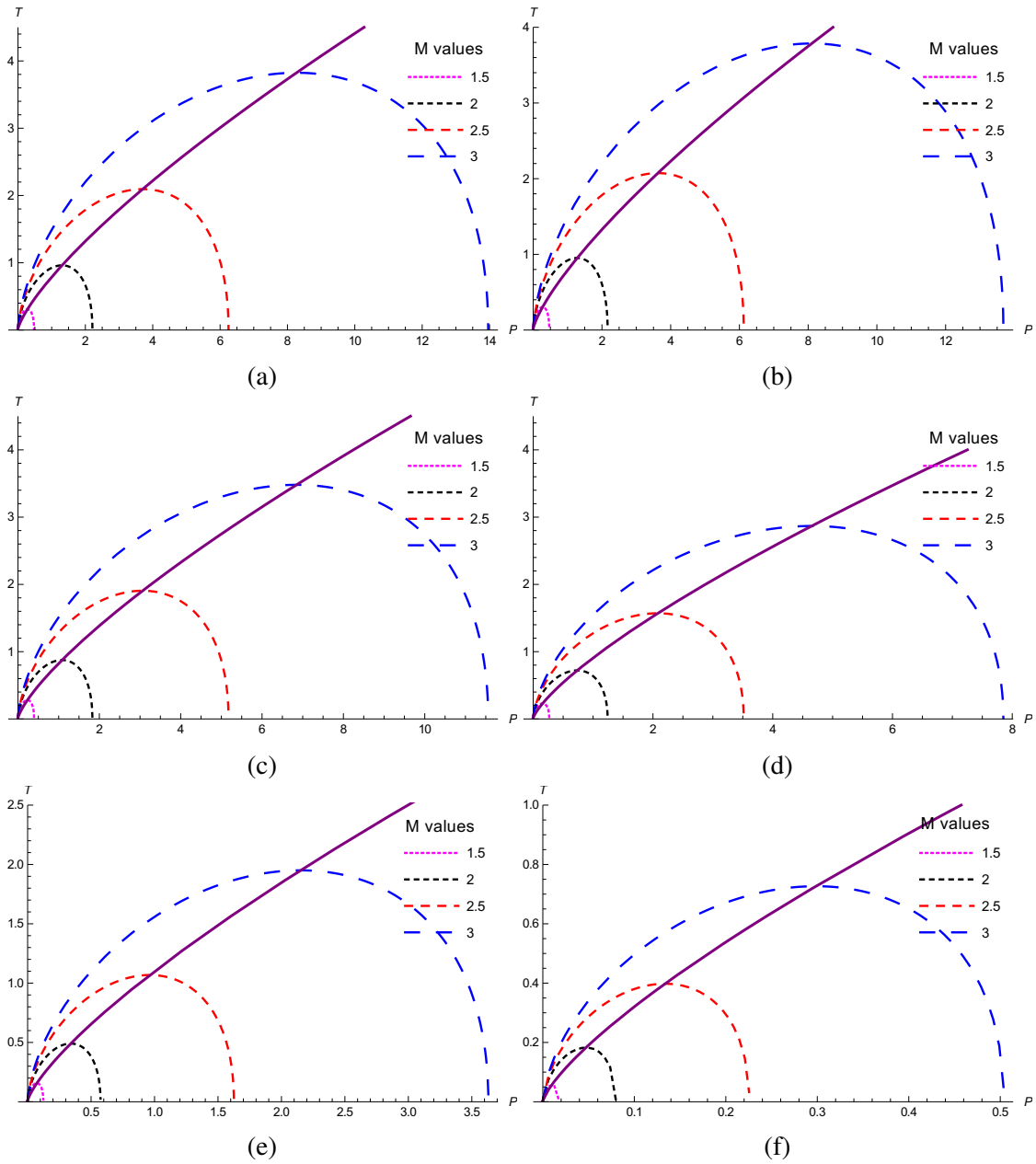


Figure 3.9: Crossing diagrams between inversion and isenthalpic curves for different values of  $\eta$ . ( $\eta = 0, 0.1, 0.3, 0.5, 0.7, 0.9$  from top to bottom and  $Q = 1$ ).

## 3.6 Conclusions

In this chapter, we have explored the thermodynamic properties of the black hole and analyzed the effect of  $\eta$  on these properties. Then the Joule-Thomson (JT) coefficient  $\mu$ , which determines the cooling and heating phase is obtained for van der Waals gas. This is followed by the calculation of inversion and isenthalpic curves for the gas.

Further, we applied the idea of JT expansion to charged AdS black hole with global monopole whereby our key ingredient was the symmetry breaking parameter  $\eta$ . The traditional JT coefficient analysis, isenthalpic, and inversion curve studies were done for this metric with different values of  $\eta$ . The result is an interesting one where we have noticed that the dependence of thermodynamic behavior on  $\eta$  is crucial. The inversion temperature and pressure both increase monotonically with  $\eta$ , which is evident from the inversion and isenthalpic curves. From the inversion curves, we conclude that the sensitivity of  $T_i$  for a given value of  $P_i$  with increasing  $\eta$  is stringent.

It is a well-known fact that in early universe the global monopole played an interesting role in density fluctuations which led to the formation of galaxies and clusters in several theoretical approaches. Hence we hope that the study of JT expansion with monopole term will be significant from different perspectives.



# Chapter 4

## Thermodynamics of Regular black holes in AdS

### Spacetime

Summary

---

*This chapter is an edited version of our article ([Ahmed Rizwan et al. 2020b](#)). We study the phase structure and the microscopic interactions in regular Bardeen AdS black holes. The stable and metastable phases in the black hole are analyzed through coexistence and spinodal curves. In the second part of the chapter, we probe the microscopic interactions of regular Bardeen AdS black holes using the novel Ruppeiner geometry.*

---

#### 4.1 Introduction

Regular black holes are the ones that do not possess a singularity at the center. Even though it is in the domain of quantum gravity theory to obtain a singularity-free solution, a phenomenological model can be constructed in classical gravity. Firstly such a regular solution was derived by Bardeen ([Bardeen et al. 1973b](#)). Later many have found that regular black holes can be an exact solution to gravity coupled with a non-linear electromagnetic source ([Ayon-Beato and Garcia 1998, 2000](#), [Hayward 2006](#)). We have studied phase transitions of regular black holes in our recent papers ([Ahmed Rizwan et al. 2019b](#), [Rajani et al. 2020](#), [Naveena Kumara et al. 2020a](#)). It is noticed that the presence of magnetic monopole charge imparts a phase structure to the regular black

holes similar to the electric charge. So we find it interesting to probe the microstructure corresponding to the magnetically charged Bardeen black holes in asymptotically AdS spacetimes.

The macroscopic picture of the black hole is used to propose a phenomenological model for black hole microstructure (Ruppeiner 2008). Even though microscopic information is not a requirement for thermodynamics, it may be used for quantum gravity studies. A prominent model for drawing microscopic information from thermodynamics is the Ruppeiner's thermodynamic geometry (Ruppeiner 1995). It is constructed on the equilibrium state space in the context of thermodynamic fluctuation theory but can be useful in studying black holes too (Ruppeiner 2008). Through Gaussian fluctuation moments, a Riemannian geometry is constructed in the thermodynamic equilibrium space, whose metric tells us about the fluctuations between the states. This method is applied to van der Waals fluids and to a variety of other statistical systems (Ruppeiner 1995, Janyszek and Mrugaa 1990, Oshima et al. 1999, Mirza and Mohammadzadeh 2008, May et al. 2013). These studies show that the thermodynamic geometry encodes the information about the microscopic interaction. The thermodynamic scalar curvature  $R$  is proportional to the correlation volume of the underlying system. The sign of  $R$  indicates the type of interaction in the microstructure, positive for repulsive and negative for attractive interactions. In recent times, there has been a lot of interest in the thermodynamic geometry to investigate critical phenomena and microstructure of various black holes in AdS spacetime (Wei and Liu 2015, Sahay 2017, Guo et al. 2019, Miao and Xu 2018, Kord Zangeneh et al. 2018, Wei and Liu 2020b, Naveena Kumara et al. 2019, 2020b, Xu et al. 2020, Chabab et al. 2018, Deng and Huang 2017, Miao and Xu 2019b, Chen et al. 2019, Du et al. 2020, Dehyadegari et al. 2017, Ghosh and Bhamidipati 2020b,a).

Recently, a novel approach for Ruppeiner geometry was developed to explore the missing information due to the singularity in the scalar curvature (Wei et al. 2019a). This is mainly due to the vanishing of heat capacity at constant volume. The new normalized scalar curvature takes care of this problem. A metric can be defined by Taylor expanding the Boltzmann entropy around the equilibrium value. The thermodynam-

cal coordinates were chosen to be the temperature and volume, and the Helmholtz free energy was chosen as the thermodynamic potential. Applying this method to the van der Waals (vdW) fluid, it was found that dominant interaction in the microstructure is attractive throughout the parameter space. Utilizing the analogy with vdW fluid, the thermodynamic geometry of a charged AdS black hole is analyzed. In contrast to the vdW fluid, the interaction is not attractive over the entire parameter space. Even though the interaction is attractive for the large black hole (LBH) everywhere and the small black hole (SBH) for most of the parameter space, there exists a weak repulsive interaction in the SBH phase at very low temperatures (Wei et al. 2019a,b). Interestingly, this behavior is not universal for all asymptotically AdS black holes. In the case of a five-dimensional neutral Gauss-Bonnet black hole, interaction similar to vdW fluid is observed, with a dominant attractive interaction throughout the SBH and LBH phases (Wei and Liu 2020b). Soon later, work is extended to  $4 - D$  Gauss-Bonnet black holes Wei and Liu (2020a). Subsequently, the microscopic interactions for  $4 - D$  AdS topological black holes dRGT massive gravity were studied (Yerra and Bhamidipati 2020b, Wu et al. 2020). The microstructure was found to be distinct, with the presence of both repulsive and attractive interactions in both the SBH and LBH phases. In our recent paper, we have investigated the microstructure of regular Hayward and Born-Infeld AdS black holes (Naveena Kumara et al. 2020c, 2021). The microscopic interactions observed are similar to the case of charged AdS black holes in the regular Hayward case. In contrast, Born-Infeld AdS black holes show a reentrant phase transition, which has a distinct microstructure. Apart from these studies, the study of microstructure using this novel method is limited to a few black holes. Motivated by the recent progress, here we explore the phase structure and microstructure of a regular Bardeen AdS black hole.

The chapter is organized as follows. In section (Sec.4.2), we review the action and derivation of the regular Bardeen black hole in AdS spacetime. In section (Sec.4.3), we mainly focus on the thermodynamics and phase structure of the black hole. Then the Ruppeiner geometry and analysis of critical features are discussed in section (Sec.4.4.1). The final section (Sec.4.5) is dedicated to the summary and conclusions.

## 4.2 Regular Bardeen AdS Black hole

The Bardeen black hole emerges as the solution to the Einstein's gravity coupled to a non-linear electrodynamics source with a negative cosmological constant  $\Lambda$ . We will consider an action,

$$\mathcal{S} = \frac{1}{16\pi} \int d^4x \sqrt{-\tilde{g}} (R - 2\Lambda - \mathcal{L}(\mathcal{F})), \quad (4.1)$$

where  $R$  denotes the Ricci scalar,  $\tilde{g}$  the determinant of metric tensor  $\tilde{g}_{\mu\nu}$ , and  $\Lambda$  is the cosmological constant.  $\mathcal{L}(\mathcal{F})$  is the Lagrangian density of non-linear electrodynamics, which is the function of the field strength  $\mathcal{F} = F_{\mu\nu}F^{\mu\nu}$  with  $F_{\mu\nu} = \partial_\mu A_\nu - \partial_\nu A_\mu$ . Variation of the action (eqn.4.1) leads to Einstein's and Maxwell's equations of motion, given by

$$G_{\mu\nu} + \Lambda g_{\mu\nu} = T_{\mu\nu}, \quad \nabla_\mu \left( \frac{\partial \mathcal{L}(\mathcal{F})}{\partial \mathcal{F}} F^{\mu\nu} \right) = 0 \quad \text{and} \quad \nabla_\mu (*F^{\nu\mu}) = 0. \quad (4.2)$$

$G_{\mu\nu}$  is the Einstein tensor and  $T_{\mu\nu} = 2 \left( \frac{\partial \mathcal{L}(\mathcal{F})}{\partial \mathcal{F}} F_{\mu\lambda} F_\nu^\lambda - \frac{1}{4} g_{\mu\nu} \mathcal{L}(\mathcal{F}) \right)$  is the energy-momentum tensor. The Lagrangian density in the case of Bardeen black holes is,

$$\mathcal{L}(\mathcal{F}) = \frac{12}{\alpha} \left( \frac{\sqrt{\alpha \mathcal{F}}}{1 + \sqrt{\alpha \mathcal{F}}} \right)^{5/2}, \quad (4.3)$$

where  $\alpha$  is a positive quantity with a dimension  $[\text{Length}]^2$ . We take the following ansatz for Maxwell's field tensor,

$$F_{\mu\nu} = 2\delta_{[\mu}^\theta \delta_{\nu]}^\phi Q(r) \sin \theta. \quad (4.4)$$

But from Maxwell's equations (eqn.4.2),  $dF = \frac{dQ(r)}{dr} dr \wedge d\theta \wedge d\phi = 0$  which require  $Q(r)$  to be a constant  $Q_m$ . For a spherically symmetric solution, the non-vanishing components of Maxwell's field tensor are  $F_{tr}$  and  $F_{\theta\phi}$ . Since we are interested in a magnetically charged regular solution, we choose gauge potential and Maxwell's field



tensor to be,

$$A_\mu = Q_m \cos \theta \delta_\mu^\phi, \quad F_{\theta\phi} = -F_{\phi\theta} = Q_m \sin \theta, \quad (4.5)$$

where  $Q_m$  is the magnetic monopole charge. The scalar function  $F$  is obtained from  $F_{\theta\phi}$  as,

$$F = \frac{2Q_m^2}{r^4}. \quad (4.6)$$

We can rewrite Lagrangian density  $\mathcal{L}(\mathcal{F})$  as a function of radial distance,

$$\mathcal{L}(r) = \frac{12}{\alpha} \left( \frac{2\alpha Q_m^2}{r^2 + 2\alpha Q_m^2} \right)^{5/2}. \quad (4.7)$$

A static spherically symmetric solution for the Einstein's equation can be put in the form,

$$ds^2 = -f(r)dt^2 + \frac{dr^2}{f(r)} + r^2 (d\theta^2 + \sin^2 \theta d\phi^2), \quad (4.8)$$

with the metric function  $f(r) = 1 - \frac{2m(r)}{r} - \frac{\Lambda r^2}{3}$ . Making use of the line element, the Einstein's equation is solved for fixing the functional form of  $m(r)$ .  $G_{tt}$  and  $G_{rr}$  components of Einstein's equation read as,

$$\frac{1}{r^2} \partial_r m(r) - \Lambda = \frac{1}{4} \mathcal{L}(r), \quad (4.9)$$

$$\frac{1}{r} \partial_r^2 m(r) - \Lambda = \left( \frac{1}{4} \mathcal{L}(r) - \frac{\partial \mathcal{L}}{\partial \mathcal{F}} F_{\theta\phi} F^{\theta\phi} \right). \quad (4.10)$$

Integrating the above differential equations, we obtain the mass function  $m(r)$  for a regular Bardeen AdS black hole as,

$$m(r) = \frac{\Lambda r^3}{6} + \frac{Mr^3}{(\beta^2 + r^2)^{3/2}}, \quad (4.11)$$

where  $M$  is the mass of the black hole and  $\beta$  is the charge parameter related to total charge  $Q_m$ ,

$$Q_m = \frac{\beta^2}{\sqrt{2\alpha}}. \quad (4.12)$$

So, the line element for Bardeen-AdS black hole is written with the metric function,

$$f(r) = 1 - \frac{2Mr^2}{(\beta^2 + r^2)^{3/2}} - \frac{\Lambda r^2}{3}. \quad (4.13)$$

### 4.3 Thermodynamics and phase structure

In this section, we review the thermodynamics of the black hole in an extended phase space, where the cosmological constant  $\Lambda$  is given the status of a dynamical variable pressure  $P$ . It can be justified from Smarr relation and the first law of black hole thermodynamics in the asymptotically AdS spacetimes. The thermodynamic pressure  $P$  is related to  $\Lambda$  as,

$$P = -\frac{\Lambda}{8\pi}. \quad (4.14)$$

Firstly, we write the first law of black hole thermodynamics and Smarr relation for the magnetically charged Bardeen AdS black hole (Fan and Wang 2016, Fan 2017),

$$dM = TdS + \Psi d\beta + VdP + \Pi d\alpha, \quad (4.15)$$

$$M = 2(TS - VP + \Pi\alpha) + \Psi\beta. \quad (4.16)$$

This can be obtained either from Komar integral, or from scaling argument presented in the paper by Kastor *et al* (Kastor *et al.* 2009). Notice that there exists additional terms  $\alpha$  and  $\Pi$ , they are the parameters related to the non-linear electromagnetic field and its conjugate potential respectively. We can write black hole mass  $M$  using the condition  $f(r_h) = 0$  at the event horizon  $r = r_h$ ,

$$M = \frac{(\beta^2 + r_h^2)^{3/2} (8\pi P r_h^2 + 3)}{6r_h^2}. \quad (4.17)$$

The Hawking temperature of the black hole is obtained as,

$$T = \left. \frac{f'(r)}{4\pi} \right|_{r=r_h} = -\frac{\beta^2}{2\pi r(\beta^2 + r_h^2)} + \frac{r_h}{4\pi(\beta^2 + r_h^2)} + \frac{2Pr_h^3}{\beta^2 + r_h^2}, \quad (4.18)$$

where we have used eqn.4.17 and eqn.4.14 for mass  $M$  and pressure  $P$ . The required thermodynamic quantities for our analysis, volume  $V$  and entropy  $S$  can be obtained from the first law,

$$V = \left( \frac{\partial M}{\partial P} \right)_{S, \beta} = \frac{4}{3} \pi (\beta^2 + r_h^2)^{3/2}, \quad (4.19)$$

$$S = \int \frac{dM}{T} = \pi r_h^2 \left[ \left( 1 - \frac{2\beta^2}{r_h^2} \right) \sqrt{1 + \frac{\beta^2}{r_h^2}} + \frac{3\beta^2}{r_h^2} \log \left( \sqrt{\beta^2 + r_h^2} + r_h \right) \right]. \quad (4.20)$$

The thermodynamic stability of black hole is specified by the heat capacity at constant pressure  $C_P$  and at constant volume  $C_V$ , which is determined as,

$$C_P = T \left( \frac{\partial S}{\partial T} \right)_P = \frac{2S(\pi\beta^2 + S)(-2\pi\beta^2 + 8PS^2 + S)}{2\pi^2\beta^4 + \pi\beta^2S(24PS + 7) + S^2(8PS - 1)}, \quad (4.21)$$

$$C_V = T \left( \frac{\partial S}{\partial T} \right)_V = 0. \quad (4.22)$$

One can obtain the equation of state,  $P = P(V, T)$ , utilising the expression for the Hawking temperature (eqn. 4.18) and thermodynamic volume (eqn. 4.20),

$$P = \frac{\left( \frac{6V}{\pi} \right)^{2/3} \left( -1 + 2\pi T \sqrt{\left( \frac{6V}{\pi} \right)^{2/3} - 4\beta^2} \right) + 12\beta^2}{2\pi \left( \left( \frac{6V}{\pi} \right)^{2/3} - 4\beta^2 \right)^2}. \quad (4.23)$$

We study the phase structure of the black hole in the canonical ensemble with a fixed monopole charge  $\beta$ . The  $P - V$  isotherms show a first-order van der Waals fluid like phase transition between two phases, namely, the *small black hole* (SBH) and the *large black hole* (LBH) phase. The critical point is obtained from the inflection point of the  $P - V$  isotherm,

$$\left. \frac{\partial P}{\partial V} \right|_{r=r_h} = \left. \frac{\partial^2 P}{\partial V^2} \right|_{r=r_h} = 0. \quad (4.24)$$

The critical quantities temperature ( $T_c$ ), pressure ( $P_c$ ) and volume ( $V_c$ ), thus obtained are given below,

$$T_c = \frac{(17 - \sqrt{273}) \sqrt{\frac{1}{2}(\sqrt{273} + 15)}}{24\pi\beta}, \quad (4.25)$$

$$P_c = \frac{\sqrt{273} + 27}{12(\sqrt{273} + 15)^2 \pi\beta^2}, \quad (4.26)$$

$$V_c = \frac{4}{3} \pi\beta^3 \left(1 + \frac{1}{2}(\sqrt{273} + 15)\right)^{3/2}. \quad (4.27)$$

Using critical quantities, we define the following reduced coordinates,

$$T_r = \frac{T}{T_c}, \quad P_r = \frac{P}{P_c}, \quad V_r = \frac{V}{V_c}. \quad (4.28)$$

We can rewrite the equation of state in the reduced parameter space as,

$$P_r = \frac{(\sqrt{273} + 15)^2 V_r^{2/3} \left(3(\sqrt{273} + 17) - 4T_r \sqrt{\sqrt{273} + 15} \sqrt{-2 + (\sqrt{273} + 17) V_r^{2/3} - \frac{18}{V_r^{2/3}}}\right)}{(\sqrt{273} + 27) \left(2 - (\sqrt{273} + 17) V_r^{2/3}\right)^2}. \quad (4.29)$$

The phase transition in a Bardeen AdS black hole was extensively studied by AG Tzikas (Tzikas 2019). But there are a couple of things left out in the analysis due to the difficulty in inverting the equation of state and solving  $r_h$  as a function of pressure and temperature,  $r_h = r_h(P, T)$ . We address this problem numerically and obtain the coexistence equation from the swallowtail behavior of Gibbs free energy.

We begin our analysis from the Gibbs free energy, which is defined as the Legendre transform of enthalpy, recall that addition of  $VdP$  term leads to the identification of mass as enthalpy  $H$ . The Gibbs free energy reads as,

$$G(P, r_h, g) = H - TS. \quad (4.30)$$

And change in the Gibbs free energy,

$$dG = -SdT + VdP + \Phi dg. \quad (4.31)$$

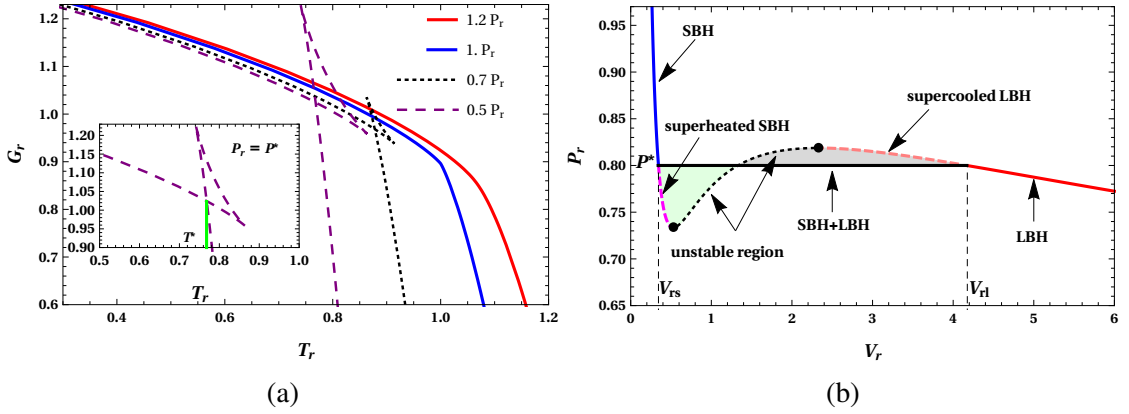


Figure 4.1: In Fig. 4.1a, the Gibbs free energy  $G_r$  is plotted as a function of reduced temperature  $T_r$  for different reduced pressure  $P_r$ . The swallow tail behaviour is exhibited when  $P_r < 1$ . In insets, a magnified view of the swallow tail at a pressure  $P_r = P^* < 1$  is shown. In Fig. 4.1b, Isotherm with reduced temperature  $T_r = T^* < 1$  under Maxwell's construction is shown. The SBH, superheated SBH, unstable region, supercooled LBH and stable LBH phases are labelled in the Fig. 4.1b.

The Gibbs energy and its change is important in determining the thermodynamic stability of a system. In an equilibrium state, when the pressure, temperature, and charge are fixed,  $G$  takes a minimal value. But often writing  $G$  explicitly as the function of temperature and pressure,  $G(P, T)$  is difficult. We can obtain the Gibbs free energy plots parametrically using eqn.4.30 and eqn.4.18. In Fig. 4.1a, we plot reduced Gibbs free energy ( $G_r$ ) as the function of reduced temperature ( $T_r$ ) for different pressures. When reduced pressure  $P_r < 1$ , we can see a “swallow tail behavior” which is a typical signature of a first-order phase transition. A close observation will reveal that there are three regions in the swallowtail, two branches corresponding to the stable SBH and LBH phases, and a tail connecting these two. As the difference in Gibbs free energy between two branches becomes zero, the transition takes place between SBH and LBH phases. At the critical pressure or below, these two branches become distinct. But they do intersect at a certain temperature  $T^*$ , where two phases coexist. We use these data to plot the coexistence curve and fit it into a coexistence equation numerically. Using the

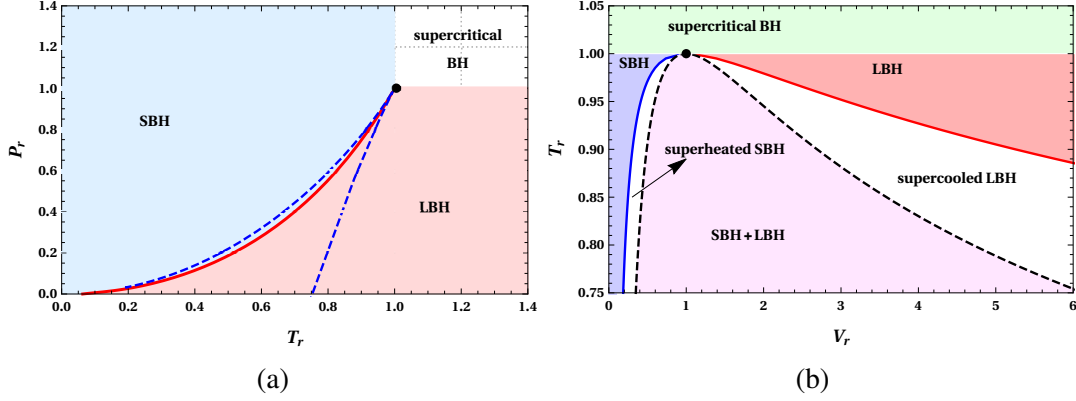


Figure 4.2: Coexistence and spinodal curves in  $P_r - T_r$  and  $T_r - V_r$  plane. The coexistence curve is shown in solid line and the spinodal curves are shown in dashed line.

fitting method, we obtain an expression for the coexistence equation,

$$P_r = -0.022 + 0.625T_r - 6.726T_r^2 + 48.312T_r^3 - 194.636T_r^4 + 511.332T_r^5 - 887.151T_r^6 + 1009T_r^7 - 722.605T_r^8 + 295.313T_r^9 - 52.4384T_r^{10}, \quad (4.32)$$

$$T_r \in (0, 1).$$

In Fig.4.2a, we have obtained  $P_r - T_r$  coexistence diagram using the fitting formula. The red line is the locus of coexistence phase pressure and temperature ( $P^*, T^*$ ). The light magenta-shaded region below the curve is the LBH phase, and the light green color region depicts the SBH phase. The black point at the coordinate (1, 1) denotes the critical point, and above that (unshaded region), differentiation of phases is impossible known as supercritical region. In Fig.4.2a, along the coexistence curve, we have also shown the spinodal curve marked by the blue dashed line. It is plotted using the condition,

$$(\partial_{V_r} T_r)_{P_r} = 0, \quad \text{or} \quad (\partial_{V_r} P_r)_{T_r} = 0. \quad (4.33)$$

The spinodal curve equation obtained from the above condition is of the form,

$$T_{rsp} = \frac{3(17 + \sqrt{273}) \left(-10 + (17 + \sqrt{273}) V_r^{2/3}\right) \sqrt{-2 + (17 + \sqrt{273}) V_r^{2/3}}}{4\sqrt{15 + \sqrt{273}} \left(-4 + (17 + \sqrt{273}) V_r^{2/3} + (17\sqrt{273} + 281) V_r^{4/3}\right)}, \quad (4.34)$$

$$P_{rsp} = \frac{3(15 + \sqrt{273})^2 \left(-12V_r^{2/3} + 9(17 + \sqrt{273}) V_r^{4/3} - (281 + 17\sqrt{273}) V_r^2\right)}{2(27 + \sqrt{273}) V_r^{2/3} \left(3(17 + \sqrt{273}) V_r^{2/3} - ((285\sqrt{273} + 4709) V_r^2 + 4)\right)}. \quad (4.35)$$

Using parametric plots, we have obtained spinodal curves, which are the locus of extreme points separating metastable SBH and LBH phases from the unstable region. And as it is evident from figures (Fig.4.2a and Fig.4.2b), the spinodal curve is the envelope of the saturated mixture of SBH and LBH phases. The spinodal curve also has a maximum at the critical point. The coexistence phase structure is shown in the  $T_r - V_r$  plane along with the spinodal curve in Fig.4.2b. Careful analysis of curves will find that there are five regions, namely SBH phase, LBH phase, supercritical phase, metastable superheated SBH, and supercooled LBH phase. In both the plots in  $P_r - T_r$  and  $T_r - V_r$  planes, the extremal point coincides with the extrema in the spinodal curves. To have more clarity, we can turn to  $P_r - V_r$  isotherms. When the reduced temperature  $T_r$  of isotherm is below 1, we can see an oscillating behavior with an inflection point at the critical point. At any temperature  $T^*$ , corresponding to coexistence  $T_r - V_r$  curve, which is obviously bounded below 1, the isotherm consists of fore mentioned five regions. In Fig.4.1b, we have presented labelled  $P_r - V_r$  plot indicating different regions. For Maxwell's construction, a vertical line is drawn at the pressure  $P^*$ . The line divides the isotherm into two equally occupied regions satisfying Maxwell's equal-area law. At the temperature,  $T^*$ , the volume of the SBH and LBH phases is  $V_s$  and  $V_l$ , respectively. The  $V_s$  and  $V_l$  are obtained from  $T_r - V_r$  coexistence curve. The terminology used here is defined parallel to the analogous van der Waals fluid system. From the  $P_r - V_r$  isotherm, we see that the SBH phase (thick blue) can exist till the pressure  $P^*$  where it has the volume  $V_s$ . When the pressure is reduced below  $P^*$ , the system moves to a superheating phase without undergoing a transition. This phase denoted by the pink dashed portion

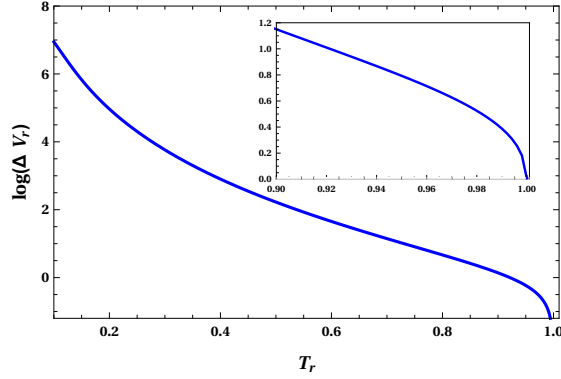


Figure 4.3:  $\log(\Delta V_r)$  vs  $T_r$ , The volume change  $\Delta V_r = V_l - V_s$  as a function of reduced temperature  $T_r$ . Magnified view near the critical point is shown in the insets.

is the superheated SBH phase. This state is metastable in the sense that it can undergo a phase transition with even small fluctuation. The end of this metastable phase is marked by a black dot which represents the spinodal curve. Further, there exists a small unstable region with a positive slope denoted by the black dotted line in Fig.4.1b. This unstable region terminates at the extremum, from there system moves to another metastable state known as supercooled LBH. The unstable region is separated from the metastable region by the spinodal curve. The supercooled LBH phase is marked as the magenta dashed line in the plot. The system continues in this state till  $P^*$ , after that system, undergoes rapid expansion with a slight change in pressure. The volume acts as an order parameter during this transition. At the critical point, the difference between the volumes of SBH and LBH phases vanishes, and they form a single supercritical phase. These regions are also portrayed in the coexistence curve in  $T_r - V_r$  plane Fig. 4.2b. Using the numerical method, we plot the volume change  $\Delta V_r = V_l - V_s$  as the function of reduced temperature  $T_r$  in Fig.4.3. It shows that  $\Delta V_r$  approaches zero at the critical point and monotonously increases when the temperature is reduced. The series expansion of  $\Delta V_r$  around the critical point reads,

$$\Delta V_r = 4.03691(1 - T_r)^{0.537073}. \quad (4.36)$$

The critical exponent is 0.537, which is approximately equal to the universal value 1/2. This result is similar to the one earlier obtained in different black holes (Wei et al. 2019a,b, Wei and Liu 2020b, Naveena Kumara et al. 2020c, Wu et al. 2020).



## 4.4 Thermodynamic Geometry

Black hole thermodynamics would appear very much in need of some microscopic foundation. This can be given by quantum gravity theories. Prominent candidates for quantum gravity are String theory and Loop quantum gravity. From the famous quote by Boltzmann, “If it is hot, it must have microstructure”. So without invoking any quantum gravity theory, one can find that the black holes have a microstructure. We can call it “atoms of spacetime,” and it is not odd to speculate the interaction between these micromolecules using the observed thermodynamics of black holes. George Ruppeiner proposed a phenomenological model for black hole microstructure in 2008 based on the theory of fluctuations. The theory of fluctuation tells us that the physical quantities describing a macroscopic body in equilibrium are almost always very nearly equal to their mean values. Nevertheless, they fluctuate, i.e., they deviate from the mean values though in a small amount. This fluctuation requires some probability distributions for the physical quantities. Thus, the probability for finding a physical quantity  $x$  to be in between  $(x_0, \dots, x_N)$  and  $(x_0 + dx_0, \dots, x_N + dx_N)$  is proportional to the number of the microstates  $\Omega$ ,

$$P(x_0, \dots, x_N) dx_0 \dots dx_N = C \Omega(x_0, \dots, x_N) dx_0 \dots dx_N. \quad (4.37)$$

Using Boltzmann’s entropy formula, from microstates we construct macroscopic thermodynamic quantities. Inverting the formula by Einstein is the starting point for fluctuation theory.

$$S = k_B \ln \Omega \Rightarrow \Omega = e^{S(x)/k_B}. \quad (4.38)$$

Substitute eqn.4.38 in the distribution eqn. 4.37,

$$P(x) dx = C \times e^{S(x)/k_B} dx. \quad (4.39)$$

Now, a Taylor expansion of  $S(x)$  around the equilibrium value  $x_0$  yields,

$$S(x) = S(x_0) + \left. \frac{\partial S}{\partial x} \right|_{x=x_0} (x - x_0) + \frac{1}{2} \left. \frac{\partial^2 S}{\partial x^2} \right|_{x=x_0} (x - x_0)^2 + \dots \quad (4.40)$$

Around the equilibrium, system will have maximum entropy,  $\left. \frac{\partial S}{\partial x} \right|_{x=x_0} = 0$ . Define the quantities in the expansion (eqn.4.40) as,

$$x - x_0 = \Delta x \quad ; \quad \left( -\frac{k_B}{\left. \frac{\partial^2 S}{\partial x^2} \right|_{x=x_0}} \right) = \langle (\Delta x)^2 \rangle = \sigma^2. \quad (4.41)$$

Substituting various terms, we can see that the probability distribution (eqn.4.39) is a Gaussian,

$$P(x)dx = C \times \exp \left( -\frac{(\Delta x)^2}{2\langle (\Delta x)^2 \rangle} \right) dx. \quad (4.42)$$

In a canonical ensemble when energy fluctuate around an average, it makes sense to define a standard deviation of the energy, that is nothing but heat capacity at constant volume  $C_V$ ,

$$\sigma_E^2 = \langle (\Delta E)^2 \rangle = \langle E^2 \rangle - \langle E \rangle^2 = k_B T^2 C_V. \quad (4.43)$$

The statistical Mechanics provides the profound result that this response functions whether it is heat capacity ( $C_V$ ) or the compressibility ( $\kappa$ ) are given exactly by the mean square fluctuations of the respective conjugate thermodynamic properties of the system.

Moving further by considering two fluctuating variables  $x^\mu$  and  $x^\nu$  having their equilibrium value  $x_0^\mu$  and  $x_0^\nu$  respectively,  $\Delta x^\mu = x^\mu - x_0^\mu$  and  $\Delta x^\nu = x^\nu - x_0^\nu$ . The probability distribution (eqn.4.39) becomes,

$$\begin{aligned} P(x)dx &= C \times \exp^{S(x)|_{x_0} + \frac{1}{2} \left. \frac{\partial^2 S}{\partial x^\mu \partial x^\nu} \right|_{x_0} \Delta x^\mu \Delta x^\nu} \\ &= \frac{1}{(2\pi)^{1/2}} \exp^{-\frac{1}{2} g_{\mu\nu} \Delta x^\mu \Delta x^\nu} \times \sqrt{\det(g_{\mu\nu})} dx, \end{aligned} \quad (4.44)$$

where  $(\Delta l)^2 = g_{\mu\nu} \Delta x^\mu \Delta x^\nu$  and  $g_{\mu\nu} = -\frac{1}{k_B} \left. \frac{\partial^2 S}{\partial x^\mu \partial x^\nu} \right|_{x_0}$ . The line element  $(\Delta l)^2$  is the distance between thermodynamic states, and it is in the form of second rank metric tensor  $g_{\mu\nu}$ . The distance between two fluctuating states is inversely proportional to the probability of fluctuation between the states. So the metric speaks about thermodynamic stability. The metric, which is the hessian of entropy function contains the response functions like heat capacity ( $C_V$ ) and compressibility ( $\kappa$ ). This approach to thermodynamics using the

differential geometry is popularly known as *thermodynamic geometry*. It is the work of Weinhold (Weinhold 1976) and Ruppeiner (Ruppeiner 1979) which brought attention to this field. The essential part of this method is the construction of a thermodynamic metric. The first such metric is proposed by Weinhold in which hessian of internal energy was the key entity, which is a function of entropy and other extensive quantity (Weinhold 1975). Later, another construction of metric was given by Ruppeiner, where, instead of internal energy, entropy is taken as generating function in the definition of hessian (Ruppeiner 1979, 1995). This new construction appears more appropriate for black hole thermodynamics since the entropy of the black hole is measured on the horizon, whereas the internal energy is at the asymptotic infinity. However, one can show that these different constructions are related to each other conformally with the inverse of temperature as a conformal factor. In the fluctuation theory of equilibrium thermodynamics, the inverse of the Ruppeiner metric gives the second moments of fluctuations. At the critical point, thermodynamic scalar curvature becomes proportional to the correlation volume of  $\xi$  of the thermodynamic system. The curvature scalar contains the underlying microscopic structure of the corresponding statistical system, which shows diverging behavior near the critical point. George Ruppeiner conjectured that the curvature scalar captures the details about the microscopic or mesoscopic interactions.

The Sign of curvature scalar  $R$  indicates the type of interactions,

$R < 0$  Attractive interactions,

$R = 0$  no interactions or very weak interactions,

$R > 0$  Repulsive interactions.

So the curvature scalar vanishes for ideal gas since there is no intermolecular interaction. Several applications of thermodynamic geometry on different black hole spacetimes revealed interesting results and newer possibilities (Ferrara et al. 1997, Aman et al. 2003, Sarkar et al. 2006, Shen et al. 2007, Sarkar et al. 2008, Ruppeiner 2008, Sahay et al. 2010a, Lala and Roychowdhury 2012, Hendi et al. 2015b, Li and Mo 2016, Sahay 2017). The interplay between geometry and microscopic structure in the ther-

modynamic geometric method is extremely useful in black hole thermodynamics since the exact knowledge of constituent information of black hole is still a debatable issue. It should be emphasized that in both ordinary thermal systems and black hole systems, thermodynamic geometry gives only a phenomenological description, not the exact microstructure.

#### 4.4.1 Microstructure of the Bardeen AdS Black Hole

In this section, we study the critical behaviour and the microstructure of the Bardeen black hole using the novel Ruppeiner geometry put forward by Wei *et.al* (Wei *et al.* 2019a), where  $T$  and  $V$  are chosen as the fluctuation coordinates. The line element is written in  $(T, V)$  coordinates as,

$$dl^2 = \frac{C_V}{T^2} dT^2 - \frac{(\partial_V P)_T}{T} dV^2. \quad (4.45)$$

And the normalized scalar curvature  $R_N$  is obtained from the above line element as,

$$R_N = RC_V = \frac{(\partial_V P)^2 - T^2 (\partial_{V,T} P)^2 + 2T^2 (\partial_V) (\partial_{V,T} P)}{2(\partial_V P)^2}. \quad (4.46)$$

We have seen from eqn. 4.22 that the heat capacity ( $C_V$ ) at constant volume vanishes for the black hole. This can result in a singularity, and this singular behavior in the curvature scalar  $R$  is rectified by multiplying it with  $C_V$ .

The normalized scalar  $R_N$  gives information about the microscopic interactions present in the black hole. The metric tensor is calculated using the line element (eqn.4.45), and  $R_N$  is obtained from the eqn.4.46.  $R_N$  hence obtained is a complicated expression  $R_N(T, V, g)$ . After converting it in the reduced coordinates  $R_N(T_r, V_r)$ , it is plotted against the reduced volume  $V_r$  with a fixed temperature is shown in Fig. 4.46. In reduced coordinates,  $R_N$  is independent of monopole charge  $g$ . From the figures (Fig.4.4a, Fig.4.4b), we can see that  $R_N$  has two divergent points below the critical point  $T_r < 1$ . And when the temperature becomes equal to the critical temperature  $T_r = 1$ , these divergences merge and shoot up at the point  $V_r = 1$  as showed in Fig.4.4c. As expected, the divergence vanishes for all temperatures above the critical temperature

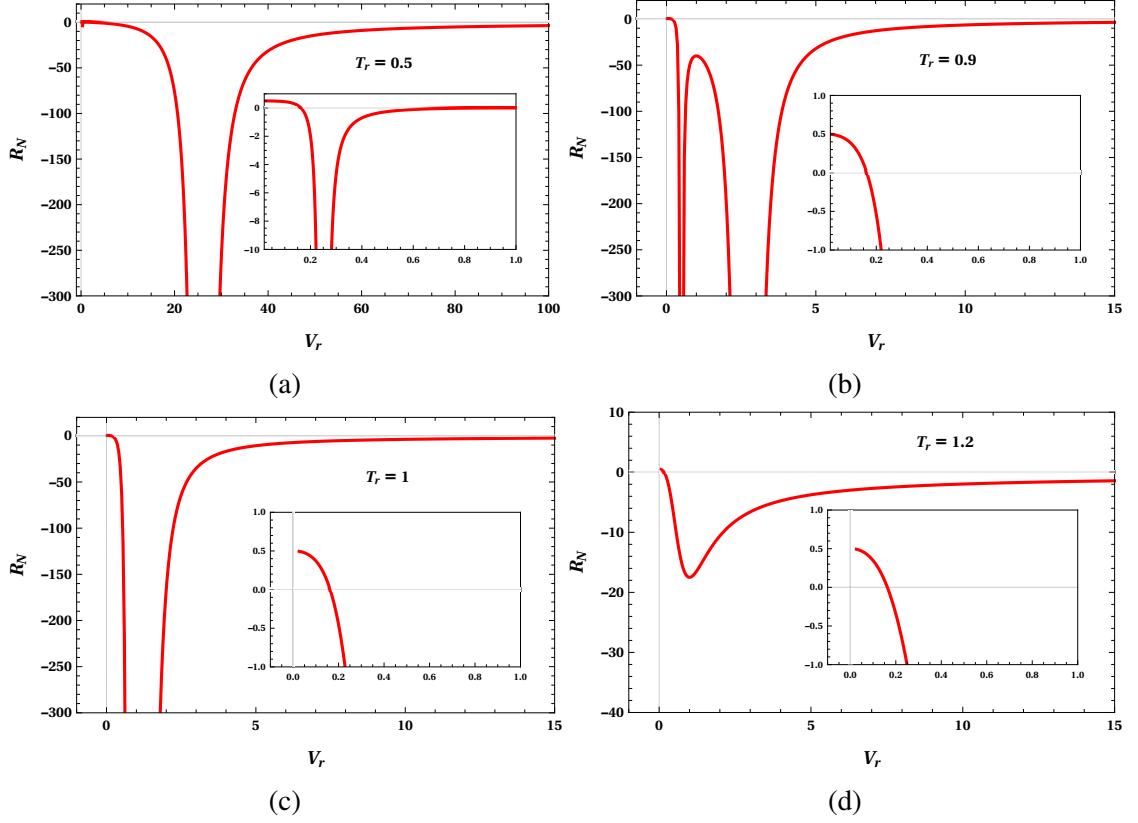


Figure 4.4: The normalised curvature scalar  $R_N$  is plotted against the reduced volume  $V_r$  at different reduced temperature  $T_r$ .

$T_r > 1$  (Fig.4.4d). This shows that the information about the phase transition and critical phenomenon is well expressed by the normalized curvature scalar  $R_N$ . Interestingly, these two divergent points correspond to the metastable points in the spinodal curves. We can notice that even though  $R_N$  is negative for most of the parameter space, there exists a small range where it is positive, which are shown in the inlets of Fig (4.4). The sign-changing curve is plotted in the  $T_r - V_r$  plane utilizing the condition scalar curvature  $R_N = 0$ .

The scalar curvature  $R_N$  vanishes and changes its sign at the point  $T_0$ , given by

$$T_0 = \frac{T_{rsp}}{2} = \frac{3(\sqrt{273} + 17) \left( (\sqrt{273} + 17) V_r^{2/3} - 10 \right) \sqrt{(\sqrt{273} + 17) V_r^{2/3} - 2}}{8\sqrt{\sqrt{273} + 15} \left( (\sqrt{273} + 17) V_r^{2/3} + (17\sqrt{273} + 281) V_r^{4/3} - 4 \right)}. \quad (4.47)$$

Sign change also happens at the point,

$$V_r = V_0 = \frac{5}{8} \sqrt{\frac{5}{2} (4709 - 285\sqrt{273})}. \quad (4.48)$$

The sign-changing curve distinguishes regions of negative  $R_N$  from positive. As we know, the scalar curvature  $R_N$  tells about the microscopic interaction. Positive  $R_N$  means a repulsive interaction, and negative  $R_N$  signifies an attractive interaction in the microstructure. To have more clarity, we have placed all three plots, coexistence, spinodal and sign-changing plots, in a single plot (Fig.4.5a). Different regions in Fig.4.5a correspond to the stable and metastable phases. The light magenta shaded region under the sign-changing curve has positive and the unshaded region has negative  $R_N$ . The region ①, area common between the spinodal curve and sign-changing curve is a saturated SBH+ LBH phase. This phase always has a repulsive interaction in the microstructure with a positive  $R_N$ . Next, the left-most region bounded inside the line  $V_r = V_0$  also has a repulsive interaction with a positive  $R_N$ . In that, region ③ is an SBH phase and region ② is a metastable superheated SBH phase. Nevertheless, there is a stable SBH portion that lies outside this positive  $R_N$  region marked with ④, which has an attractive interaction in the microstructure. All other phases, supercooled LBH as well as stable LBH phase, have negative  $R_N$ , with dominant attractive interaction. It affirms that there exists attractive and repulsive interaction in the black hole microstructure, a hint of this is observed in the  $R - V_r$  plot (Fig.4.4).

In Fig. 4.5b, normalized curvature scalar  $R_N$  is plotted as a function of temperature along the coexistence line. This is obtained numerically from the  $P_r - T_r$  coexistence fitting equation. Both of the branches, SBH and LBH, diverge to infinity at the critical temperature  $T_r = 1$ . Besides this, we can see that sign of  $R_N$  is always negative for the LBH phase, but the same is not true for the SBH phase. As shown in inlets of Fig. 4.5b, in the small temperature range, there exists a region with positive  $R_N$ . Even though the scalar curvature decreases with temperature for both the branches, the LBH branch never attains positive  $R_N$ . Like in the previous plot (Fig.4.4), this also leads to the conclusion that there exists attractive and repulsive interaction in the microstructure of the SBH phase. We also notice that the intensity of attractive interaction in the

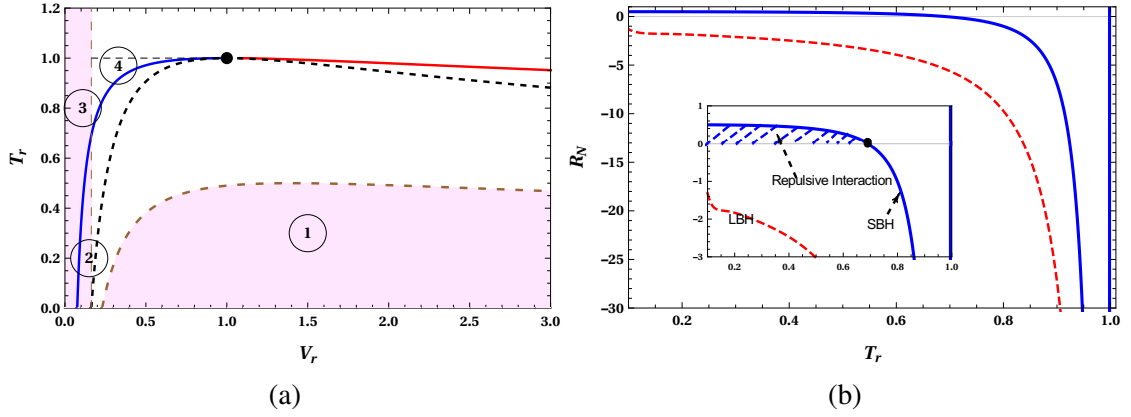


Figure 4.5: Fig.4.5a: The sign-changing curve of  $R_N$  along with the coexistence and spinodal curves. Fig.4.5b: The behaviour of normalised curvature scalar  $R_N$  along the coexistence line. The red (solid) line and blue (dashed) line correspond to a large black hole and a small black hole, respectively. The inlet shows the region where the SBH branch takes a positive  $R_N$  value.

SBH phase is stronger than that of the LBH phase. It can happen due to the strong correlation between the black hole molecules in the SBH phase than in the loosely correlated LBH phase. This behavior is similar to the van der Waals liquid-gas system, where the attractive interaction in the liquid phase is more intense than in the gaseous phase.

Finally, we can find the critical exponent corresponding to the divergence of  $R_N$  along the coexistence line for the SBH and LBH branches. This can be obtained numerically assuming that  $R_N$  has the form,

$$R_N \sim (1 - T_r)^p. \quad (4.49)$$

Taking logarithm on both sides, it reduces to,

$$\ln |R_N| = -p \ln(1 - T_r) + q. \quad (4.50)$$

We have numerically generated data for  $R_N$  as a function of coexistence temperature  $T_r$  in the range 0.9 to 0.999. Along the SBH branch, we can fit the data as,

$$\log |R| = -1.90021 \log(1 - T_r) - 1.37767. \quad (4.51)$$

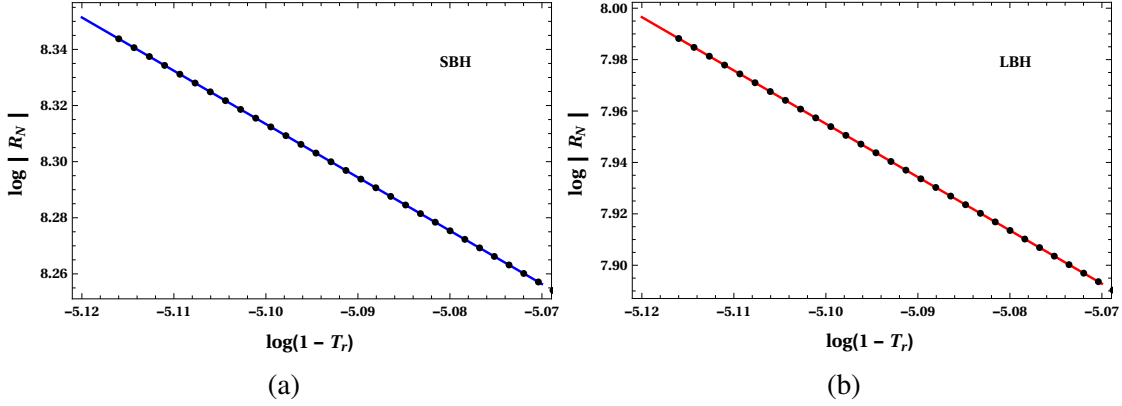


Figure 4.6: The behaviour of scalar curvature  $\ln |R_N|$  near the critical point is shown in terms of  $\ln(1 - T_r)$  for the case of LBH in Fig.4.6b and SBH in Fig.4.6a. The numerical data points are marked by black dots and line obtained from fitting formula are in solid blue line for SBH and in red line for LBH phase.

Similarly, for LBH branch, we obtain,

$$\log |R| = -2.07412 \log(1 - T_r) - 2.62298. \quad (4.52)$$

We have plotted these equations separately for SBH and LBH phases in the figure (Fig. 4.6a, 4.6b) along with the numerical data points. These plots show great consistency in the solid lines and numerical data. Apart from the numerical errors, the results show that the critical exponent  $p$  is approximately equal to 2. From equations (eqn.4.51) and (eqn.4.52), we can write,

$$R_N (1 - T_r)^2 = -\exp^{-(1.37767+2.62298)/2} = -0.135291. \quad (4.53)$$

This ratio is slightly higher than the universal ratio  $-1/8$  found in the vdW system and other AdS black holes. Taking the numerical errors into account, the result we obtained is very close to the universal ratio.

## 4.5 Summary and Conclusions

In this chapter, we have concentrated mainly on studying the thermodynamics and microstructure of regular Bardeen AdS black holes. Information about the coexistence phases missing in earlier studies in the literature is addressed. We have dedicated initial



sections for obtaining coexistence  $P_r - T_r$  equations from the Gibbs free energy plots. The Gibbs free energy in reduced coordinates is plotted as a function of reduced temperature  $T_r$  with a fixed pressure  $P_r$ . The appearance of swallowtail behavior in these plots below the critical pressure is used to generate data for obtaining the coexistence equation. As it is difficult to obtain the coexistence equation analytically in Bardeen black holes, from Maxwell's equal-area law or Gibbs free energy, we have used the fitting formula. Through the coexistence equation, different regions in  $P_r - V_r$  isotherm are analyzed at a reduced temperature  $T_r < 1$ . It is noticed that a first-order phase transition analogous to the vdW system takes place between stable SBH and LBH phases. Besides, there exists metastable superheated SBH and supercooled LBH phases. The stable and metastable phases are distinguished from each other by plotting a spinodal curve. The unstable regions are removed through Maxwell's constructions. These distinct phases in the black hole are studied through the coexistence and spinodal curves in  $P_r - T_r$  and  $T_r - V_r$  planes. The change in volume  $\Delta V_r = V_{rl} - V_{rs}$  acts as an order parameter during the SBH-LBH phase transition. Near the critical point, the critical exponent is calculated, which matches with the universal value of  $1/2$ .

In the second half of the chapter, we have studied thermodynamics through Ruppeiner geometry. The novel method proposed by Wei *et al.* is used to calculate the thermodynamic scalar curvature (Wei *et al.* 2019a). Using the reduced equation of state for Bardeen black hole, novel scalar curvature is calculated and plotted against reduced volume  $V_r$  at different temperatures. The critical behavior is well captured in the plots with the appearance and disappearance of divergences below and above the critical point. Moreover, it is noticed that scalar curvature attains both positive and negative values in the plots. The sign of  $R_N$  encodes the information about the microscopic interactions. This leads one to an inference that both attractive and repulsive interaction exists in the black hole microstructure. To have more details on the microstructure, we have analyzed the behavior of scalar curvature along the coexistence curve. In the absence of analytical expression for the coexistence curve, we depend on the numerical methods for obtaining  $R_N$  vs.  $T_r$  plots for SBH and LBH branches. Both the branches diverge to negative infinity at critical point  $T_r = 1$ . Except for the divergence, the mi-

crostructure of the SBH and LBH are distinct. The LBH phase always has a larger  $|R_N|$  than the SBH branch.

Moreover, the SBH branch attains positive  $R_N$  in the small temperature range. This is in agreement with  $R_N - V_r$  plots, SBH microstructure has repulsive as well as attractive interactions, but the LBH microstructure has only attractive interactions. This is in contrast to the vdW fluid system, where only attractive dominant interactions are present between the molecules. Our results imply that the phase transition leads to a change in the microstructure of the regular Bardeen AdS black holes. A similar type of behavior is observed in charged AdS black holes and regular Hayward AdS black holes. But this feature is not universal; in the five-dimensional neutral Gauss-Bonnet black hole case, only attractive interaction present in the entire parameter space similar to van der Waals fluid. In Born-Infeld AdS black holes and massive gravity theories, the nature of interaction depends on the value of coupling and massive parameter, respectively. Our result is interesting as it establishes that the microscopic interaction in regular black holes is generic in nature. As an extension to our work, it is interesting to probe the repulsive interactions in the other regular black holes as well.

# Chapter 5

## Effect of Quintessence on Phase transitions and Thermodynamic geometry of Regular black holes

Summary

---

*This chapter is an edited version of our article ([Ahmed Rizwan et al. 2019b](#)). We investigate the thermodynamics and geometrothermodynamics of regular Bardeen-AdS black holes with quintessence. The thermodynamics of the black hole is studied using temperature-entropy ( $T - S$ ), Pressure-Volume ( $P - v$ ), and Gibbs energy plots, which indicate a critical behavior. Using the concept of thermodynamic Ruppeiner and Weinhold geometry, we calculated the thermodynamic curvature scalar  $R_R$  and  $R_W$  in the quintessence dark energy regime ( $\omega = -2/3$ ). While these curvature scalars enable us to identify the critical behavior, they do not show divergence at the phase transition points observed in specific heat studies. To resolve this puzzle, we have adopted the method of geometrothermodynamics proposed by Hernando Quevedo.*

---

### 5.1 Introduction

The accelerated expansion of the universe is due to the presence of an exotic field called Dark energy. Quintessence is one among different models for dark energy ([Ford 1987](#), [Kiselev 2003](#), [TsujiKawa 2013](#)). The cosmic source for inflation has the equation of state  $p_q = \omega\rho_q$  ( $-1 < \omega < -1/3$ ), and  $\omega = -2/3$  corresponds to quintessence dark

energy regime. The energy density for quintessence has the form  $\rho_q = -\frac{a}{2} \frac{3\omega}{r^{3(\omega+1)}}$ , which is positive for usual quintessence. Several attempts have been made to explore the effects of quintessence on the black hole, with Kiselev's phenomenological approach being the notable one (Kiselev 2003). By using Kiselev's phenomenological model, we can construct a regular-Bardeen black hole surrounded by quintessence. According to the model, the quintessence comes from a fluid with the energy-momentum tensor,

$$\begin{aligned} T_r^r &= T_t^t = \rho_q, \\ T_\theta^\theta &= T_\phi^\phi = -\frac{1}{2}\rho_q(3\omega + 1), \\ \rho_q &= -\frac{a}{2} \frac{3\omega}{r^{3(\omega+1)}}, \end{aligned}$$

$\omega$  and  $a$  are the state parameter and the normalization constant related to quintessence energy density  $\rho_q$ . Solving the Einstein equations, we can obtain metric for a regular-Bardeen AdS black hole with quintessence (Saleh et al. 2018, Fan 2017, Li 2014, Kiselev 2003) (detailed steps given in Appx.F),

$$ds^2 = -f(r)dt^2 + \frac{dr^2}{f(r)} + r^2 d\theta^2 + r^2 \sin^2 \theta d\phi^2,$$

$$\text{with } f(r) = \left(1 - \frac{2\mathcal{M}(r)}{r} + \frac{r^2}{l^2} - \frac{a}{r^{3\omega+1}}\right).$$

Phase transitions in black holes surrounded by quintessence are widely studied. Thermodynamics of Reissner-Nordström and regular black holes surrounded by quintessence were investigated by various groups (Yi-Huan and Zhong-Hui 2011, Thomas et al. 2012, Tharanath and Kuriakose 2013, Li 2014, Fan 2017, Saleh et al. 2018, Rodrigue et al. 2020).

This chapter is organized as follows. In section 5.2, thermodynamics of regular Bardeen black hole surrounded by quintessence is studied in the extended phase space. In the next section 5.3, thermodynamic geometry for the black hole is constructed using Weinhold and Ruppeiner metric, followed by geometrothermodynamics. Conclusion is written in the final section 5.4.

## 5.2 Thermodynamics of the black hole

First law of thermodynamics for the Bardeen black hole must be modified to include quintessence as follows,

$$dM = TdS + \Psi d\beta + VdP + \mathcal{A}da. \quad (5.1)$$

Where  $\Psi$  is the potential conjugate to the magnetic charge  $\beta$  and  $\mathcal{A}$  is a quantity conjugate to quintessence parameter  $a$ .

$$\mathcal{A} = \left( \frac{\partial M}{\partial a} \right)_{S,\beta,P} = -\frac{1}{2r_h^{3\omega}}. \quad (5.2)$$

As we have mentioned earlier, in the extended phase space, the cosmological constant is considered as thermodynamic pressure.

$$P = -\frac{\Lambda}{8\pi}, \quad \Lambda = -\frac{3}{l^2}. \quad (5.3)$$

We can derive Hawking temperature (eqn. 5.4) from the first law, which can be combined with the area law to obtain the equation of state (eqn. 5.5).

$$T = \frac{1}{4} \sqrt{\beta^2 + \frac{S}{\pi}} S^{-\frac{3\omega}{2} - \frac{5}{2}} \left( 3a\pi^{\frac{3\omega}{2} + \frac{1}{2}} (\pi\beta^2(\omega + 1) + S\omega) + S^{\frac{3\omega}{2} + \frac{1}{2}} (-2\pi\beta^2 + 8PS^2 + S) \right), \quad (5.4)$$

$$P = \frac{1}{8\pi} \left[ \frac{8\pi T}{\sqrt{4\beta^2 + v^2}} + 32\beta^2 v^{-3\omega-5} (v^{3\omega+1} - 3a8^\omega(\omega + 1)) - 3a8^{\omega+1}\omega v^{-3(\omega+1)} - \frac{4}{v^2} \right]. \quad (5.5)$$

where  $v = 2r_h$  is specific volume. Using the above equations the  $P - v$  and  $T - S$  curves are plotted in figure (Fig. 5.1a, Fig. 5.1b). These two plots clearly show critical phenomena around the critical points. The critical points are obtained from the conditions,

$$\frac{\partial P}{\partial v} = 0, \quad \frac{\partial^2 P}{\partial v^2} = 0. \quad (5.6)$$

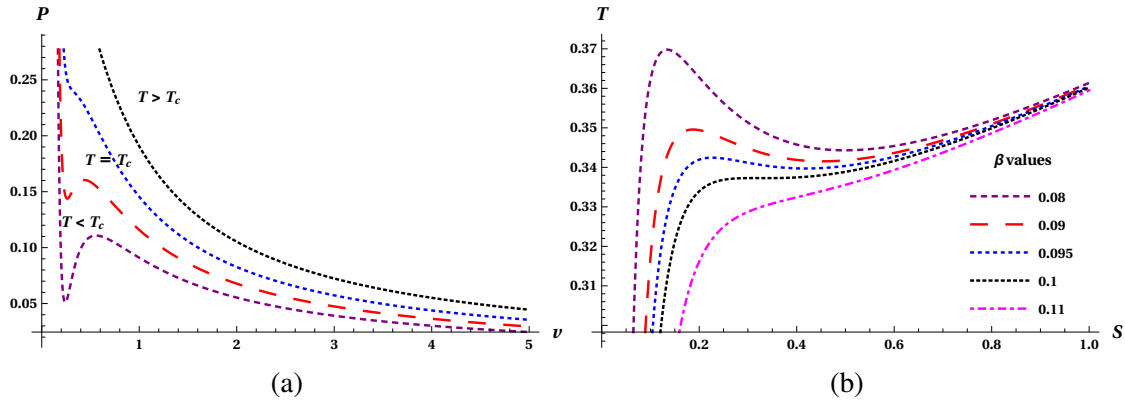


Figure 5.1: To the left we have  $P - v$  diagram for regular AdS black hole surrounded by quintessence ( $a = 0.07$ ,  $\beta = 0.1$ ,  $\omega = -2/3$ ,  $T_c = 0.36$ ). In the right side  $T - S$  plot for different values of  $\beta$  is shown.

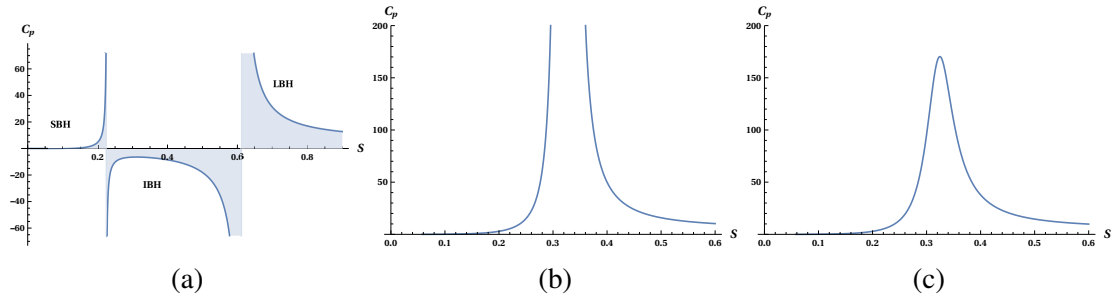


Figure 5.2: Specific heat versus entropy diagram for regular AdS black hole surrounded by quintessence ( $a = 0.07$ ,  $\beta = 0.1$ ,  $\omega = -\frac{2}{3}$ ). (Fig. 5.2a) for  $P = P_c$ , (Fig. 5.2b) for  $P < P_c$ , (Fig. 5.2c) for  $P > P_c$ .

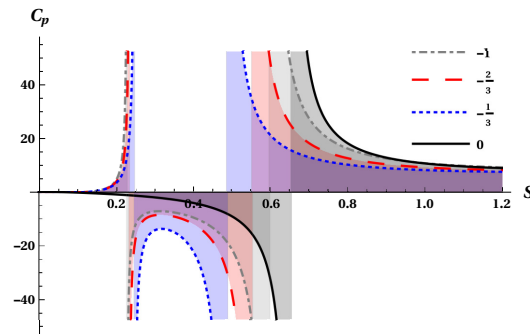


Figure 5.3: Specific heat for different  $\omega$  values

Table 5.1: Critical points are found using eqn. 5.6 with quintessence state parameter  $\omega = -1, -2/3, -1/3$ . The ratio  $\frac{P_c v_c}{T_c}$  is calculated for each case.

$\omega$	$P_c$	$v_c$	$T_c$	$\frac{P_c v_c}{T_c}$
-1	0.2155	0.6426	0.3485	0.3973
-2/3	0.2073	0.6422	0.3376	0.3945
-1/3	0.1926	0.6426	0.3241	0.3819

In the absence of quintessence, the critical volume ( $V_c$ ), critical temperature ( $T_c$ ) and critical pressure ( $P_c$ ) of regular Bardeen-AdS black hole are obtained, which are as follows,

$$V_c = 2\sqrt{2}\beta\sqrt{2 + \sqrt{10}} \quad , T_c = \frac{25(13\sqrt{10} + 31)}{432\pi\beta(2\sqrt{10} + 5)^{3/2}} \quad ,$$

$$P_c = \frac{5\sqrt{10} - 13}{432\pi\beta^2}.$$

Using the critical quantities, we can calculate  $\frac{P_c v_c}{T_c}$  ratio.

$$\frac{P_c v_c}{T_c} = \frac{(-26 + 10\sqrt{10})(5 + 2\sqrt{10})^{3/2}\sqrt{2(2 + \sqrt{10})}}{775 + 325\sqrt{10}}.$$

which is numerically equal to 0.381931. For Reissner-Nordström AdS black hole, this ratio matches with that of a Van der Waals gas ( $\frac{P_c v_c}{T_c} = 3/8$ ).

The presence of quintessence affects the phase transition. As the analytic expression is difficult to obtain, the critical quantities are obtained numerically for the state parameter  $\omega = -1, -2/3, -1/3$  (Table 5.1). An increase in the value of  $\omega$  from  $-1$  to  $0$  leads to a decrease in the ratio, which approaches  $3/8$ .

In statistical mechanics, a phase transition is characterized by divergences in second moments like specific heat, compressibility, and susceptibility. Hence to study more details of phase transition, we focus on the heat capacity of the system. Sign of heat capacity tells about the thermodynamic stability of black holes, which is positive for

stable and negative for unstable. The heat capacity at constant pressure is given by,

$$C_P = T \left( \frac{\partial S}{\partial T} \right)_P = \frac{2S (\pi\beta^2 + S) \left( S (\sqrt{\pi}(8PS + 1) - 2a\sqrt{S}) + \beta^2 (\pi a\sqrt{S} - 2\pi^{3/2}) \right)}{\sqrt{\pi} (\beta^4 (8\pi^2 - 3\pi^{3/2}a\sqrt{S}) + S^2(8PS - 1) + 4\pi\beta^2 S)}$$

$C_P - S$  plot is obtained from this equation, which shows critical behavior Fig. 5.2 below certain pressure ( $P_c$ ). Fig. 5.2 shows that below the critical pressure  $P < P_c$ , there are two singular points, which reduce to one when  $P = P_c$ , and above  $P > P_c$ , this divergence disappears. In Fig. 5.2b, there are three distinct regions separated by two singular points. The Small black hole (SBH) and large black hole (LBH) regions with positive specific heat, and the intermediate black hole (IBH) with negative specific heat. As the positive specific heat regions are thermodynamically stable, phase transition takes place between the small black hole and a large black hole. From Fig.5.3, we observe that the quintessence state parameter  $\omega$  shifts the SBH-LBH transition to lower entropy values. The specific heat plotted with  $\omega = -1, -\frac{1}{3}, -\frac{2}{3}$  and 0 shows the deviation. When  $\omega = 0$ , the intermediate region vanishes. Only two regions exist, one with negative and the other with positive specific heat; the behavior is similar to that of a regular Bardeen black hole (Tharanath and Kuriakose 2013).

The small-large black hole phase transition observed in this black hole is analogous to the liquid-gas transition in Van der Waals gas like in Reissner-Nordström AdS black holes. The notable difference compared to Van der Waals gas is the ratio  $\frac{P_c v_c}{T_c}$ , which does not appear to be a constant value  $3/8$ , as the critical temperature  $T_c$  depends on the quintessence.

### 5.3 Quintessence and Thermodynamic Geometry

After Albert Einstein's theory of gravity based on differential geometry became a great success, the method of differential geometry was identified as a mathematical language for various gauge fields. It was Gibbs (Gibbs 1948) in the later part of the 19th century and Caratheodory (Carathéodory 1909) in 1909, to use these ideas of differential geometry in classical thermodynamics. Hermann (Hermann 1973) and Mrugala (Mrugala 1978) applied differential geometry to the thermodynamic phase space using its con-



tact structure. Then Weinhold ([Weinhold 1975](#)) and later Ruppeiner ([Ruppeiner 1979, 1995](#)) constructed thermodynamic metric to study phase transitions and microscopic interactions in thermodynamic systems. Geometrothermodynamics is another geometric formalism for the classical thermodynamics developed by H. Quevedo ([Quevedo 2007](#)). The phase transition of the system can be seen in the divergence behavior of this curvature scalar near the critical point.

Thermodynamic geometry is applied to van der Waals gas and different statistical models including magnetic models ([Ruppeiner 1995](#), [Janyszek and Mrugaa 1990](#), [Oshima et al. 1999](#), [Mirza and Mohammadzadeh 2008](#), [May et al. 2013](#)). Considering black hole as a thermodynamic system, the geometric formalism is used to study the critical behavior of black holes during phase transitions ([Ruppeiner 2008](#), [Aman et al. 2003](#), [Sarkar et al. 2006](#), [Shen et al. 2007](#), [Sarkar et al. 2008](#), [Sahay et al. 2010b,a](#), [Banerjee et al. 2011b,a](#), [Biswas and Chakraborty 2011](#), [Akbar et al. 2011](#), [Niu et al. 2012](#), [Bellucci and Tiwari 2012](#), [Lala and Roychowdhury 2012](#), [Wei and Liu 2013](#), [Yi-Wen et al. 2013](#), [Suresh et al. 2014](#), [Zhang et al. 2015a](#), [Mansoori et al. 2015](#), [Zhang et al. 2015b](#), [Hendi et al. 2015b](#), [Soroushfar et al. 2016](#), [Li and Mo 2016](#), [Sahay 2017](#), [Chaturvedi et al. 2017](#)). But there were inconsistencies in the position of critical point, as specific heat diverges at a point different from where scalar curvature diverges ([Janke et al. 2010](#), [Wei et al. 2012](#), [Suresh et al. 2014](#)). The Legendre invariance was found to be the key factor behind these discrepancies. Taking Legendre invariance into account a metric was constructed by Quevedo et al. ([Quevedo 2007, 2008](#), [Alvarez et al. 2008](#)), which resolved the issue. Quevedo's formalism named as Geometrothermodynamics(GTD) is applied to various black holes ([Bravetti et al. 2013](#), [Quevedo et al. 2012](#), [Tharanath et al. 2015](#), [Sanchez 2016](#), [Quevedo et al. 2016](#), [Hu et al. 2017](#), [Channuie and Momeni 2018](#)) including regular black holes ([Akbar et al. 2012](#)).

In this section, we investigate thermodynamic phase transitions based on geometric formalism proposed by Weinhold, Ruppeiner, and Quevedo. The divergent behavior of curvature scalar plotted against entropy reflects the existence of critical points corresponding to the thermodynamic phase transition.

### 5.3.1 Weinhold Geometry

The Weinhold metric is defined adhoc in the thermodynamic equilibrium space as the Hessian of the internal energy  $M$ ,

$$ds_W^2 = g_{ij}^W dx^i dx^j = \partial_i \partial_j M(S, N^a) dx^i dx^j, \quad (i, j = 1, 2),$$

where  $N^a$  represents any other thermodynamic extensive variables. Here, mass  $M$  is the function of entropy  $S$  and extensive variable  $\beta$ , which is the monopole charge. A Hessian is defined as a square matrix containing second derivative of energy with respect to the entropy and other extensive parameters (Weinhold 1975, 1976),

$$g^W = \begin{bmatrix} M_{,SS} & M_{,S\beta} \\ M_{,\beta S} & M_{,\beta\beta} \end{bmatrix}.$$

Using the expression for mass of the black hole, the components of metric tensor turns out to be,

$$g_{SS} = \frac{\beta^4 (8\pi^2 - 3\pi^{3/2} a \sqrt{S}) + S^2 (8PS - 1) + 4\pi\beta^2 S}{8\sqrt{\pi} S^3 \sqrt{\pi\beta^2 + S}}, \quad (5.7)$$

$$g_{S\beta} = g_{\beta S} = \frac{\beta (\beta^2 (3\sqrt{\pi} a \sqrt{S} - 6\pi) + S(8PS - 3))}{4S^2 \sqrt{\beta^2 + \frac{S}{\pi}}}, \quad (5.8)$$

$$g_{\beta\beta} = \frac{(2\pi\beta^2 + S) (\sqrt{\pi}(8PS + 3) - 3a\sqrt{S})}{2S\sqrt{\pi\beta^2 + S}}. \quad (5.9)$$

From metric tensor  $g_{ij}^W$ , one can calculate curvature scalar, which is found to be a complicated expression,  $R_W(S, P, b, \omega, a)$ . Plotting the curvature  $R_W$  versus entropy  $S$ , we have studied its divergence behavior, which occurs at multiple points Fig. 5.4. Even at the critical point ( $P_c=0.207$  for  $a=0.07$  and  $\beta = 0.1$ ),  $R_W$  shows multiple divergences Fig. 5.6a) which are different from that of the critical value of entropy ( $S$ ) observed in specific heat plots. From these randomly located diverging points, we can infer only

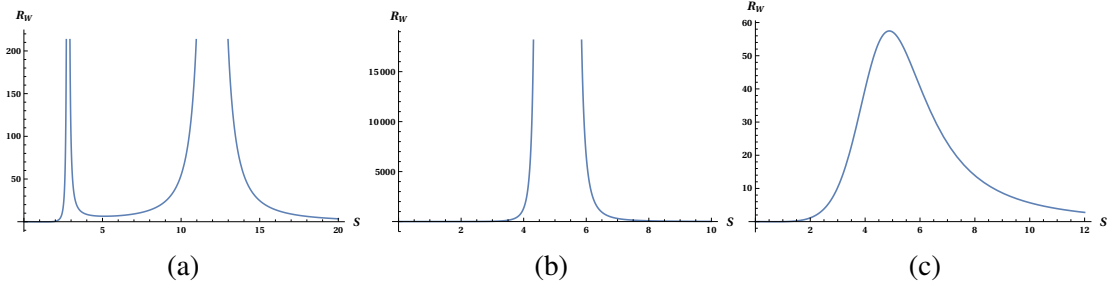


Figure 5.4: Curvature divergence plots for Weinhold metric. In all three plots quintessence parameter and monopole charge are fixed,  $a = 0.5$  and  $\beta = 1$ . Pressure is  $P = 0.01$  in (5.4a),  $P = 0.01264$  in (5.4b) and  $P = 0.0141$  in (5.4c).

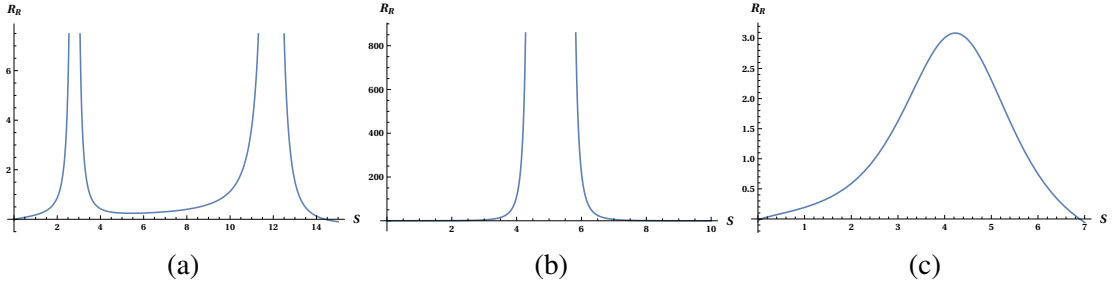


Figure 5.5: Curvature divergence plots for Ruppeiner metric. In all three plots quintessence parameter and monopole charge are fixed,  $a = 0.5$  and  $\beta = 1$ . Pressure is  $P = 0.01$  in (5.5a),  $P = 0.01264$  in (5.5b) and  $P = 0.0141$  in (5.5c).

the critical behavior of the system but not the exact phase transition points. As there is no agreement between the divergence points in Weinhold geometry and specific heat study, next, we focus on Ruppeiner geometry.

### 5.3.2 Ruppeiner Geometry

The Ruppeiner metric is defined as a Hessian of the entropy function  $S$  of the system instead of the internal energy  $M$  as in the Weinhold case. But one can transform the Ruppeiner metric, which is a function of  $M$  and  $\beta$  originally, to the same coordinate system used in the Weinhold metric, i.e.,  $S$  and  $\beta$ . Technically, their geometries are related to each other conformally (Ruppeiner 1979, 1995, 2008, 2010).

The Ruppeiner metric in the thermodynamic space states is given as ,

$$g_{ij}^R = -\partial_i \partial_j S(M, x^\alpha), \quad (i, j = 1, 2),$$

$$g^R = \begin{bmatrix} S_{,MM} & S_{,M\beta} \\ S_{,\beta M} & S_{,\beta\beta} \end{bmatrix}.$$

Because of the conformal property, the line elements in Ruppeiner and Weinhold formalism are related as

$$dS_R^2 = -\frac{dS_W^2}{T}. \quad (5.10)$$

Using eqn.5.7, eqn.5.8, eqn.5.9 and eqn.5.4 the components of Ruppeiner metric tensor are easily obtained as ,

$$g_{SS} = \frac{\sqrt{\pi} \left( b^4 \left( 8\pi^2 - 3\pi^{3/2} a\sqrt{S} \right) + 4\pi b^2 S + S^2 (8PS - 1) \right)}{2S (\pi b^2 + S) \left( b^2 \left( \pi a\sqrt{S} - 2\pi^{3/2} \right) + S \left( \sqrt{\pi} (8PS + 1) - 2a\sqrt{S} \right) \right)}, \quad (5.11)$$

$$g_{S\beta} = g_{\beta S} = \frac{\pi^{3/2} b \left( b^2 \left( 6\pi - 3\sqrt{\pi} a\sqrt{S} \right) + S(3 - 8PS) \right)}{(\pi b^2 + S) \left( b^2 \left( 2\pi^{3/2} - \pi a\sqrt{S} \right) - S \left( \sqrt{\pi} (8PS + 1) - 2a\sqrt{S} \right) \right)}, \quad (5.12)$$

$$g_{\beta\beta} = \frac{2\pi S \left( 2\pi b^2 + S \right) \left( \sqrt{\pi} (8PS + 3) - 3a\sqrt{S} \right)}{(\pi b^2 + S) \left( b^2 \left( \pi a\sqrt{S} - 2\pi^{3/2} \right) + S \left( \sqrt{\pi} (8PS + 1) - 2a\sqrt{S} \right) \right)}. \quad (5.13)$$

The curvature tensor  $R_R$  calculated from the above metric  $g_{ij}^R$  is again a complicated expression like in the Weinhold case. The obtained curvature function is plotted against entropy  $S$  to study the critical behavior (Fig. 5.5 and Fig. 5.6b).

The Fig.5.6b shows that at the critical point  $P_c = 0.207$ , there are multiple divergence around  $S = 0.06$  and  $S = 0.48$ , which does not correspond to the critical value of entropy ( $S = 0.32$ ). From these multiple singularities for curvature scalar, it is difficult to identify the critical points from Ruppeiner geometry. But it is interesting that Ruppeiner geometry indicates a phase transition even though it cannot identify the exact transition points (Fig.5.5), like Weinhold geometry. This kind of anomaly was found in Kehagias-Sfetsos black hole (Janke et al. 2010) and in Gauss-Bonnet Born-Infeld massive gravity theories (Hendi et al. 2016, 2015a). In both Weinhold and Ruppeiner geometries, we note that the number of divergence points reduces of curvature scalar decreases when the pressure increases and gradually disappear.

### 5.3.3 Geometrothermodynamics

In this approach, the metric is constructed from a Legendre invariant thermodynamic potential and their derivatives with respect to the extensive variables. For geometrothermodynamic calculations, we will consider  $2n + 1$  dimensional thermodynamic phase space  $\mathcal{T}$ . This phase space is constructed using the coordinates  $\{\Phi, E^a, I^a\}$ , where  $\Phi$  is thermodynamic potential and  $E^a$  and  $I^a$  are extensive and intensive variables. Then Gibbs one-form is introduced as  $\Theta = d\Phi - \delta_{ab}I^a E^b$ , satisfying  $\Theta \wedge (d\Theta) \neq 0$ . Defining a Legendre invariant metric  $G$  on  $\mathcal{T}$ ,

$$G = (d\Phi - \delta_{ab}I^a E^b)^2 + (\delta_{ab}I^a E^b)(\eta_{cd}I^c E^d), \quad (5.14)$$

$$\eta_{cd} = \text{diag}(-1, 1, \dots, 1). \quad (5.15)$$

$\mathcal{T}$ ,  $\Theta$  and  $G$  constitutes a Riemann contact manifold. Following this we define an  $n$  dimensional Riemannian submanifold  $\varepsilon \subset \mathcal{T}$ , which is the space of equilibrium thermodynamic states (equilibrium manifold) via a smooth map  $\varphi : \varepsilon \rightarrow \mathcal{T}$ . The Quevedo metric, which is similar to Ruppeiner and Weinhold metric, is defined on this equilibrium submanifold using the inverse map  $\varphi^*(G)$ .

$$g^Q = \varphi^*(G) = \left( E^c \frac{\partial \Phi}{\partial E^c} \right) \left( \eta_{ab} \delta^{bc} \frac{\partial^2 \Phi}{\partial E^c \partial E^d} dE^a dE^d \right). \quad (5.16)$$

In our case we consider a 5 dimensional phase space with the coordinates  $Z_A = \{M, S, \beta, T, \Theta\}$ , where  $S, \beta$  are extensive variables and  $T, \Theta$  are their dual intensive variables. Then we have the fundamental Gibbs one form as,

$$\Theta = dM - TdS - \Psi d\beta. \quad (5.17)$$

Now we can write the Quevedo metric as follows,

$$g^Q = (SM_S + \beta M_\beta) \begin{bmatrix} -M_{SS} & 0 \\ 0 & M_{\beta\beta} \end{bmatrix}. \quad (5.18)$$

Using the Quevedo metric, we calculate the corresponding curvature, which is a com-

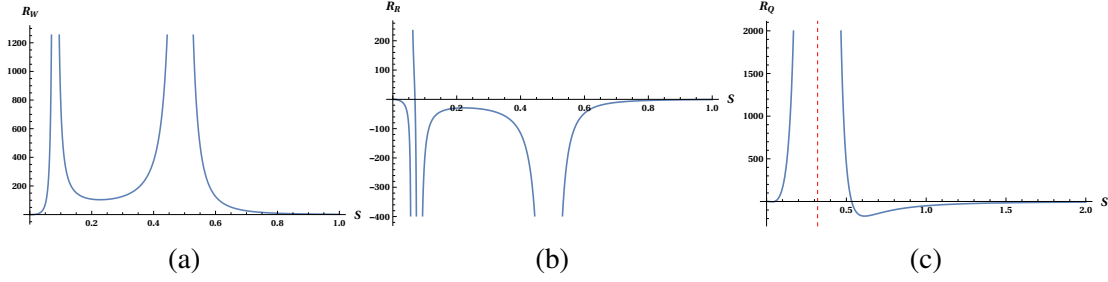


Figure 5.6: Curvature divergence plots for Weinhold (Fig. 5.6a), Ruppeiner (Fig. 5.6b) and Quevedo metric (5.6c) around critical point ( $a = 0.5, \beta = 0.1$  and  $P_c = 0.207$ ).

plicated expression having the following form,

$$R_Q = \frac{f(S, \beta, P, a)}{g(S, \beta, P, a)}, \quad (5.19)$$

which is interesting as it has a diverging behavior. Using the plots of curvature scalar  $R_Q$ , we investigate the divergence. In Fig.5.6c, we can see a divergence peaked at  $S \approx 0.32$ , same as in the specific heat case. Contrary to what we obtained in Weinhold and Ruppeiner geometries, the singular point of curvature scalar in geometrothermodynamics exactly matches the specific heat singular point.

## 5.4 Conclusion

In this chapter, we have studied thermodynamics and thermodynamic geometry of a regular Bardeen-AdS black hole surrounded by a quintessence. In the thermodynamic study, we observed a critical behavior from  $P - v$  and  $T - S$  plots. Further confirmation was obtained from the specific heat plots. The discontinuity in the specific heat at  $S = 0.32$  indicates a phase transition of the system. We analyzed the effect of quintessence in the phase transitions through the state parameter  $\omega$ . The critical values for pressure ( $P_c$ ), volume ( $v_c$ ) and temperature ( $T_c$ ) are obtained for  $\omega = -1, -\frac{2}{3}$  and  $-\frac{1}{3}$  case. The ratio  $\frac{P_c v_c}{T_c}$  showed slight decrease with increase of  $\omega$  from -1 to  $-\frac{1}{3}$ .

Following the study of black hole phase transition in the thermodynamic approach, we carried out the geometrical investigation of the same. In the literature, it is a well-known fact that the divergence behavior of curvature scalar also reflects the existence of critical points. If we accept that the criticality of specific heat is the definition of phase transition, the thermodynamic geometry, which shows divergence at the same point,

turns out to be the correct geometrical description of the same phenomena. For the metric under consideration, we found that, even though the Ruppeiner and Weinhold geometries reflect the singularity of curvature scalar, it can only be taken as the indication of phase transition but not the accurate description of the same, as the diverging points do not coincide with that of specific heat. There were multiple divergence and mismatch in the thermodynamic scalar of Weinhold and Ruppeiner geometries. This indicates an anomaly; to overcome this we have used Quevado's geometrothermodynamics. The main problem with the Weinhold and Ruppeiner geometry is that they were not Legendre invariant and thus depend on the choice of thermodynamic potential. However, geometrothermodynamics being Legendre invariant, reproduces critical point exactly.





# Chapter 6

## Heat engine in the Regular AdS black holes surrounded by Quintessence

Summary

---

*This chapter is an edited version of our article (Rajani et al. 2020). We investigate heat engine models constructed in the regular Bardeen-AdS black hole with quintessence. The presence of a quintessence field improves the heat engine efficiency significantly. An analytical expression for heat engine efficiency is derived in terms of the quintessence dark energy parameters. We find that the quintessence parameter  $a$  increases the efficiency, whereas the state parameter  $\omega_q$  decreases the efficiency.*

---

### 6.1 Introduction

The discovery of the heat engine was a revolution in human history. It was a time when people cannot imagine a machine moving on its-own without a horse in front. Even though rudimentary models were there from 1st century, it was firstly idealized by Nicolas Sadi Carnot in 1824. A heat engine converts the heat available from a heat source (hot reservoir) to mechanical work, and the remaining heat is rejected to a heat sink (cold reservoir) at a lower temperature. A working substance in the engine is brought from a higher state temperature to a lower state temperature. Any substance with non-zero heat capacity can be chosen as a working substance, usually a gas or

liquid. It generates work while transferring heat to the colder sink. During the process, the working substance goes through a cycle, e.g., Stirling cycle, Otto cycle, Diesel cycle. These heat engines are used in automobiles and thermal power stations; even there are some natural heat engines.

Black holes being a thermal system exhibiting van der Waals fluid analogy, it is natural to construct a heat engine out of black holes. Such an innovative engine known as *holographic heat engine* is designed recently by Clifford V. Johnson (Johnson 2014). Holographic is termed due to the significance of heat engine in the holographic picture of spacetime. The heat cycles in bulk trigger a renormalization flow in the dual field theory. Thus, the holographic heat engine fills the missing link between extended thermodynamics and holography. These phenomena can happen only in systems with large degrees of freedom where thermal effects dominate over quantum ones. Black hole as a heat engine is in particular, exhibits this thermal dominance. This proposal has drawn considerable attention and the concept of holographic heat engines were later generalised to various other black holes (Jafarzade and Sadeghi 2017, Setare and Adami 2015, Johnson 2016a, Zhang and Liu 2016, Johnson 2016b, Belhaj et al. 2015, Wei and Liu 2017, Mo and Li 2018, Hendi et al. 2018, Xu et al. 2017, Mo et al. 2017, Hennigar et al. 2017, Zhang et al. 2018, Yerra and Bhamidipati 2020a, Yerra and Chandrasekhar 2019).

In this chapter, we extend the concept of a heat engine to regular Bardeen AdS black hole, which possesses no singularity at the origin. A further effect of the quintessence field on efficiency is also studied. This chapter is organized as follows. In section (Sec.6.2), we discuss the heat engine model in the regular Bardeen AdS black hole. In section (Sec.6.3), regular black holes with quintessence is considered, and their effect on efficiency is scrutinized. The chapter ends with results and discussions, which are presented in section (Sec.6.4).

## 6.2 Regular black hole as a Heat Engine

In this section, we calculate the efficiency of the heat engine constructed by taking regular Bardeen AdS black hole as a working substance. As shown in Fig. 6.1b, a simple heat cycle includes a pair of isotherms at high temperature  $T_H$  and low temperature  $T_C$ .

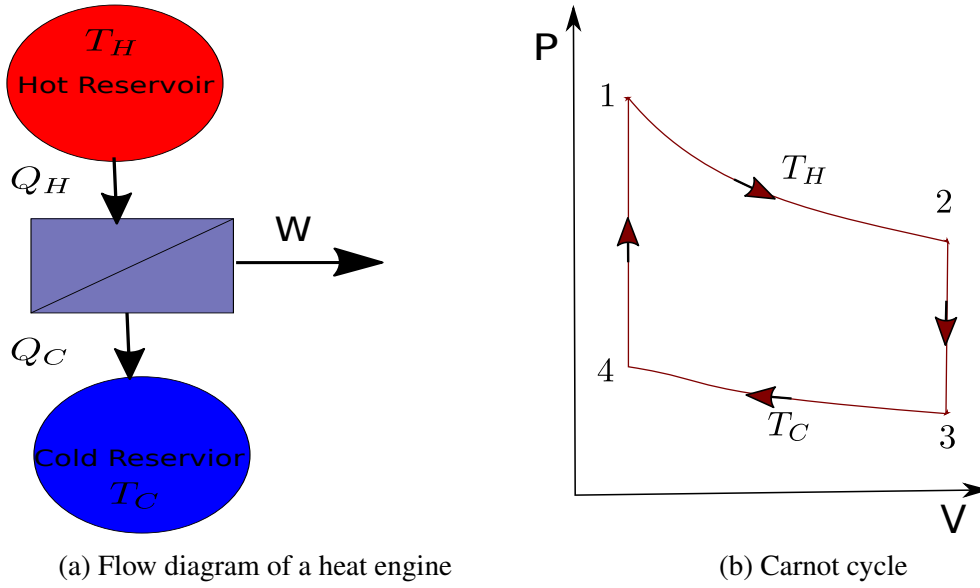


Figure 6.1: Schematic diagram of a traditional heat engine

These two paths are connected either by isochoric(constant volume) paths as in Stirling cycle or adiabatic(no heat exchange) paths as in Carnot cycle. During isothermal expansion, ( $1 \rightarrow 2$ ),  $Q_H$  amount of heat is being absorbed, and it will exhaust  $Q_C$  amount of heat during isothermal compression ( $3 \rightarrow 4$ ). The paths ( $2 \rightarrow 3$ ) and ( $4 \rightarrow 1$ ) are isochoric paths. But for static black holes, entropy and volume are dependent on each other. So adiabats and isochores are alike, meaning no difference between the Carnot engine and Stirling engine. The efficiency of the heat engine is given by,

$$\eta = \frac{W}{Q_H} = \frac{\oint PdV}{Q_H}. \quad (6.1)$$

It can be compared with the efficiency Carnot heat engine cycle  $\eta_c$ , which is the theoretical maximum possible value.

$$\eta_c = 1 - \frac{Q_C}{Q_H} = 1 - \frac{T_C}{T_H}. \quad (6.2)$$

The total work done along one complete cycle can be obtained as,

$$\begin{aligned} W_{tot} &= W_{1 \rightarrow 2} + W_{3 \rightarrow 4} = P_1(V_2 - V_1) + P_4(V_4 - V_3) \\ &= \frac{4(P_1 - P_4) \left( (\pi\beta^2 + S_2)^{3/2} - (\pi\beta^2 + S_1)^{3/2} \right)}{3\sqrt{\pi}}. \end{aligned} \quad (6.3)$$

For static black holes, the heat capacity at constant volume  $C_V = 0$ . From that, one can conclude that no heat exchange takes place in the isochoric paths ( $2 \rightarrow 3$ ) and ( $4 \rightarrow 1$ ). Therefore we have to compute heat exchanged  $Q_H$  during the isothermal process  $1 \rightarrow 2$ ,

$$\begin{aligned} Q_H &= \int_{T_1}^{T_2} C_P(P_1, T) dT = \int_{S_1}^{S_2} C_P \left( \frac{\partial T}{\partial S} \right) dS = \int_{S_1}^{S_2} T dS = M_2 - M_1, \\ &= \frac{(\pi\beta^2 + S_2)^{3/2} (8P_1 S_2 + 3)}{6\sqrt{\pi} S_2} - \frac{(\pi\beta^2 + S_1)^{3/2} (8P_1 S_1 + 3)}{6\sqrt{\pi} S_1}. \end{aligned} \quad (6.4)$$

Using eqn. 6.1, eqn.6.3 and eqn. 6.4, the efficiency of the engine is calculated as,

$$\eta = \frac{W}{Q_H} = \frac{8(P_1 - P_4) \left( (\pi\beta^2 + S_2)^{3/2} - (\pi\beta^2 + S_1)^{3/2} \right)}{\frac{(\pi\beta^2 + S_2)^{3/2} (8P_1 S_2 + 3)}{S_2} - \frac{(\pi\beta^2 + S_1)^{3/2} (8P_1 S_1 + 3)}{S_1}}. \quad (6.5)$$

The upper bound of efficiency is set by the Carnot cycle, which is obtained from eqn.6.2. As we can observe from schematic diagram (Fig. 6.1b), higher temperature  $T_H$  is  $T_2$  and lower temperature  $T_C$  is  $T_4$ . Hence the Carnot engine efficiency is,

$$\eta_C = 1 - \frac{\sqrt{S_2} (\pi\beta^2 + S_2) (-2\pi\beta^2 + 8P_4 S_1^2 + S_1)}{\sqrt{S_1} (\pi\beta^2 + S_1) (-2\pi\beta^2 + 8P_1 S_2^2 + S_2)}. \quad (6.6)$$

The efficiency  $\eta$  and the ratio  $\eta/\eta_C$  are plotted against entropy  $S_2$  using eqn.6.5 and eqn.6.6. As we can see in Fig. 6.2a the heat engine efficiency monotonously increases with  $S_2$  (corresponding volume  $V_2$ ) for all values of  $\beta$ , which implies that the increase in volume difference between small black hole ( $V_1$ ) and large black hole ( $V_2$ ) increases the efficiency. However, this trend does not continue forever as the efficiency reaches saturation values after a certain value of  $S_2$ . The dependence on charge  $\beta$  also visible from the same figure; the rates of increment are different for different  $\beta$  values. The

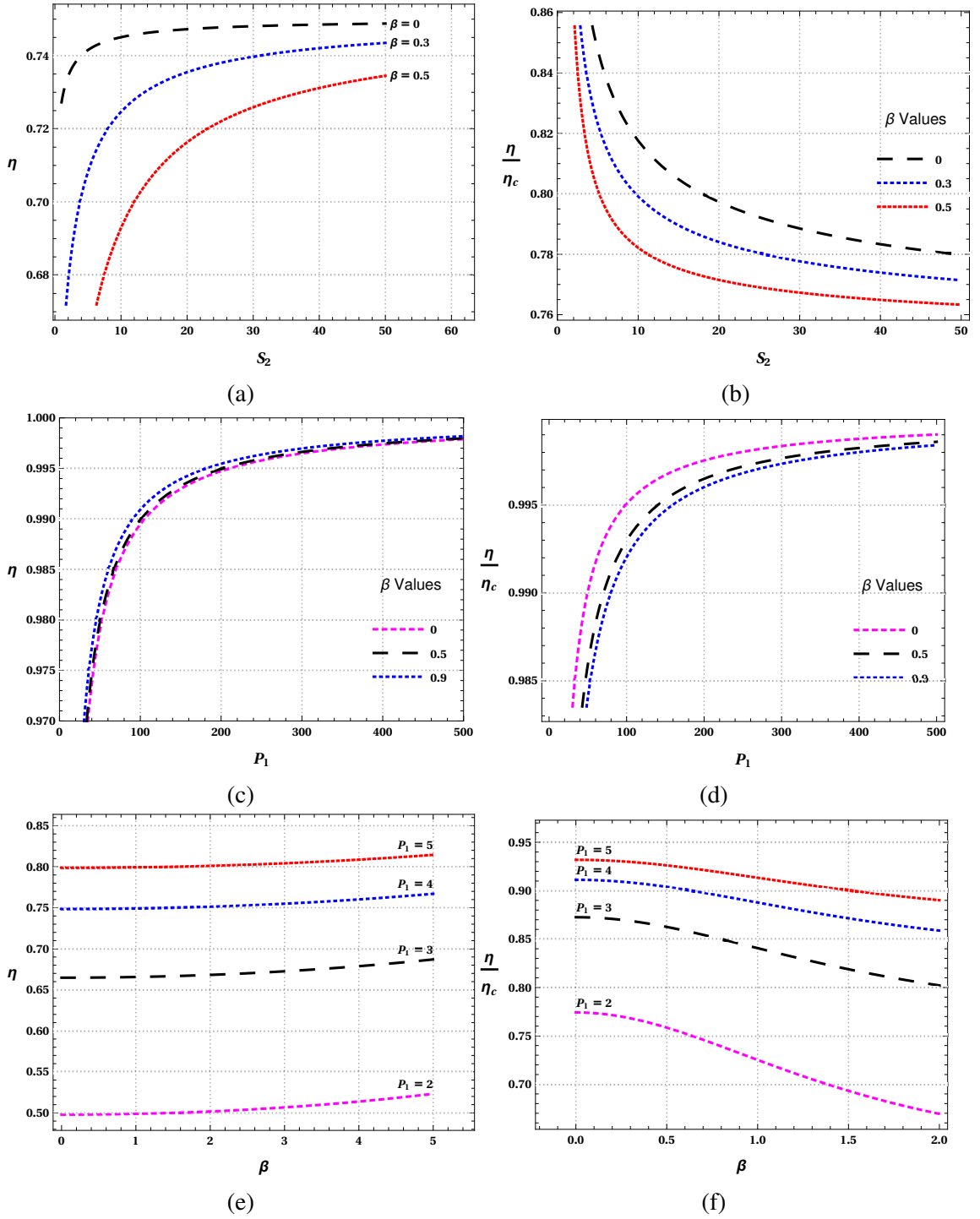


Figure 6.2: The variation of efficiency  $\eta$  of the engine with regular Bardeen black hole as the working substance and the ratio  $\eta/\eta_c$  with different variables. In Fig. 6.2a and 6.2b, the entropy dependence is shown with different values of  $\beta$ . Here we take  $P_1 = 4, P_4 = 1$  and  $S_1 = 1$ . In the second set of figures Fig. 6.2c and Fig. 6.2d, the variation with pressure is studied with different values of  $\beta$ . In this case we take  $P_4 = 1, S_2 = 4$  and  $S_1 = 1$ . In the last set figure Fig. 6.2e and Fig. 6.2f, the behavior against charge  $\beta$  with different values of  $P_1$  is displayed. Here we take  $S_2 = 20, P_4 = 1$  and  $S_1 = 10$ . The parameters  $P_1, P_4, S_1$  and  $S_4$  are chosen accordingly for the proper display of the nature of the plots.

plot  $\eta/\eta_C$  versus  $S_2$  in Fig. 6.2b is consistent with second law, as it is bounded below 1. With the increase in charge  $\beta$ , the ratio decreases. We also investigate the dependence of efficiency  $\eta$  on pressure  $P_1$ , the pressure at the source, which is shown in Fig. 6.2c and 6.2d. Those two figures clearly show that the efficiency of the engine will approach the maximum possible value as the pressure approaches infinity. Before concluding this section, we also mention that the monopole charge  $\beta$  has a positive effect on efficiency, i.e., the higher the charge, the higher is the efficiency (Fig. 6.2e, Fig. 6.2f).

### 6.3 Influence of Quintessence on efficiency

Following the work of Hang Liu and Meng, we study the effect of dark energy on thermodynamics and heat engine efficiency of regular black holes (Liu and Meng 2017). Quintessence is one of the candidates for dark energy, which leads to the accelerated expansion of the universe (Kiselev 2003, Tsujikawa 2013). The real scalar field acts as a cosmic source having equation of state  $p_q = \omega_q \rho_q$  ( $-1 < \omega_q < -1/3$ ). The density of quintessence field is given by,

$$\rho_q = -\frac{a}{2} \frac{3\omega_q}{r^{3(\omega_q+1)}}. \quad (6.7)$$

Kiselev was the first one to study the effects of quintessence on a black hole (Kiselev 2003). Since then, there were many studies in black holes surrounded by quintessence, to mention a few, in the contexts of gauge gravity duality (Chen et al. 2013) and quasi-normal modes (Chen and Jing 2005). Phase transitions in Reissner-Nordström and regular black holes with this exotic field were also studied (Yi-Huan and Zhong-Hui 2011, Thomas et al. 2012, Li 2014, Fan 2017, Saleh et al. 2018, Rodrigue et al. 2020). When we include quintessence term in the metric of regular Bardeen AdS black hole,  $f(r)$  is modified to

$$f(r) = 1 - \frac{2Mr^2}{(\beta^2 + r^2)^{3/2}} - \frac{a}{r^{3\omega_q+1}} - \frac{\Lambda r^2}{3}. \quad (6.8)$$

Where  $a$  is the normalization constant or strength parameter related to quintessence density and  $\omega_q$  is the state parameter. Now we proceed as in the earlier sections to

obtain an expression for the efficiency of the engine. Using the defining condition of an event horizon,  $f(r_h) = 0$ , one can calculate the black hole mass as

$$M = -\frac{1}{6} (\beta^2 + r_h^2)^{3/2} r^{-3(\omega_q+1)} \left( 3a + (-8\pi P r_h^2 - 3) r_h^{3\omega_q+1} \right). \quad (6.9)$$

We can write the expression for temperature as,

$$T = \frac{r_h^{-3\omega_q-2} \left( 3a (\beta^2 (\omega_q + 1) + r_h^2 \omega_q) + r_h^{3\omega_q+1} (-2\beta^2 + 8\pi P r_h^4 + r_h^2) \right)}{4\pi (\beta^2 + r_h^2)}. \quad (6.10)$$

The heat capacity at constant pressure is,

$$C_P = \frac{2S(\pi\beta^2+S) \left( 3a\pi^{\frac{3\omega_q+1}{2}} (\pi\beta^2(\omega_q+1)+S\omega_q) + S^{\frac{3\omega_q+1}{2}} (-2\pi\beta^2+8PS^2+S) \right)}{S^{\frac{3\omega_q+1}{2}} f_1(S) - 3a\pi^{\frac{3\omega_q+1}{2}} f_2(S)}, \quad (6.11)$$

where,

$$\begin{aligned} f_1(S) &= (2\pi^2\beta^4 + \pi\beta^2S(24PS + 7) + S^2(8PS - 1)), \\ f_2(S) &= (\pi^2\beta^4(3\omega_q^2 + 5\omega_q + 2) + \pi\beta^2S(6\omega_q^2 + 7\omega_q + 4) + S^2\omega_q(3\omega_q + 2)). \end{aligned}$$

Then we compute the heat  $Q_H$  along the process  $1 \rightarrow 2$  (the earlier arguments on no heat transfer for isochoric processes still holds),

$$\begin{aligned} Q_H &= \int_{T_1}^{T_2} C_P(P_1, T) dT = M_2 - M_1, \\ &= \frac{1}{6\sqrt{\pi}} \left\{ (\pi\beta^2 + S_1)^{3/2} S_1^{-\frac{3}{2}(\omega_q+1)} \left[ 3a\pi^{\frac{3\omega_q+1}{2}} - (8P_1S_1 + 3)S_1^{\frac{3\omega_q+1}{2}} \right] \right. \\ &\quad \left. + (\pi\beta^2 + S_2)^{3/2} S_2^{-\frac{3}{2}(\omega_q+1)} \left[ (8P_1S_2 + 3)S_2^{\frac{3\omega_q+1}{2}} - 3a\pi^{\frac{3\omega_q+1}{2}} \right] \right\}. \quad (6.12) \end{aligned}$$

Having all the required quantities, the heat engine efficiency is expressed in terms of quintessence parameters  $a$  and  $\omega_q$  as,

$$\eta = \frac{8(P_1 - P_4) \left( (\pi\beta^2 + S_2)^{3/2} - (\pi\beta^2 + S_1)^{3/2} \right)}{f(S_1) + f(S_2)}. \quad (6.13)$$

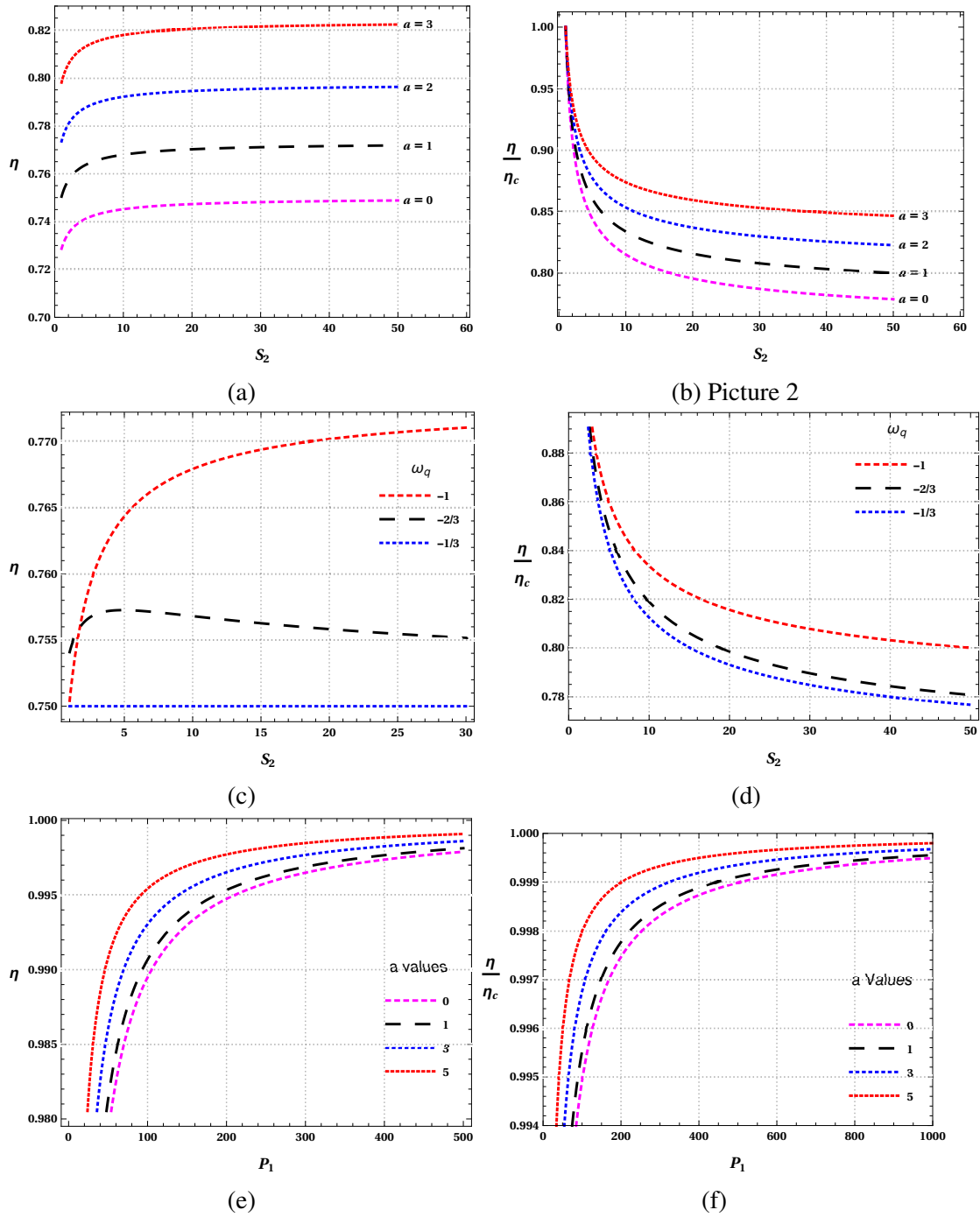


Figure 6.3: *The effect of quintessence on the efficiency  $\eta$  of the engine and on the ratio  $\eta/\eta_c$  with different variables. In the first set of figures Fig.6.3a and Fig.6.3b, the variation with entropy is displayed with different values of  $a$ . Here we take  $P_1 = 4, P_4 = 1, S_1 = 1, \omega_q = -1$  and  $\beta = 0.1$ . In the second set of figures Fig.6.3c and Fig.6.3d, the variation with entropy for different values of  $\omega_q$  is shown. In this case we take  $P_1 = 4, P_4 = 1, S_1 = 1, a = 1$  and  $\beta = 0.1$ . In the last set Fig. 6.3e and Fig. 6.3f, the dependence on pressure for different values of  $a$  is observed with  $P_4 = 1, S_1 = 1, S_2 = 4, \omega_q = -1$  and  $\beta = 0.1$ . Here also the fixed parameters are chosen appropriately for the proper observation of the effect.*



where

$$f(S) = (\pi\beta^2 + S)^{\frac{3}{2}} S^{-\frac{3}{2}(\omega_q+1)} \left[ 3a\pi^{\frac{3\omega_q}{2}+\frac{1}{2}} - (8P_1S + 3)S^{\frac{3\omega_q}{2}+\frac{1}{2}} \right].$$

The efficiency of the Carnot engine is also obtained as earlier,

$$\eta_C = 1 - \frac{(\pi\beta^2 + S_2) S_1^{-\frac{3\omega_q}{2}-1} S_2^{\frac{3\omega_q}{2}+1} g(S_1, P_4)}{(\pi\beta^2 + S_1) g(S_2, P_1)}, \quad (6.14)$$

where,

$$g(S, P) = \left( 3a\pi^{\frac{3\omega_q}{2}+\frac{1}{2}} (\pi\beta^2(\omega_q + 1) + S\omega_q) + S^{\frac{3\omega_q}{2}+\frac{1}{2}} (-2\pi\beta^2 + 8PS^2 + S) \right).$$

The heat engine efficiency depends on pressure  $P$ , entropy  $S$ , monopole charge  $\beta$  and quintessence parameters  $a$  and  $\omega_q$ . The above expressions reduce to the previous case when quintessence parameters  $a = 0$  and  $\omega_q = 0$ . There is a significant increment in the efficiency against  $S_2$  when we increase the quintessence strength  $a$  with other parameters being fixed (Fig. 6.3a). This change is visible in the ratio plot also (Fig. 6.3b). The plot for efficiency versus  $S_2$  for different values of  $\omega_q$  show similar functional behaviour in Fig. 6.3c and Fig. 6.3d. But there is a difference in the physical effect; higher values of  $\omega_q$  lead to smaller efficiency. With  $\omega_q = -1$ , the black hole shows higher efficiency than  $\omega_q = -1/3$  case, where efficiency takes a constant value of 0.75. This is not a surprising result because the quintessence density ( $\rho_q$ ) decreases with an increase in  $\omega_q$  (6.7). Then we study the role of pressure  $P_1$  on  $\eta$  and  $\eta/\eta_C$  with different values of quintessence strength  $a$  shown in Fig.6.3e and Fig.6.3f, where the functional appearance remains same. The efficiency and its ratio improve with higher pressures and with quintessence. But it is noticed that there is a faster convergence to limiting value 1 in the quintessence case. The effect of quintessence on the efficiency of a regular black hole heat engine is summarised in Table6.1.

At the final stage of our investigation, we focus on the action of quintessence parameter  $a$  and  $\omega_q$ . For all three values of  $\omega_q$ , efficiency increases exponentially when it is plotted against quintessence constant  $a$  (Fig.6.4a). The scenario remains the same for the ratio plot, with an exception at  $\omega_q = -1/3$ , which has a slight decaying nature

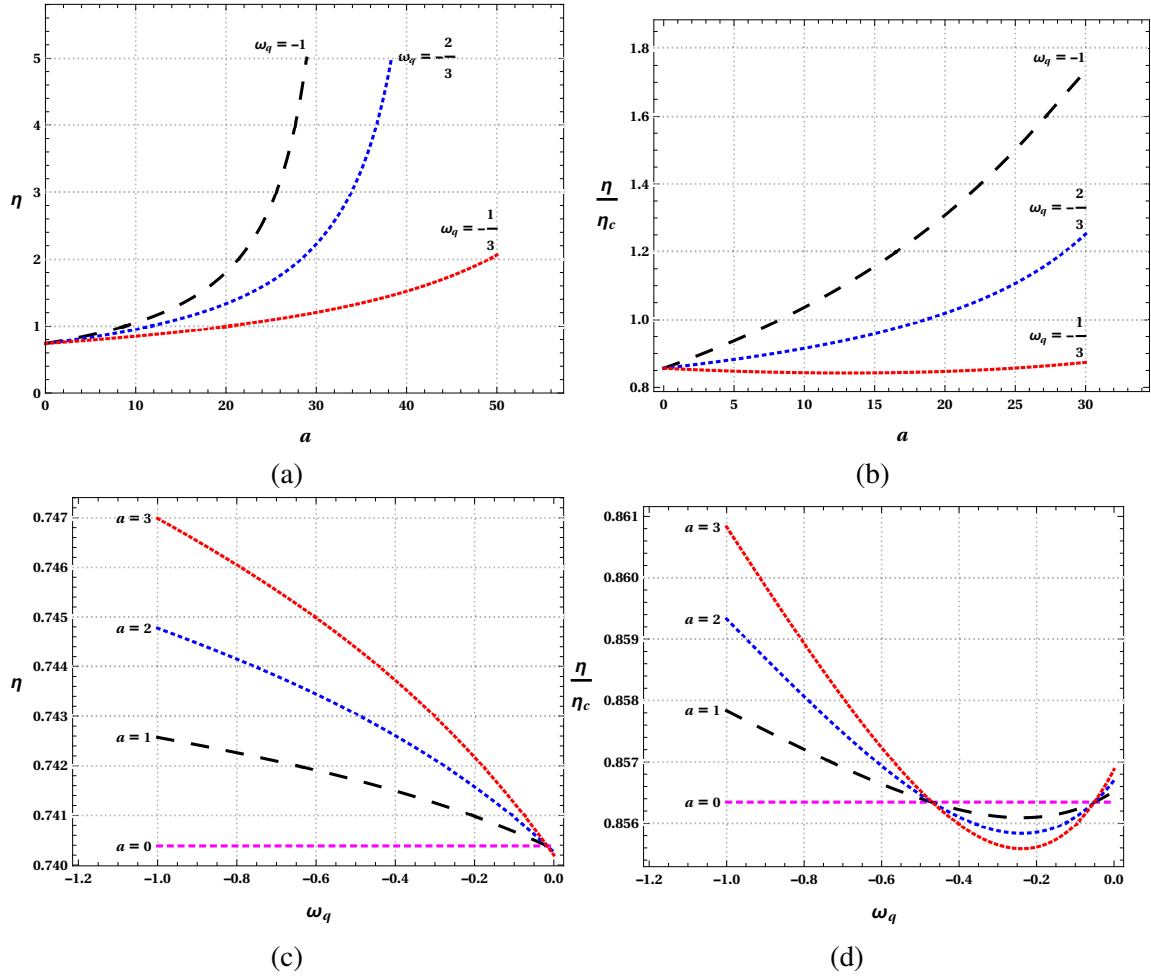


Figure 6.4: *The effect of quintessence on the efficiency  $\eta$  of the engine and on the ratio  $\eta/\eta_c$  with different variables. In the Fig.6.4a and Fig.6.4b the dependence on  $a$  is studied with different values of  $\omega_q$ . Here we take  $P_1 = 4, P_4 = 1, S_1 = 1, S_2 = 4$  and  $\beta = 0.1$ . In the second set of figures (Fig.6.4c and Fig.6.4d) behaviour against state parameter  $\omega$  with different values of  $a$  is shown. In this case we take  $P_1 = 4, P_4 = 1, S_1 = 1, S_2 = 4$  and  $\beta = 0.1$ .*

Table 6.1: Deviation in heat engine efficiency  $\eta$ , with variation of quintessence equation of state parameter  $\omega_q$  and strength parameter  $a$ .

$a$	$\omega_q$	$\eta$	$a$	$\omega_q$	$\eta$
1	-1/3	0.800	3	-1/3	0.804
1	-2/3	0.809	3	-2/3	0.833
1	-1	0.817	3	-1	0.859

initially (Fig.6.4b). We note that in these two plots, the efficiency shoots over unity which is a clear violation of the second law of thermodynamics. To avoid this unphysical situation we must be careful enough to choose quintessence parameters. In Fig.6.4c and Fig.6.4d, we present the effect of  $\omega_q$  on  $\eta$  and  $\eta/\eta_C$  for different values of  $a$ . In the light of earlier point, quintessence density ( $\rho_q$ ) decreases with increasing  $\omega_q$ , the efficiency is higher for smaller values of  $\omega_q$ . This inference is drawn by considering the physically meaningful range  $-1 < \omega_q < -1/3$ .

## 6.4 Conclusions and Discussions

Regular black holes are of great interest in physics as they do not possess singularity. In this chapter, we demonstrated that the regular Bardeen AdS black hole could be used as an engine to extract energy. The efficiency of the engine is improved by immersing the black hole system in a quintessential field, which has the motivations from cosmology where quintessence can be interpreted as a candidate for dark energy.

In this chapter, we constructed a heat engine by taking the regular Bardeen black hole as a working substance. A cycle in the  $P - V$  plane is assigned for the black hole with two isotherms and isochores. The efficiency of the engine is calculated by using the work is done and heat absorbed during the cycle. As it is customary to compare the efficiency of any engine with the Carnot engine, we have compared our results with the corresponding Carnot efficiency. Detailed analysis of the dependence of efficiency  $\eta$  on  $S_2$  (entropy of LBH phase),  $P_1$  (pressure in SBH phase) and  $\beta$  (monopole charge) are done. Among the several observations, we emphasize that the increase in entropy difference between the SBH phase ( $S_1$ ) and LBH phase ( $S_2$ ) increases the efficiency of the engine. We have made a successful attempt to improve the efficiency of the engine

by adding a quintessence field. The heat engine efficiency depends on the quintessence parameters  $\omega_q$  and  $a$ . We have presented a detailed discussion on the improvement of engine efficiency with quintessence parameters. The quintessence parameter  $a$  increases the efficiency, and  $\omega_q$  decreases the efficiency  $\eta$ . We observed a drop in the efficiency  $\eta$  in the quintessence range  $-1 < \omega_q < -1/3$ . This happens because quintessence matter density ( $\rho_q$ ) decreases with an increase in  $\omega_q$  value. It is worth mentioning that accelerated expansion of the universe takes place in this quintessence range of  $\omega_q$ . And in this range, the presence of quintessence matter around the black hole improves the efficiency of the heat engine. The effect of intensity of quintessential matter field on the heat engine efficiency of regular black holes underlines the importance of quintessence in black hole thermodynamics. This result is promising when one considers the quintessence as a viable model for dark energy. We expect that our study in this regard will shed light on the thermodynamics of quintessential AdS black holes.

# Chapter 7

## Summary and Future Work

---

*“And I cherish more than anything else the Analogies, my most trustworthy masters. They know all the secrets of Nature, and they ought to be least neglected in Geometry” - Johannes Kepler*

---

This thesis focuses on aspects of black hole thermodynamics in anti-de Sitter spacetime. Black hole thermodynamics is a subject that helps a theoretical physicist to unveil the deep connection between gravitation, quantum theory, and statistical physics. The subject is mainly motivated by the emergent nature of spacetime. The gravitational field does not possess any fundamental degrees of freedom, rather emerges as an effective theory of an underlying many-body system. These ideas are well understood in anti-de Sitter (AdS) space, where AdS-gravity finds a dual conformal field theoretic (CFT) description on its boundary. The *AdS/CFT* correspondence appears to be an outcome of spacetime’s emergent nature from a non-gravitational condensed matter system. We were motivated by the emergent gravity approach proposed by T. Jacobson and several others, based on the connection between horizon thermodynamics and gravity. This approach does not invoke any quantum gravity theory and relies on Boltzmann’s argument “If you can heat it, it should have a microstructure”. So the existence of horizon temperature directly implies ‘atoms of spacetime’ at the microstructure. But as in hydrodynamics, gravity is very immune to these ‘atoms of spacetime.’ Inspired by these

advances, we have focused our studies on black hole thermodynamics, mainly the van der Waals fluid analogy of the horizon.

The thermodynamics of black holes in AdS spacetime was devoid of the consistency between the first law and Smarr relation. The required consistency is brought by treating the cosmological constant ( $\Lambda$ ) as a thermodynamical variable, pressure. With the identification, the black hole phase space is extended with the  $PdV$  term in the first-law. This has to lead to a new arena of *black hole chemistry*. In the extended phase space, the asymptotically AdS black holes undergo a vdW like first-order phase transition between a *small black hole* (SBH) and *large black hole* phase (LBH). Subsequently, an enormous amount of research conducted in phase transitions of asymptotically-AdS black holes found that all belong to the same universality class of the vdW system. In addition, we have also analyzed other manifestations of vdW fluid analogy, including Joule-Thomson expansion and heat engine in asymptotically AdS black holes.

In the first chapter of the thesis, a brief history of theoretical physics is presented; also, the properties of AdS space and its CFT correspondence is introduced. In the second chapter, we have reviewed the laws of black hole thermodynamics in light of Komar Integrals and charge conservations in gravity. In the later parts of the chapter, an extended version of thermodynamics in the AdS space is analyzed using the concept of black hole enthalpy.

In chapter 3, we have studied the thermodynamics of charged AdS black holes in the presence of a global monopole. A detailed analysis of critical behavior in the black hole is carried out. The classical van der Waals analogy is drawn from  $P - v$  isotherms which is followed by Gibbs free energy study and coexistence curves. The critical exponents calculated, matches with the universality class. In the last section of the chapter, we have included the study of Joule-Thomson (JT) expansion in the presence of a global monopole. During the JT expansion, the mass remains constant, so it is also called the isenthalpic process. This process will result in either heating or cooling in the final phase. We studied the effect of the global monopole parameter on the inversion tem-

perature and isenthalpic curves. The obtained result is compared with Joule–Thomson expansion of van der Waals fluid and the similarities were noted. It is observed that the presence of a global monopole has a drastic effect on the JT coefficient.

In chapter 4, we have extended our studies to regular Bardeen black holes. The stable SBH and LBH phase, metastable superheated SBH and supercooled LBH phase, and supercritical phases are analyzed deeply through numerical techniques. Further, using the novel Ruppeiner geometry, we have studied the microscopic interactions in the stable phases. A difference in the microscopic interaction is found in the SBH phase. There exists a repulsive interaction in the SBH phase during the low-temperature regime.

The study of black hole thermodynamics of regular black holes is continued in chapter 5 with an additional quintessence field. The critical behavior and effect of the quintessence parameter is scrutinized. It is observed that the quintessence parameter shifts the transition to the lower entropy values. In the second part of the chapter, the concept of thermodynamic geometry is applied. Using the Ruppeiner, Weinhold, and Quevedo geometry, the curvature scalar divergence is analyzed. It is found that in the quintessence black hole case, the divergence in the curvature scalar of Ruppeiner and Weinhold metric does not represent the phase transition. The Quevedo metric is more suitable here as the curvature scalar divergence matches with the specific heat studies.

In chapter 6, taking the vdW analogy further, a black hole heat engine is constructed in a regular Bardeen black hole. The efficiency of the engine is calculated using the work done and heat absorbed during the process. In the final sections of the chapter, the heat engine efficiency is improved by adding a quintessence field. Then the analytical expression for the efficiency is calculated in terms of quintessence parameters. Besides the natural extension of black hole thermodynamics, the study of a heat engine is significant in the holographic picture of spacetime. The heat cycles in bulk trigger a renormalization flow in the dual field theory. Thus, the holographic heat engine fills the missing link between extended thermodynamics and holography.

Besides the works mentioned in the thesis chapters, we have done some work on photon orbits and Reentrant phase transitions (RPT) in AdS black holes. In photon orbit studies on regular black holes, we found that the photon orbit radius and minimum impact parameter have some signatures of the phase transition in extended phase space. Our study hints at a relationship between gravity and thermodynamics (Naveena Kumara et al. 2020a, Hegde et al. 2020). We have also worked out Reentrant phase transitions in Born-Infeld AdS black holes (Naveena Kumara et al. 2021). RPT is another fascinating feature observed in nicotine/water mixture, nematic/smectic liquid crystals, etc., where a monotonic change in the thermodynamic variable results in two (or more) phases, with the same initial and final macrostate. A similar kind of *RPT* occurs in black holes between Large /Intermediate/Large black hole phases. The motivation behind that was to find out the underlying micro-molecules behind this exotic phenomenon using Ruppeiner’s phenomenological approach. Apart from these works, we have recently written an article on the BSW (Banados, Silk, and West) mechanism for rotating black holes with an anisotropic matter field (Ahmed Rizwan et al. 2020a). It is shown that a rotating black hole can act as a particle accelerator, which appeared as a possible candidate for highly energetic astrophysical phenomena like active galactic nuclei, gamma-ray bursts, and ultrahigh-energy cosmic rays.

## Outlook and Future Directions

Recent progress in astrophysical research from LIGO/Virgo collaborations and event horizon telescope (EHT) has inspired us to search signatures for black hole thermodynamics from the observational data. During the ring-down phase of binary black hole mergers, a perturbed black hole emits gravitational waves in the form of quasinormal radiation. There exists a connection between photon orbit radius measured from EHT and quasinormal modes observed in GW events. One can find a relation by calculating the Lyapunov exponent associated with divergence of radial velocity and imaginary parts of QNMs. Interestingly, the Lyapunov exponent comes in quantum gravity theories as the out-of-time ordered correlators which measure the amount of chaos. There are several ways to extend our work,

1. An immediate and interesting extension would be the study of the vdW like be-



havior and other manifestations of the analogy in light of gauge/gravity duality. Mainly to ponder the reasons behind the phase transitions in black holes on the grounds of quantum theories of gravity.

2. Another possibility is to further extend the vdW-like fluid analogy of black holes to other exotic everyday phenomena. That can establish a new link between black hole physics and many-body systems.
3. Another direction is the thermodynamics in de Sitter spacetime, which is more sensible in cosmology. Holographic heat engine and Joule-Thomson expansion can find a new meaning in the de-Sitter patch of the universe.
4. Finally, with the availability of data from Ligo/Virgo and EHT, I hope to link these observational aspects with quantum gravity theories. In particular, black hole shadow, quasinormal modes, and echoes have a deep connection with AdS/CFT correspondence. One of the directions in this regard is through the Lyapunov exponent. Holographic dual operator for out-of-time-ordered-correlator can answer at least some questions.



# Appendices



# Appendix A

## Differential Forms

A differential  $p$ -form is an antisymmetric  $(0, p)$  tensor. In an  $n$ -dimensional space-time, there are  $\frac{n!}{p!(n-p)!}$  linearly independent  $p$ -forms. Meaning in 4-dimensions, there can be one independent 0-form and four 1-forms. The advantage of writing in the language of differential form is that it can be integrated and differentiated in an elegant way. From  $p$ -form  $A$  and  $q$ -form  $B$ , we can form a  $p + q$  form by taking the wedge product  $A \wedge B$ , which is an antisymmetric tensor product.

$$(A \wedge B)_{\mu_1 \dots \mu_{p+q}} = \frac{(p+q)!}{p!q!} A_{[\mu_1 \dots \mu_p} B_{\mu_{p+1} \dots \mu_{p+q}]} \quad (\text{A.1})$$

In case of wedge product of two 1-forms,

$$(A \wedge B)_{\mu\nu} = A_\mu B_\nu - A_\nu B_\mu = 2A_{[\mu} B_{\nu]} \quad (\text{A.2})$$

The exterior derivative turns a  $p$ -form into  $p + 1$  form by antisymmetrised partial differentiation and it is a tensor.

$$(dA)_{\mu_1 \dots \mu_{p+1}} = (p+1) \partial_{[\mu_1} A_{\mu_2 \dots \mu_{p+1}]} \quad (\text{A.3})$$

The exterior derivative of a 0-form is simply a gradient,

$$(d\phi)_\mu = \partial_\mu \phi \quad (\text{A.4})$$

For product of a  $p$ -form  $A$  and  $q$ -form  $B$ , exterior derivative is given by

$$d(A \wedge B) = (dA) \wedge B + (-1)^p A \wedge (dB). \quad (\text{A.5})$$

Another operation on an  $n$ -dimensional manifold is the Hodge duality, done using a Hodge dual star operator which maps a  $p$ -form to a  $(n-p)$ form,

$$(*A)_{\mu_1 \dots \mu_{n-p}} = \frac{1}{p!} \varepsilon^{\nu_1 \dots \nu_p}{}_{\mu_1 \dots \mu_{n-p}} A_{\nu_1 \dots \nu_p}, \quad (\text{A.6})$$

where  $\varepsilon$  is the Levi-Civita tensor, which is obtained from Levi-Civita symbol  $\tilde{\varepsilon}$ . We can obtain back the original form by applying Hodge star operator twice,

$$**A = (-1)^{s+p(n-p)} A, \quad (\text{A.7})$$

where  $s$  is the number of negative eigen values of the metric, for Lorentzian and Euclidean signature,  $s$  is  $-1$  and  $+1$  respectively. The Levi-Civita symbol is defined as,

$$\tilde{\varepsilon}_{\mu_1 \mu_2 \dots \mu_n} = \begin{cases} +1, & \text{if } \mu_1 \mu_2 \dots \mu_n \text{ is an even permutation of } 1 \dots (n-1) \\ -1, & \text{if } \mu_1 \mu_2 \dots \mu_n \text{ is an odd permutation of } 1 \dots (n-1) \\ 0, & \text{otherwise} \end{cases} \quad (\text{A.8})$$

The Levi-Civita symbol is an antisymmetric object which does not transform like a tensor but transforms very close to a tensor; such objects often are called tensor densities. Nevertheless, tensor densities can be converted to a tensor by multiplying with  $|g|^{w/2}$  where  $w$  is the weight of the density. The weight is the power of Jacobian in the transformation equation. Note that the determinant of a metric is a tensor density with weight  $-2$ . Hence multiplying the Levi-Civita symbol of weight 1 with  $|g|^{1/2}$  can promote it to a tensor. Levi-Civita tensor is given by,

$$\varepsilon_{\mu_1 \mu_2 \dots \mu_n} = \sqrt{|g|} \tilde{\varepsilon}_{\mu_1 \mu_2 \dots \mu_n}. \quad (\text{A.9})$$

In Euclidean spacetime, Levi-Civita symbol is not different from tensor as  $\sqrt{|g|} = 1$ . We can also show that the Levi-Civita tensor is infact the volume element.

$$\sqrt{|g|}d^n x = \sqrt{|g|}dx^0 \wedge \cdots \wedge dx^{n-1} = \frac{1}{n!}\epsilon_{\mu_1 \dots \mu_n} dx^{\mu_1} \wedge \cdots \wedge dx^{\mu_n}. \quad (\text{A.10})$$

ie, the integral of function  $f(x)$  in a  $n$ -dimensional manifold can be written in abstract form as,

$$\int f(x) \sqrt{|g|}d^n x = \int f(x) \epsilon. \quad (\text{A.11})$$

Raising and lowering of indices in the Levi-Civita tensor requires a metric tensor. Through the Levi-Civita tensor, Hodge dual has a dependency on the metric. The contraction of indices on Levi-Civita tensor gives the antisymmetrised product of Kronecker delta. Contracting  $p$ -indices,

$$\epsilon^{\mu_1 \mu_2 \dots \mu_p \alpha_1 \dots \alpha_{n-p}} \epsilon_{\mu_1 \mu_2 \dots \mu_p \beta_1 \dots \beta_{n-p}} = (-1)^s p! (n-p)! \delta_{\beta_1}^{[\alpha_1} \dots \delta_{\beta_{n-p}}^{\alpha_{n-p}]}. \quad (\text{A.12})$$

If you want to contract all the indices except one,  $p = n - 1$ , then

$$\epsilon^{\mu_1 \mu_2 \dots \mu_p \alpha} \epsilon_{\mu_1 \mu_2 \dots \mu_p \beta} = (-1)^s (n-1)! \delta_{\beta}^{\alpha}. \quad (\text{A.13})$$

In 3-dimensional Euclidean space, Hodge dual of a wedge product of two 1-forms turns out to be a normal cross product, giving a 1-form.

$$*(A \wedge B) = \epsilon_i^{jk} A_j B_k. \quad (\text{A.14})$$

This is a peculiar feature in 3-dimensions; two dual vectors can be identified with a third dual vector.





# Appendix B

## Stoke's Theorem

The form notation presents an elegant way of deriving Stoke's theorem in coordinate free notation. First step is to notice that a  $(n - 1)$ -form  $\omega$  can be written as Hodge dual of 1-form  $V$  in an  $n$ -dimensional manifold.

$$\omega = *V. \tag{B.1}$$

This can be written in component form using definition (Appendix A.6),

$$\begin{aligned} \omega_{\mu_1 \dots \mu_{n-1}} &= (*V)_{\mu_1 \dots \mu_{n-1}}, \\ &= \varepsilon^{\nu}_{\mu_1 \dots \mu_{n-1}} V_{\nu}. \end{aligned}$$

The exterior derivative of  $(n - 1)$ -form  $\omega$ ,  $d\omega$  is a  $n$ -form.

$$\begin{aligned} (d\omega)_{\lambda \mu_1 \dots \mu_{n-1}} &= (d*V)_{\lambda \mu_1 \dots \mu_{n-1}}, \\ &= n \nabla_{[\lambda} (\varepsilon_{|\nu| \mu_1 \dots \mu_{n-1}}] V^{\nu}), \\ &= n \varepsilon_{\nu [\mu_1 \dots \mu_{n-1}} \nabla_{\lambda]} V^{\nu}. \end{aligned} \tag{B.2}$$

Any  $n$ -form by definition can be written as a function  $f(x)$  times  $\varepsilon$  or Hodge dual of  $f(x)$ . ie,

$$\begin{aligned} d\omega &= *f(x) = f(x)\varepsilon, \\ \text{or } *d\omega &= **f(x) = f(x). \end{aligned} \quad (\text{B.3})$$

Taking dual on both sides of equation (AppendixB.2),

$$\begin{aligned} *(d\omega)_{\lambda\mu_1\dots\mu_{n-1}} &= *(n\varepsilon_{\nu[\mu_1\dots\mu_{n-1}}\nabla_{\lambda]}V^\nu), \\ &= \frac{n}{n!}\varepsilon^{\lambda\mu_1\dots\mu_{n-1}}(\varepsilon_{\nu[\mu_1\dots\mu_{n-1}}\nabla_{\lambda]}V^\nu), \\ &= \frac{1}{(n-1)!}(-1)^s(n-1)!\delta_\nu^\lambda\nabla_\lambda V^\nu = (-1)^s\nabla_\nu V^\nu. \end{aligned} \quad (\text{B.4})$$

In the final step, we have used property of Levi-Civita symbol on contraction of indices.

Now we can write,

$$d\omega = *((-1)^s\nabla_\nu V^\nu) = \nabla_\nu V^\nu\sqrt{|g|}d^n x. \quad (\text{B.5})$$

We know from vector calculus that the divergence of a vector can be written as,

$$\nabla_\nu V^\nu = \frac{1}{\sqrt{|g|}}\partial_\nu(\sqrt{|g|}V^\nu). \quad (\text{B.6})$$

Putting things together, left hand side of Stoke's theorem becomes,

$$\int_M d\omega = \int_M d^n x \partial_\nu(\sqrt{|g|}V^\nu). \quad (\text{B.7})$$

The right hand side of Stoke's theorem involves the induced volume on the boundary.

The volume on the boundary or on the particular hypersurface is written in terms of induced metric  $\gamma_{ij}$  on the hypersurface,

$$\hat{\varepsilon} = \sqrt{|\gamma|}d^{n-1}y. \quad (\text{B.8})$$

Thus r.h.s of Stoke's theorem becomes,

$$\int_{\partial M} \omega = \int_{\partial M} d^{n-1}y \sqrt{|\gamma|} n_\nu V^\nu. \quad (\text{B.9})$$

where  $y$  is the coordinate on the boundary  $\partial M$  and  $n^\nu$  is the unit normal to  $\partial M$ . When a hypersurface is the boundary of a certain region,  $n^\nu$  can be pointing inwards or outwards. If the boundary is time-like (space-like), then unit normal  $n^\nu$  should be chosen to be pointing inward(outward). Hence, Stoke's theorem takes the form,

$$\int_M d^n x \partial_\nu \left( \sqrt{|g|} V^\nu \right) = \int_{\partial M} d^{n-1}y \sqrt{|\gamma|} n_\nu V^\nu. \quad (\text{B.10})$$



# Appendix C

## Komar Integrals in Various Notations

The expression for conserved charge  $Q$  is written in different forms,

$$Q = - \int_R d(*J) = - \int_\Sigma *J. \quad (\text{C.1})$$

$$\text{Or, } Q = - \int_R d^n x \sqrt{|g|} \nabla_\mu J^\mu = - \int_\Sigma d^{n-1} y \sqrt{|\gamma|} n_\mu J^\mu. \quad (\text{C.2})$$

Formula in terms of Killing vector

$$- \int_\Sigma d^{n-1} y \sqrt{|\gamma|} n_\mu J^\mu = - \int_\Sigma d^{n-1} y \sqrt{|\gamma|} n_\mu R^{\mu\nu} \xi_\nu, \quad (\text{C.3})$$

$$= - \int_{\partial\Sigma} d^2 x \sqrt{|\alpha|} n_\mu \sigma_\nu \nabla^\mu \xi^\nu. \quad (\text{C.4})$$

In more sophisticated notation,

$$Q = \int_\Sigma dS_\mu R^{\mu\nu} \xi_\nu = \int_{\partial\Sigma} dS_{\mu\nu} \nabla^\mu \xi^\nu, \quad (\text{C.5})$$

where  $dS_a = n_\mu \sqrt{|\gamma|} d^{n-1} y$  and  $dS_{\mu\nu} = (n_\mu \sigma_\nu - n_\nu \sigma_\mu) \sqrt{|\alpha|} d^2 x$ . In differential form,

$$Q = - \int_\Sigma *J = - \int_\Sigma (d * d\xi) = - \int_{\partial\Sigma} *d\xi. \quad (\text{C.6})$$

Sometimes also written as,

$$Q = - \int_{\partial\Sigma} \varepsilon_{\alpha\beta\mu\nu} \nabla^\mu \xi^\nu. \quad (\text{C.7})$$



## Appendix D

# Komar Integral for Schwarzschild Black Hole

The unit normal to the hypersurface ( $\Sigma$ )  $n_\mu$  and to the boundary of hypersurface  $\partial\Sigma$  is very similar to RN- black hole case discussed earlier.

$$n_\mu = \left( -\sqrt{\left(1 - \frac{2GM}{r}\right)}, 0, 0, 0 \right) \text{ and } \sigma_\mu = \left( 0, \frac{1}{\sqrt{\left(1 - \frac{2GM}{r}\right)}}, 0, 0 \right). \quad (\text{D.1})$$

Schwarzschild spacetime is static and stationary, hence killing vector is time-like,  $\xi^\mu = \partial_t = (1, 0, 0, 0)$ . Now we can evaluate integral for Komar mass,

$$M_{Komar} = \frac{1}{4\pi G} \int_{\partial\Sigma} d^2x \sqrt{|\alpha|} n_\mu \sigma_\nu \nabla^\mu \xi^\nu. \quad (\text{D.2})$$

Where,

$$n_\mu \sigma_\nu \nabla^\mu \xi^\nu = n_0 \sigma_1 \nabla^0 \xi^1 = -\nabla^0 \xi^1. \quad (\text{D.3})$$

And,

$$\nabla^0 \xi^1 = g^{00} \nabla_0 \xi^1 = g^{00} \left( \partial_0 \xi^1 + \Gamma^1_{0\lambda} \xi^\lambda \right), \quad (\text{D.4})$$

$$= g^{00} \Gamma^1_{00} \xi^0 = -\frac{1}{\left(1 - \frac{2GM}{r}\right)} \frac{GM}{r^2} \left(1 - \frac{2GM}{r}\right), \quad (\text{D.5})$$

$$= -\frac{GM}{r^2}. \quad (\text{D.6})$$

Substituting these things in equation(D.2), we get

$$\begin{aligned} M_{Komar} &= \frac{1}{4\pi G} \int_{s^2} d\theta d\phi r^2 \sin \theta \left( \frac{GM}{r^2} \right), \\ &= \frac{1}{4\pi G} 4\pi (GM) = M. \end{aligned} \quad (\text{D.7})$$



# Appendix E

## Surface Gravity and Killing Horizon

From Frobenius theorem, any vector  $\vec{V}$  is hypersurface orthogonal, if  $\vec{V}$  is orthogonal to every tangent vectors on the hypersurface.

$$V_{[\mu} \partial_\nu V_{\alpha]} = 0. \quad (\text{E.1})$$

Applying it for Killing vector field  $\xi_\mu$  on the horizon,

$$\begin{aligned} \xi_{[\mu} \nabla_\nu \xi_{\alpha]} &= 0, \\ &= \frac{1}{3} (\xi_\mu \nabla_{[\nu} \xi_{\alpha]} - \xi_\nu \nabla_{[\mu} \xi_{\alpha]} + \xi_\alpha \nabla_{[\mu} \xi_{\nu]}), \\ &= \frac{1}{3} (\xi_\mu \nabla_\nu \xi_\alpha - \xi_\nu \nabla_\mu \xi_\alpha + \xi_\alpha \nabla_{[\mu} \xi_{\nu]}), \\ \implies -2\xi_{[\mu} \nabla_{\nu]} \xi_\alpha &= \xi_\alpha \nabla_{[\mu} \xi_{\nu]} = \xi_\alpha \nabla_\mu \xi_\nu. \end{aligned} \quad (\text{E.2})$$

In last step, we have used Killing equation and definition of antisymmetric tensor,

$$\nabla_{[\mu} \xi_{\nu]} = \frac{1}{2} (\nabla_\mu \xi_\nu - \nabla_\nu \xi_\mu) = \nabla_\mu \xi_\nu.$$

We have obtained the relation,

$$\xi_\alpha \nabla_\mu \xi_\nu = -2\xi_{[\mu} \nabla_{\nu]} \xi_\alpha. \quad (\text{E.3})$$

Multiply equation (Appendix E.3) by antisymmetric  $\nabla^\mu \xi^\nu$  tensor which dissolves the antisymmetric part in the r.h.s,

$$\begin{aligned}
(\nabla^\mu \xi^\nu) \xi_\alpha (\nabla_\mu \xi_\nu) &= -2 (\nabla^\mu \xi^\nu) \xi_{[\mu} \nabla_{\nu]} \xi_\alpha, \\
&= -2 (\nabla^\mu \xi^\nu) \xi_\mu \nabla_\nu \xi_\alpha, \\
&= -2 (\xi_\mu \nabla^\mu \xi^\nu) (\nabla_\nu \xi_\alpha), \\
&= -2 \kappa \xi^\nu \nabla_\nu \xi_\alpha = -2 \kappa^2 \xi_\alpha.
\end{aligned} \tag{E.4}$$

We observe the expressions for the surface gravity  $\kappa$  as,

$$\kappa^2 = -\frac{1}{2} (\nabla^\mu \xi^\nu) (\nabla_\mu \xi_\nu). \tag{E.5}$$

# Appendix F

## Bardeen Black Hole with a Quintessence

We start with a static spherically symmetric metric *ansatz* in four dimensions such that,

$$ds^2 = - \left( 1 - \frac{2m(r)}{r} \right) dt^2 + \frac{dr^2}{\left( 1 - \frac{2m(r)}{r} \right)} + r^2 (d\theta^2 + \sin^2 \theta d\phi^2). \quad (\text{F.1})$$

The field equation can be written as,

$$G_{\mu\nu} + \Lambda g_{\mu\nu} = T_{\mu\nu}^{(q)} + T_{\mu\nu}^{(NL)}. \quad (\text{F.2})$$

where  $G_{\mu\nu} = R_{\mu\nu} - \frac{1}{2}g_{\mu\nu}R$ , and  $g_{\mu\nu}$  are the Einstein field tensor and the metric tensor, respectively.  $R_{\mu\nu}$  and  $R$  are, respectively, the Ricci tensor and Ricci scalar. Whereas,  $T_{\mu\nu}^{(q)}$ , and  $T_{\mu\nu}^{(NL)}$  are, respectively, the energy-momentum tensors for quintessence field and the nonlinear electrodynamics. The independent components of the field equations are written as,

$$\begin{aligned} \frac{2m'(r)}{r^2} - \Lambda &= T_t^{(q)} + T_t^{(NL)}, \\ \frac{m''(r)}{r} - \Lambda &= T_\theta^{(q)} + T_\theta^{(NL)}, \end{aligned} \quad (\text{F.3})$$

where,

$$T_t^{t(q)} = T_r^{r(q)} = \rho_q = \frac{3a\omega_q}{r^{3(\omega_q+1)}},$$

$$T_t^{t(NL)} = T_r^{r(NL)} = 2\mathcal{L}(r) = \frac{6M\beta^2}{(r^2 + \beta^2)^{5/2}}. \quad (\text{F.4})$$

$$T_\theta^{\theta(q)} = T_\phi^{\phi(q)} = -\frac{1}{2}\rho_q(3\omega_q + 1) = -\frac{a}{2} \frac{3\omega_q(3\omega_q + 1)}{r^{3(\omega_q+1)}}, \quad (\text{F.5})$$

$$T_\theta^{\theta(NL)} = T_\phi^{\phi(NL)} = 2 \left( \mathcal{L}(r) - \frac{\partial \mathcal{L}}{\partial r} \left( \frac{\partial \mathcal{F}}{\partial r} \right)^{-1} F^{\theta\phi} F_{\theta\phi} \right) = \frac{3M\beta^2(3r^2 - 2\beta^2)}{(r^2 + \beta^2)^{7/2}}.$$

Substituting for  $T_r^{r(q)}$  and  $T_r^{r(NL)}$ , we have

$$\frac{2m'(r)}{r^2} - \Lambda = \frac{3a\omega_q}{r^{3(\omega_q+1)}} + \frac{6M\beta^2}{(r^2 + \beta^2)^{5/2}},$$

$$m'(r) = \frac{\Lambda r^2}{2} + \frac{a}{2} \frac{3\omega_q}{r^{(3\omega_q+1)}} + \frac{3M\beta^2 r^2}{(r^2 + \beta^2)^{5/2}}. \quad (\text{F.6})$$

Integrating the above equation, we get

$$m(r) = \int_0^r dr \frac{\Lambda r^2}{2} + \int_0^r dr \frac{a}{2} \frac{3\omega_q}{r^{(3\omega_q+1)}} + \int_0^r dr \frac{3M\beta^2 r^2}{(r^2 + \beta^2)^{5/2}},$$

$$m(r) = \frac{\Lambda r^3}{6} + \frac{a}{2} \frac{1}{r^{(3\omega_q+1)}} + \frac{Mr^2}{(r^2 + \beta^2)^{3/2}}. \quad (\text{F.7})$$

Therefore, the metric function reads

$$f(r) = 1 - \frac{2m(r)}{r} = 1 - \frac{2M r^2}{(r^2 + \beta^2)^{3/2}} - \frac{a}{r^{(3\omega_q+1)}} - \frac{\Lambda r^2}{3}. \quad (\text{F.8})$$

This way, we can get the required solution for the regular Bardeen black hole with a quintessence.

# Bibliography

- Akbar, M., Quevedo, H., Saifullah, K., Sanchez, A., and Taj, S. (2011). Thermodynamic Geometry Of Charged Rotating BTZ Black Holes. *Phys. Rev. D*, 83:084031.
- Akbar, M., Salem, N., and Hussein, S. A. (2012). Thermodynamics of the bardeen regular black hole. *Chinese Physics Letters*, 29(7):070401.
- Altamirano, N., Kubiznak, D., and Mann, R. B. (2013). Reentrant phase transitions in rotating anti-de Sitter black holes. *Phys. Rev. D*, 88(10):101502.
- Alvarez, J. L., Quevedo, H., and Sanchez, A. (2008). Unified geometric description of black hole thermodynamics. *Phys. Rev. D*, 77:084004.
- Aman, J. E., Bengtsson, I., and Pidokrajt, N. (2003). Geometry of black hole thermodynamics. *Gen. Rel. Grav.*, 35:1733.
- Appels, M., Gregory, R., and Kubiznak, D. (2016). Thermodynamics of Accelerating Black Holes. *Phys. Rev. Lett.*, 117(13):131303.
- Appels, M., Gregory, R., and Kubiznak, D. (2017). Black Hole Thermodynamics with Conical Defects. *JHEP*, 05:116.
- Ayon-Beato, E. and Garcia, A. (1998). Regular black hole in general relativity coupled to nonlinear electrodynamics. *Phys. Rev. Lett.*, 80:5056–5059.
- Ayon-Beato, E. and Garcia, A. (2000). The Bardeen model as a nonlinear magnetic monopole. *Phys. Lett.*, B493:149–152.
- Banerjee, A., Chatterjee, S., and Sen, A. A. (1996). Global monopole in Kaluza-Klein space-time. *Class. Quant. Grav.*, 13:3141–3149.

- Banerjee, R., Ghosh, S., and Roychowdhury, D. (2011a). New type of phase transition in Reissner Nordström–AdS black hole and its thermodynamic geometry. *Phys. Lett. B*, 696:156–162.
- Banerjee, R., Modak, S. K., and Samanta, S. (2011b). Second Order Phase Transition and Thermodynamic Geometry in Kerr-AdS Black Hole. *Phys. Rev. D*, 84:064024.
- Bardeen, J. M., Carter, B., and Hawking, S. W. (1973a). The Four laws of black hole mechanics. *Commun. Math. Phys.*, 31:161–170.
- Bardeen, J. M., Carter, B., and Hawking, S. W. (1973b). The Four laws of black hole mechanics. *Commun. Math. Phys.*, 31:161–170.
- Barriola, M. and Vilenkin, A. (1989). Gravitational field of a global monopole. *Phys. Rev. Lett.*, 63:341–343.
- Bekenstein, J. D. (1972). Black holes and the second law. *Lett. Nuovo Cim.*, 4:737–740.
- Bekenstein, J. D. (1973). Black holes and entropy. *Phys. Rev. D*, 7:2333–2346.
- Bekenstein, J. D. (1974). Generalized second law of thermodynamics in black hole physics. *Phys. Rev. D*, 9:3292–3300.
- Belhaj, A., Chabab, M., El Moumni, H., Masmar, K., Sedra, M. B., and Segui, A. (2015). On heat properties of ads black holes in higher dimensions. *Journal of High Energy Physics*, 2015(5):149.
- Belhaj, A., Chabab, M., El Moumni, H., and Sedra, M. B. (2012). On Thermodynamics of AdS Black Holes in Arbitrary Dimensions. *Chin. Phys. Lett.*, 29:100401.
- Bellucci, S. and Tiwari, B. N. (2012). Thermodynamic geometry and topological einstein–yang–mills black holes. *Entropy*, 14(6):1045–1078.
- Biswas, R. and Chakraborty, S. (2011). Black Hole Thermodynamics in Horava Lifshitz Gravity and the Related Geometry. *Astrophys. Space Sci.*, 332:193.
- Bravetti, A., Momeni, D., Myrzakulov, R., and Altaibayeva, A. (2013). Geometrothermodynamics of myers-perry black holes. *Advances in High Energy Physics*, 2013.

- Brown, J. D. and Teitelboim, C. (1988). Neutralization of the Cosmological Constant by Membrane Creation. *Nucl. Phys. B*, 297:787–836.
- Caldarelli, M. M., Cognola, G., and Klemm, D. (2000). Thermodynamics of Kerr-Newman-AdS black holes and conformal field theories. *Class. Quant. Grav.*, 17:399–420.
- Carathéodory, C. (1909). Untersuchungen über die Grundlagen der Thermodynamik. *Mathematische Annalen*, 67(3):355–386.
- Chabab, M., El Moumni, H., Iraoui, S., Masmar, K., and Zhizeh, S. (2018). More Insight into Microscopic Properties of RN-AdS Black Hole Surrounded by Quintessence via an Alternative Extended Phase Space. *Int. J. Geom. Meth. Mod. Phys.*, 15(10):1850171.
- Chamblin, A., Emparan, R., Johnson, C. V., and Myers, R. C. (1999a). Charged AdS black holes and catastrophic holography. *Phys. Rev. D*, 60:064018.
- Chamblin, A., Emparan, R., Johnson, C. V., and Myers, R. C. (1999b). Holography, thermodynamics and fluctuations of charged AdS black holes. *Phys. Rev. D*, 60:104026.
- Channuie, P. and Momeni, D. (2018). On the Scalar-Vector-Tensor Gravity: Black Hole, Thermodynamics and Geometrothermodynamics. *Phys. Lett. B*, 785:309–314.
- Chaturvedi, P., Das, A., and Sengupta, G. (2017). Thermodynamic Geometry and Phase Transitions of Dyonic Charged AdS Black Holes. *Eur. Phys. J. C*, 77(2):110.
- Chen, S. and Jing, J. (2005). Quasinormal modes of a black hole surrounded by quintessence. *Classical and Quantum Gravity*, 22:4651–4657.
- Chen, S. and Jing, J. (2013). Gravitational field of a slowly rotating black hole with a phantom global monopole. *Class. Quant. Grav.*, 30:175012.
- Chen, S., Liu, X., Liu, C., and Jing, J. (2013).  $P - V$  criticality of AdS black hole in  $f(R)$  gravity. *Chin. Phys. Lett.*, 30:060401.

- Chen, S., Pan, Q., and Jing, J. (2013). Holographic superconductors in quintessence AdS black hole spacetime. *Classical and Quantum Gravity*, 30(14):145001.
- Chen, S., Wang, L., Ding, C., and Jing, J. (2010). Holographic superconductors in the AdS black hole spacetime with a global monopole. *Nucl. Phys.*, B836:222–231.
- Chen, Y., Li, H., and Zhang, S.-J. (2019). Microscopic explanation for black hole phase transitions via Ruppeiner geometry: Two competing factors—the temperature and repulsive interaction among BH molecules. *Nucl. Phys. B*, 948:114752.
- Dehyadegari, A., Sheykhi, A., and Montakhab, A. (2017). Critical behavior and microscopic structure of charged AdS black holes via an alternative phase space. *Phys. Lett.*, B768:235–240.
- Deng, G.-M., Fan, J., Li, X., and Huang, Y.-C. (2018). Thermodynamics and phase transition of charged AdS black holes with a global monopole. *Int. J. Mod. Phys. A*, 33(03):1850022.
- Deng, G.-M. and Huang, Y.-C. (2017).  $Q$ - $\Phi$  criticality and microstructure of charged AdS black holes in  $f(R)$  gravity. *Int. J. Mod. Phys.*, A32(35):1750204.
- Dirac, P. A. M. (1927). Quantum theory of emission and absorption of radiation. *Proc. Roy. Soc. Lond. A*, 114:243.
- Dolan, B. P. (2011). Pressure and volume in the first law of black hole thermodynamics. *Class. Quant. Grav.*, 28:235017.
- Du, Y.-Z., Zhao, H.-H., and Zhang, L.-C. (2020). Microstructure and Continuous Phase Transition of the Einstein-Gauss-Bonnet AdS Black Hole. *Adv. High Energy Phys.*, 2020:6395747.
- Dyson, F. J. (1949). The S matrix in quantum electrodynamics. *Phys. Rev.*, 75:1736–1755.
- Einstein, A. (1911). On The influence of gravitation on the propagation of light. *Annalen Phys.*, 35:898–908.



- Einstein, A. (1915a). Explanation of the Perihelion Motion of Mercury from the General Theory of Relativity. *Sitzungsber. Preuss. Akad. Wiss. Berlin (Math. Phys. )*, 1915:831–839.
- Einstein, A. (1915b). Zur Allgemeinen Relativitätstheorie. *Sitzungsber. Preuss. Akad. Wiss. Berlin (Math. Phys. )*, 1915:778–786. [Addendum: *Sitzungsber. Preuss. Akad. Wiss. Berlin (Math. Phys. )* 1915, 799–801 (1915)].
- Einstein, A. (1936). Lens-Like Action of a Star by the Deviation of Light in the Gravitational Field. *Science*, 84:506–507.
- Fan, Z.-Y. (2017). Critical phenomena of regular black holes in anti-de Sitter spacetime. *Eur. Phys. J.*, C77(4):266.
- Fan, Z.-Y. and Wang, X. (2016). Construction of Regular Black Holes in General Relativity. *Phys. Rev.*, D94(12):124027.
- Ferrara, S., Gibbons, G. W., and Kallosh, R. (1997). Black holes and critical points in moduli space. *Nucl. Phys. B*, 500:75–93.
- Feynman, R. P. (1950). Mathematical formulation of the quantum theory of electromagnetic interaction. *Phys. Rev.*, 80:440–457.
- Finkelstein, D. (1958). Past-future asymmetry of the gravitational field of a point particle. *Phys. Rev.*, 110:965–967.
- Flores-Alfonso, D. and Quevedo, H. (2019). Extended thermodynamics of self-gravitating skyrmions. *Classical and Quantum Gravity*, 36(15):154001.
- Ford, L. H. (1987). Cosmological-constant damping by unstable scalar fields. *Phys. Rev. D*, 35:2339–2344.
- Ghosh, A. and Bhamidipati, C. (2020a). Thermodynamic geometry and interacting microstructures of BTZ black holes.
- Ghosh, A. and Bhamidipati, C. (2020b). Thermodynamic geometry for charged Gauss-Bonnet black holes in AdS spacetimes. *Phys. Rev.*, D101(4):046005.

- Gibbs, J. (1948). *The Collected Works. Vol. 1. Thermodynamics*. Yale University Press.
- Glashow, S. L. (1961). Partial-symmetries of weak interactions. *Nuclear Physics*, 22(4):579–588.
- Gunasekaran, S., Mann, R. B., and Kubiznak, D. (2012). Extended phase space thermodynamics for charged and rotating black holes and Born-Infeld vacuum polarization. *JHEP*, 11:110.
- Guo, X.-Y., Li, H.-F., Zhang, L.-C., and Zhao, R. (2019). Microstructure and continuous phase transition of a Reissner-Nordstrom-AdS black hole. *Phys. Rev. D*, 100(6):064036.
- Hawking, S. W. (1975). Particle Creation by Black Holes. *Commun. Math. Phys.*, 43:199–220. [167(1975)].
- Hawking, S. W. and Page, D. N. (1983). Thermodynamics of Black Holes in anti-De Sitter Space. *Commun. Math. Phys.*, 87:577.
- Hayward, S. A. (2006). Formation and evaporation of regular black holes. *Phys. Rev. Lett.*, 96:031103.
- Hegde, K., Naveena Kumara, A., Ahmed Rizwan, C. L., Ali, M. S., and M, A. K. (2020). Null Geodesics and Thermodynamic Phase Transition of Four-Dimensional Gauss-Bonnet AdS Black Hole.
- Hendi, S., Panah, B. E., Panahiyan, S., Liu, H., and Meng, X.-H. (2018). Black holes in massive gravity as heat engines. *Physics Letters B*, 781:40 – 47.
- Hendi, S. H., Li, G.-Q., Mo, J.-X., Panahiyan, S., and Eslam Panah, B. (2016). New perspective for black hole thermodynamics in Gauss–Bonnet–Born–Infeld massive gravity. *Eur. Phys. J. C*, 76(10):571.
- Hendi, S. H., Panahiyan, S., Eslam Panah, B., and Momennia, M. (2015a). A new approach toward geometrical concept of black hole thermodynamics. *Eur. Phys. J. C*, 75(10):507.

- Hendi, S. H., Sheykhi, A., Panahiyan, S., and Eslam Panah, B. (2015b). Phase transition and thermodynamic geometry of einstein-maxwell-dilaton black holes. *Phys. Rev. D*, 92:064028.
- Hendi, S. H. and Vahidinia, M. H. (2013). Extended phase space thermodynamics and  $p - v$  criticality of black holes with a nonlinear source. *Phys. Rev. D*, 88:084045.
- Hennigar, R. A., McCarthy, F., Ballon, A., and Mann, R. B. (2017). Holographic heat engines: general considerations and rotating black holes. *Classical and Quantum Gravity*, 34(17):175005.
- Hermann, R. (1973). *Geometry, physics, and systems*. Pure and applied mathematics. M. Dekker.
- Hu, Y., Chen, J., and Wang, Y. (2017). Geometrothermodynamics of van der waals black hole. *General Relativity and Gravitation*, 49(12):148.
- Jafarzade, K. and Sadeghi, J. (2017). The thermodynamic efficiency in static and dynamic black holes. *International Journal of Theoretical Physics*, 56(11):3387–3399.
- Janke, W., Johnston, D. A., and Kenna, R. (2010). Geometrothermodynamics of the Kehagias-Sfetsos Black Hole. *J. Phys. A*, 43(42):425206.
- Janyszek, H. and Mrugaa, R. (1990). Riemannian geometry and stability of ideal quantum gases. *Journal of Physics A: Mathematical and General*, 23(4):467–476.
- Johnson, C. V. (2014). Holographic Heat Engines. *Class. Quant. Grav.*, 31:205002.
- Johnson, C. V. (2016a). Born–infeld AdS black holes as heat engines. *Classical and Quantum Gravity*, 33(13):135001.
- Johnson, C. V. (2016b). Gauss–bonnet black holes and holographic heat engines beyond largeN. *Classical and Quantum Gravity*, 33(21):215009.
- Jusufi, K., Werner, M. C., Banerjee, A., and Övgün, A. (2017). Light Deflection by a Rotating Global Monopole Spacetime. *Phys. Rev. D*, 95(10):104012.

- Kastor, D., Ray, S., and Traschen, J. (2009). Enthalpy and the Mechanics of AdS Black Holes. *Class. Quant. Grav.*, 26:195011.
- Kerr, R. P. (1963). Gravitational field of a spinning mass as an example of algebraically special metrics. *Phys. Rev. Lett.*, 11:237–238.
- Kibble, T. W. B. (1976). Topology of Cosmic Domains and Strings. *J. Phys. A*, 9:1387–1398.
- Kiselev, V. V. (2003). Quintessence and black holes. *Class. Quant. Grav.*, 20:1187–1198.
- Kord Zangeneh, M., Dehyadegari, A., Sheykhi, A., and Mann, R. B. (2018). Microscopic Origin of Black Hole Reentrant Phase Transitions. *Phys. Rev. D*, 97(8):084054.
- Kubiznak, D. and Mann, R. B. (2012). P-V criticality of charged AdS black holes. *JHEP*, 07:033.
- Kubiznak, D., Mann, R. B., and Teo, M. (2017). Black hole chemistry: thermodynamics with Lambda. *Class. Quant. Grav.*, 34(6):063001.
- Lala, A. and Roychowdhury, D. (2012). Ehrenfest’s scheme and thermodynamic geometry in born-infeld ads black holes. *Phys. Rev. D*, 86:084027.
- Landau, L. D. L. D., Lifshitz [U+FE20]s [U+FE21], E. M. E. M., Pitaevskii, L. P. L. P., Sykes, J. B., and Kearsley, M. J. (1980). *Statistical physics. Part 1*. Elsevier Butterworth Heinemann.
- Li, G.-Q. (2014). Effects of dark energy on P–V criticality of charged AdS black holes. *Phys. Lett. B*, 735:256–260.
- Li, G.-Q. and Mo, J.-X. (2016). Phase transition and thermodynamic geometry of  $f(r)$  ads black holes in the grand canonical ensemble. *Phys. Rev. D*, 93:124021.
- Link, F. (1936). Photometric consequences of the einstein deviation. *Comptes Rendus*, 202:917–19.

- Liu, H. and Meng, X.-H. (2017). Effects of dark energy on the efficiency of charged ads black holes as heat engines. *The European Physical Journal C*, 77(8):556.
- Magnon, A. (1985). On Komar integrals in asymptotically anti-de Sitter space-times. *J. Math. Phys.*, 26:3112–3117.
- Maldacena, J. M. (1999). The Large N limit of superconformal field theories and supergravity. *Int. J. Theor. Phys.*, 38:1113–1133.
- Mansoori, S. A. H., Mirza, B., and Fazel, M. (2015). Hessian matrix, specific heats, Nambu brackets, and thermodynamic geometry. *JHEP*, 04:115.
- May, H.-O., Mausbach, P., and Ruppeiner, G. (2013). Thermodynamic curvature for attractive and repulsive intermolecular forces. *Phys. Rev. E*, 88:032123.
- Miao, Y.-G. and Xu, Z.-M. (2018). On thermal molecular potential among micro-molecules in charged AdS black holes. *Phys. Rev. D*, 98:044001.
- Miao, Y.-G. and Xu, Z.-M. (2019a). Interaction potential and thermo-correction to the equation of state for thermally stable Schwarzschild Anti-de Sitter black holes. *Sci. China Phys. Mech. Astron.*, 62(1):10412.
- Miao, Y.-G. and Xu, Z.-M. (2019b). Microscopic structures and thermal stability of black holes conformally coupled to scalar fields in five dimensions. *Nucl. Phys. B*, 942:205–220.
- Mirza, B. and Mohammadzadeh, H. (2008). Ruppeiner geometry of anyon gas. *Phys. Rev. E*, 78:021127.
- Mo, J.-X. and Li, G.-Q. (2018). Holographic heat engine within the framework of massive gravity. *Journal of High Energy Physics*, 2018(5):122.
- Mo, J.-X., Liang, F., and Li, G.-Q. (2017). Heat engine in the three-dimensional space-time. *Journal of High Energy Physics*, 2017(3):10.
- Mrugala, R. (1978). Geometrical formulation of equilibrium phenomenological thermodynamics. *Reports on Mathematical Physics*, 14(3):419 – 427.

- Newman, E. T., Couch, R., Chinnapared, K., Exton, A., Prakash, A., and Torrence, R. (1965). Metric of a Rotating, Charged Mass. *J. Math. Phys.*, 6:918–919.
- Newman, E. T. and Janis, A. I. (1965). Note on the Kerr spinning particle metric. *J. Math. Phys.*, 6:915–917.
- Newton, I. (1687). *Philosophiæ Naturalis Principia Mathematica*. England.
- Niu, C., Tian, Y., and Wu, X.-N. (2012). Critical phenomena and thermodynamic geometry of reissner-nordström-anti-de sitter black holes. *Phys. Rev. D*, 85:024017.
- Nordström, G. (1918). On the Energy of the Gravitation field in Einstein’s Theory. *Koninklijke Nederlandse Akademie van Wetenschappen Proceedings Series B Physical Sciences*, 20:1238–1245.
- Ökcü, O. and Aydiner, E. (2017). Joule–Thomson expansion of the charged AdS black holes. *Eur. Phys. J. C*, 77(1):24.
- Ökcü, O. and Aydiner, E. (2018). Joule–Thomson expansion of Kerr–AdS black holes. *Eur. Phys. J. C*, 78(2):123.
- Oshima, H., Obata, T., and Hara, H. (1999). Riemann scalar curvature of ideal quantum gases obeying gentile’s statistics. *Journal of Physics A: Mathematical and General*, 32(36):6373–6383.
- Page, D. N. (2005). Hawking radiation and black hole thermodynamics. *New J. Phys.*, 7:203.
- Quevedo, H. (2007). Geometrothermodynamics. *J. Math. Phys.*, 48:013506.
- Quevedo, H. (2008). Geometrothermodynamics of black holes. *Gen. Rel. Grav.*, 40:971–984.
- Quevedo, H., Quevedo, M. N., and Sánchez, A. (2016). Einstein-Maxwell-dilaton phantom black holes: Thermodynamics and geometrothermodynamics. *Phys. Rev. D*, 94(2):024057.

- Quevedo, H., Sanchez, A., Taj, S., and Vazquez, A. (2012). Geometrothermodynamics in Horava-Lifshitz gravity. *J. Phys. A*, 45:055211.
- Reissner, H. (1916). Über die eigengravitation des elektrischen feldes nach der einsteinschen theorie. *Annalen der Physik*, 355(9):106–120.
- Rodrigue, K. K. J., Saleh, M., Thomas, B. B., and Crepin, K. T. (2020). Thermodynamic phase transition and global stability of the regular Hayward black hole surrounded by quintessence. *Mod. Phys. Lett. A*, 35(16):2050129.
- Ruppeiner, G. (1979). Thermodynamics: A riemannian geometric model. *Phys. Rev. A*, 20:1608–1613.
- Ruppeiner, G. (1995). Riemannian geometry in thermodynamic fluctuation theory. *Rev. Mod. Phys.*, 67:605–659.
- Ruppeiner, G. (2008). Thermodynamic curvature and phase transitions in kerr-newman black holes. *Phys. Rev. D*, 78:024016.
- Ruppeiner, G. (2010). Thermodynamic curvature measures interactions. *American Journal of Physics*, 78(11):1170–1180.
- Ruppeiner, G. (2016). Some early ideas on the metric geometry of thermodynamics. *Journal of Low Temperature Physics*, 185(3-4):246–261.
- Sahay, A. (2017). Restricted thermodynamic fluctuations and the ruppeiner geometry of black holes. *Phys. Rev. D*, 95:064002.
- Sahay, A., Sarkar, T., and Sengupta, G. (2010a). On the Thermodynamic Geometry and Critical Phenomena of AdS Black Holes. *JHEP*, 07:082.
- Sahay, A., Sarkar, T., and Sengupta, G. (2010b). On the Thermodynamic Geometry and Critical Phenomena of AdS Black Holes. *JHEP*, 07:082.
- Salam, A. (1968). Weak and Electromagnetic Interactions. *Conf. Proc. C*, 680519:367–377.

- Saleh, M., Thomas, B. B., and Kofane, T. C. (2018). Thermodynamics and Phase Transition from Regular Bardeen Black Hole Surrounded by Quintessence. *Int. J. Theor. Phys.*, 57(9):2640–2647.
- Sanchez, A. (2016). Geometrothermodynamics of black holes in Lorentz noninvariant massive gravity. *Phys. Rev. D*, 94(2):024037.
- Sarkar, T., Sengupta, G., and Nath Tiwari, B. (2006). On the thermodynamic geometry of BTZ black holes. *JHEP*, 11:015.
- Sarkar, T., Sengupta, G., and Nath Tiwari, B. (2008). Thermodynamic Geometry and Extremal Black Holes in String Theory. *JHEP*, 10:076.
- Schwarzschild, K. (1916). On the gravitational field of a mass point according to Einstein's theory. *Sitzungsber. Preuss. Akad. Wiss. Berlin (Math. Phys. )*, 1916:189–196.
- Schwinger, J. (1948). On quantum-electrodynamics and the magnetic moment of the electron. *Phys. Rev.*, 73:416–417.
- Setare, M. R. and Adami, H. (2015). Polytropic black hole. *Phys. Rev. D*, 91:084014.
- Shen, J.-y., Cai, R.-G., Wang, B., and Su, R.-K. (2007). Thermodynamic geometry and critical behavior of black holes. *Int. J. Mod. Phys. A*, 22:11–27.
- Shi, X. and Li, X. (1991). The gravitational field of a global monopole. *Classical and Quantum Gravity*, 8(4):761.
- Smarr, L. (1973). Mass formula for Kerr black holes. *Phys. Rev. Lett.*, 30:71–73. [Erratum: *Phys.Rev.Lett.* 30, 521–521 (1973)].
- Soroushfar, S., Saffari, R., and Kamvar, N. (2016). Thermodynamic geometry of black holes in  $f(R)$  gravity. *Eur. Phys. J. C*, 76(9):476.
- Spallucci, E. and Smailagic, A. (2013). Maxwell's equal area law for charged Anti-deSitter black holes. *Phys. Lett. B*, 723:436–441.



- Suresh, J., Tharanath, R., Varghese, N., and Kuriakose, V. C. (2014). The thermodynamics and thermodynamic geometry of the Park black hole. *Eur. Phys. J. C*, 74:2819.
- 't Hooft, G. and Veltman, M. J. G. (1972). Regularization and Renormalization of Gauge Fields. *Nucl. Phys. B*, 44:189–213.
- Teitelboim, C. (1985). THE COSMOLOGICAL CONSTANT AS A THERMODYNAMIC BLACK HOLE PARAMETER. *Phys. Lett. B*, 158:293–297.
- Ahmed Rizwan**, C. L., Kumara A., N., Vaid, D., and Ajith, K. M. (2019a). Joule-Thomson expansion in AdS black hole with a global monopole. *Int. J. Mod. Phys.*, A33(35):1850210.
- Ahmed Rizwan**, C. L., Naveena Kumara, A., Hegde, K., Ali, M. S., and M, A. K. (2020a). Rotating Black Hole with an Anisotropic Matter Field as a Particle Accelerator.
- Ahmed Rizwan**, C. L., Naveena Kumara, A., Hegde, K., and Vaid, D. (2020b). Co-existent Physics and Microstructure of the Regular Bardeen Black Hole in Anti-de Sitter Spacetime. *Annals Phys.*, 422:168320.
- Ahmed Rizwan**, C. L., Naveena Kumara, A., Rajani, K., Vaid, D., and Ajith, K. (2019b). Effect of Dark Energy in Geometrothermodynamics and Phase Transitions of Regular Bardeen AdS Black Hole. *Gen. Rel. Grav.*, 51(12):161.
- Naveena Kumara**, A., Ahmed Rizwan, C. L., Ajith, K. M., and Ali, M. S. (2020a). Photon Orbits and Thermodynamic Phase Transition of Regular AdS Black Holes. *Phys. Rev. D*, 102(8):084059.
- Naveena Kumara**, A., Ahmed Rizwan, C. L., Hegde, K., Ali, M. S., and M, A. K. (2021). Ruppeiner Geometry, Reentrant Phase transition and Microstructure of Born-Infeld AdS Black Hole. *Phys. Rev. D*, 103(4):044025.

- Naveena Kumara, A., Ahmed Rizwan, C. L., Hegde, K., M., A. K., and Ali, M. S.** (2020b). Microstructure and continuous phase transition of a regular Hayward black hole in anti-de Sitter spacetime.
- Naveena Kumara, A., Ahmed Rizwan, C. L., Vaid, D., and Ajith, K. M.** (2019). Critical Behaviour and Microscopic Structure of Charged AdS Black Hole with a Global Monopole in Extended and Alternate Phase Spaces.
- Naveena Kumara, A., Rizwan, C. A., Hegde, K., and M, A. K.** (2020c). Repulsive Interactions in the Microstructure of Regular Hayward Black Hole in Anti-de Sitter Spacetime. *Phys. Lett. B*, 807:135556.
- Rajani, K. V., Ahmed Rizwan, C. L., Naveena Kumara, A., Vaid, D., and Ajith, K. M.** (2020). Regular Bardeen AdS black hole as a heat engine. *Nucl. Phys. B*, 960:115166.
- Tharanath, R. and Kuriakose, V. C. (2013). Thermodynamics and Spectroscopy of Schwarzschild black hole surrounded by Quintessence. *Mod. Phys. Lett. A*, 28:1350003.
- Tharanath, R., Suresh, J., and Kuriakose, V. C. (2015). Phase transitions and Geometrothermodynamics of Regular black holes. *Gen. Rel. Grav.*, 47(4):46.
- Thomas, B. B., Saleh, M., and Kofane, T. C. (2012). Thermodynamics and phase transition of the Reissner-Nordstroem black hole surrounded by quintessence. *Gen. Rel. Grav.*, 44:2181–2189.
- Tomonaga, S. (1946). On a Relativistically Invariant Formulation of the Quantum Theory of Wave Fields\*. *Progress of Theoretical Physics*, 1(2):27–42.
- Tsujikawa, S. (2013). Quintessence: A Review. *Class. Quant. Grav.*, 30:214003.
- Tzikas, A. G. (2019). Bardeen black hole chemistry. *Phys. Lett. B*, 788:219–224.
- Vilenkin, A. (1985). Cosmic Strings and Domain Walls. *Phys. Rept.*, 121:263–315.
- Wald, R. M. (2001). The thermodynamics of black holes. *Living Rev. Rel.*, 4:6.

- Wei, S.-W. and Liu, Y.-X. (2013). Critical phenomena and thermodynamic geometry of charged gauss-bonnet ads black holes. *Phys. Rev. D*, 87:044014.
- Wei, S.-W. and Liu, Y.-X. (2015). Insight into the Microscopic Structure of an AdS Black Hole from a Thermodynamical Phase Transition. *Phys. Rev. Lett.*, 115(11):111302. [Erratum: *Phys.Rev.Lett.* 116, 169903 (2016)].
- Wei, S.-W. and Liu, Y.-X. (2017). Charged AdS black hole heat engines. *arXiv e-prints*, page arXiv:1708.08176.
- Wei, S.-W. and Liu, Y.-X. (2020a). Extended thermodynamics and microstructures of four-dimensional charged Gauss-Bonnet black hole in AdS space. *Phys. Rev. D*, 101(10):104018.
- Wei, S.-W. and Liu, Y.-X. (2020b). Intriguing microstructures of five-dimensional neutral Gauss-Bonnet AdS black hole. *Phys. Lett. B*, 803:135287.
- Wei, S.-W., Liu, Y.-X., and Mann, R. B. (2019a). Repulsive Interactions and Universal Properties of Charged Anti-de Sitter Black Hole Microstructures. *Phys. Rev. Lett.*, 123(7):071103.
- Wei, S.-W., Liu, Y.-X., and Mann, R. B. (2019b). Ruppeiner Geometry, Phase Transitions, and the Microstructure of Charged AdS Black Holes. *Phys. Rev. D*, 100(12):124033.
- Wei, S.-W., Liu, Y.-X., Wang, Y.-Q., and Guo, H. (2012). Thermodynamic Geometry of Black Hole in the Deformed Horava-Lifshitz Gravity. *EPL*, 99(2):20004.
- Weinberg, S. (1967). A model of leptons. *Phys. Rev. Lett.*, 19:1264–1266.
- Weinhold, F. (1975). Metric geometry of equilibrium thermodynamics. *The Journal of Chemical Physics*, 63(6):2479–2483.
- Weinhold, F. (1976). Metric geometry of equilibrium thermodynamics. v. aspects of heterogeneous equilibrium. *The Journal of Chemical Physics*, 65(2):559–564.

- Witten, E. (1998). Anti-de Sitter space, thermal phase transition, and confinement in gauge theories. *Adv. Theor. Math. Phys.*, 2:505–532. [89(1998)].
- Wu, B., Wang, C., Xu, Z.-M., and Yang, W.-L. (2020). Ruppeiner geometry and thermodynamic phase transition of the black hole in massive gravity.
- Xu, H., Sun, Y., and Zhao, L. (2017). Black hole thermodynamics and heat engines in conformal gravity. *International Journal of Modern Physics D*, 26(13):1750151.
- Xu, Z.-M., Wu, B., and Yang, W.-L. (2020). Fine micro-thermal structures for Reissner-Nordström black hole. *Chin. Phys. C*, 44(9):095106.
- Yerra, P. K. and Bhamidipati, C. (2020a). Critical heat engines in massive gravity. *Class. Quant. Grav.*, 37(20):205020.
- Yerra, P. K. and Bhamidipati, C. (2020b). Ruppeiner Geometry, Phase Transitions and Microstructures of Black Holes in Massive Gravity.
- Yerra, P. K. and Chandrasekhar, B. (2019). Heat engines at criticality for nonlinearly charged black holes. *Mod. Phys. Lett. A*, 34(27):1950216.
- Yi-Huan, W. and Zhong-Hui, C. (2011). Thermodynamic properties of a reissner—nordström quintessence black hole. *Chinese Physics Letters*, 28(10):100403.
- Yi-Wen, H., Gang, C., and Ming-Jian, L. (2013). Legendre transformations and the thermodynamic geometry of 5d black holes. *Chinese Physics C*, 37(3):035101.
- Zemansky, M. W., Dittman, R., and Chattopadhyay, A. K. (2011). *Heat and thermodynamics*. Tata McGraw Hill Education Private Limited.
- Zhang, J., Li, Y., and Yu, H. (2018). Accelerating ads black holes as the holographic heat engines in a benchmarking scheme. *The European Physical Journal C*, 78(8):645.
- Zhang, J.-L., Cai, R.-G., and Yu, H. (2015a). Phase transition and thermodynamical geometry for Schwarzschild AdS black hole in  $AdS_5 \times S^5$  spacetime. *JHEP*, 02:143.

- Zhang, J.-L., Cai, R.-G., and Yu, H. (2015b). Phase transition and thermodynamical geometry of Reissner-Nordström-AdS black holes in extended phase space. *Phys. Rev. D*, 91(4):044028.
- Zhang, M. and Liu, W.-B. (2016).  $f(r)$  black holes as heat engines. *International Journal of Theoretical Physics*, 55(12):5136–5145.
- Zhao, H.-H., Zhang, L.-C., Ma, M.-S., and Zhao, R. (2015). Phase transition and Clapeyron equation of black holes in higher dimensional AdS spacetime. *Class. Quant. Grav.*, 32(14):145007.
- Zhao, R., Zhao, H.-H., Ma, M.-S., and Zhang, L.-C. (2013). On the critical phenomena and thermodynamics of charged topological dilaton AdS black holes. *Eur. Phys. J. C*, 73:2645.

## LIST OF PUBLICATIONS

### 1. Peer Reviewed International Journals:

1. **C.L. Ahmed Rizwan**, A. Naveena Kumara, Deepak Vaid and K.M. Ajith  
“*Joule-Thomson expansion in AdS black hole with a global monopole*”  
**International Journal of Modern Physics A 33 (2018), 1850210**,  
DOI: [10.1142/S0217751X1850210X](https://doi.org/10.1142/S0217751X1850210X), [arXiv:1805.11053](https://arxiv.org/abs/1805.11053).
2. **C.L. Ahmed Rizwan**, A. Naveena Kumara, Kartheek Hegde and Deepak Vaid  
“*Coexistent Physics and Microstructure of the Regular Bardeen Black Hole in Anti-de Sitter Spacetime*”  
**Annals of Physics 422 (2020), 168320**,  
DOI: [10.1016/j.aop.2020.168320](https://doi.org/10.1016/j.aop.2020.168320), [arXiv:2008.06472](https://arxiv.org/abs/2008.06472).
3. **C.L. Ahmed Rizwan**, A. Naveena Kumara, K.V. Rajani, Deepak Vaid and K.M. Ajith  
“*Effect of Dark Energy in Geometrothermodynamics and Phase Transitions of Regular AdS black hole*”  
**General Relativity and Gravitation 51 (2019), 12, 161**,  
DOI: [10.1007/s10714-019-2649-4](https://doi.org/10.1007/s10714-019-2649-4), [arXiv:1811.10838](https://arxiv.org/abs/1811.10838).
4. K.V. Rajani, **C.L. Ahmed Rizwan**, A. Naveena Kumara, Deepak Vaid and K.M. Ajith  
“*Regular Bardeen AdS black hole as a heat engine*”  
**Nuclear Physics B 960 (2020), 115166**,  
DOI: [10.1016/j.nuclphysb.2020.115166](https://doi.org/10.1016/j.nuclphysb.2020.115166) , [arXiv:1904.06914](https://arxiv.org/abs/1904.06914).
5. A. Naveena Kumara, **C.L. Ahmed Rizwan**, Shreyas Punacha, K.M. Ajith and Md Sabir Ali  
“*Photon orbits and thermodynamic phase transition of regular AdS black holes*”  
**Physical Review D 102 (2020) 8, 084059**,  
DOI: [10.1103/PhysRevD.102.084059](https://doi.org/10.1103/PhysRevD.102.084059), [arXiv:1912.11909](https://arxiv.org/abs/1912.11909).

6. A. Naveena Kumara, **C.L. Ahmed Rizwan**, Kartheek Hegde, K.M. Ajith  
“*Repulsive Interactions in the Microstructure of Regular Hayward Black Hole in Anti-de Sitter Spacetime*”  
**Physics Letters B 807 (2020) 135556**,  
DOI: [10.1016/j.physletb.2020.135556](https://doi.org/10.1016/j.physletb.2020.135556), [arXiv:2003.10175](https://arxiv.org/abs/2003.10175).
7. A. Naveena Kumara, **C.L. Ahmed Rizwan**, Kartheek Hegde, Md Sabir Ali and K.M. Ajith  
“*Ruppeiner Geometry, Reentrant Phase transition and Microstructure of Born-Infeld AdS Black Hole*”  
**Physical Review D 103 (2021) 4, 044025**,  
DOI: [10.1103/PhysRevD.103.044025](https://doi.org/10.1103/PhysRevD.103.044025), [arXiv:2007.07861](https://arxiv.org/abs/2007.07861).
8. **C.L. Ahmed Rizwan**, A. Naveena Kumara, Kartheek Hegde, Md Sabir Ali and K.M. Ajith  
“*Rotating Black Hole with an Anisotropic Matter Field as a Particle Accelerator*”  
**Classical and Quantum Gravity 38 (2021) 7, 075030**,  
DOI: [10.1088/1361-6382/abe2d9](https://doi.org/10.1088/1361-6382/abe2d9), [arXiv:2008.01426](https://arxiv.org/abs/2008.01426).
9. K.V. Rajani, **C.L. Ahmed Rizwan**, A. Naveena Kumara, Deepak Vaid, Md Sabir Ali  
“*Joule-Thomson Expansion of Regular Bardeen AdS Black Hole Surrounded by Static Anisotropic Quintessence Field*”  
**Physics of Dark Universe 32, (2021) 5, 100825** ,  
DOI: [10.1016/j.dark.2021.100825](https://doi.org/10.1016/j.dark.2021.100825), [arXiv:2002.03634](https://arxiv.org/abs/2002.03634).
10. Kartheek Hegde, A. Naveena Kumara, **C.L. Ahmed Rizwan**, Md Sabir Ali, K.M. Ajith  
“*Null Geodesics and Thermodynamic Phase Transition of Four-Dimensional Gauss-Bonnet AdS Black Hole*”  
**Annals of Physics 429 (2021) 168461**,  
DOI: [10.1016/j.aop.2021.168461](https://doi.org/10.1016/j.aop.2021.168461), [arXiv:2007.10259](https://arxiv.org/abs/2007.10259).

11. A. Naveena Kumara, **C.L. Ahmed Rizwan**, Kartheek Hegde, K.M Ajith, Md Sabir Ali,  
“*Microstructure and continuous phase transition of a regular Hayward black hole in anti-de Sitter spacetime*”,  
**Progress of Theoretical and Experimental Physics** May 21 (2021)  
DOI: [10.1093/ptep/ptab065](https://doi.org/10.1093/ptep/ptab065), [arXiv:2003.00889](https://arxiv.org/abs/2003.00889).

### ArXiv Preprints:

1. A. Naveena Kumara, **C.L. Ahmed Rizwan**, Deepak Vaid, K.M. Ajith  
“*Critical Behaviour and Microscopic Structure of Charged AdS Black Hole with a Global Monopole in Extended and Alternate Phase Spaces*”  
Submitted to **Nuclear Physics B**, [arXiv:1906.11550](https://arxiv.org/abs/1906.11550).
2. A. Naveena Kumara, **C.L. Ahmed Rizwan**, Kartheek Hegde Md Sabir Ali, KM Ajith  
“*Microstructure and continuous phase transition of a regular Hayward black hole in anti-de Sitter spacetime*”  
Submitted to **Physics Letters B**, [arXiv:2003.00889](https://arxiv.org/abs/2003.00889).
3. Kartheek Hegde, A. Naveena Kumara, **C.L. Ahmed Rizwan**, Md Sabir Ali, K.M. Ajith  
“*Thermodynamics, Phase Transition and Joule Thomson Expansion of novel 4-D Gauss Bonnet AdS Black Hole*”  
Submitted to **Physics Letters B**, [arXiv:2003.08778](https://arxiv.org/abs/2003.08778).
4. A. Naveena Kumara, **C.L. Ahmed Rizwan**, Kartheek Hegde, Md Sabir Ali, K.M. Ajith  
“*Microstructure of five-dimensional neutral Gauss-Bonnet black hole in anti-de Sitter spacetime via  $P-V$  criticality*”  
Submitted to **Physical Review D**, [arXiv:2006.13907](https://arxiv.org/abs/2006.13907).



5. A. Naveena Kumara, **C.L. Ahmed Rizwan**, Kartheek Hegde, Md Sabir Ali, K.M. Ajith  
“*Rotating 4D Gauss-Bonnet black hole as particle accelerator*”  
Submitted to **Modern Physics Letters A**, [arXiv:2004.04521](#).
6. Kartheek Hegde, A Naveena Kumara, **C.L. Ahmed Rizwan**, Md Sabir Ali, K.M. Ajith  
“*Thermodynamics, photon sphere and thermodynamic geometry of Eloy Ayon Beato – Garcia Spacetime*”  
Submitted to **Nuclear Physics B** , [arXiv:2104.08091](#).
7. Md Sabir Ali, A. Naveena Kumara, Kartheek Hegde, **C.L. Ahmed Rizwan**, K.M. Ajith  
“*Greybody factor for an electrically charged regular-de Sitter black holes in d-dimensions*”, [arXiv:2105.05730](#).
8. A. Naveena Kumara, Shreyas Punacha, Kartheek Hegde, **C.L. Ahmed Rizwan**, K.M. Ajith  
“*Dynamics and kinetics of phase transition for regular AdS black holes in general relativity coupled to non-linear electrodynamics*”, [arXiv:2106.11095](#) .

## 2. Peer Reviewed International Journal proceedings:

1. **C.L. Ahmed Rizwan** and Deepak Vaid . “Second order phase transition in thermodynamic geometry and holographic superconductivity in low-energy stringy black holes”. *AIP Conf. Proc.***1953**, 040026, (2018), DOI: [10.1063/1.5032646](https://doi.org/10.1063/1.5032646).
2. **C.L. Ahmed Rizwan**, A. Naveena Kumara and Ananthram K.S. “Effect of Global monopole on the microscopic structure of RN-AdS black hole”. *Springer Proc.Phys.* **248**, 81-85 (2020). DOI: [10.1007/978-981-15-6292-1-10](https://doi.org/10.1007/978-981-15-6292-1-10).
3. A. Naveena Kumara, **C.L. Ahmed Rizwan** and K.M. Ajith. “Criticality of Charged AdS Black Hole with a Global Monopole”. *Springer Proc.Phys.* **248**, 75-79 (2020). DOI: [10.1007/978-981-15-6292-1-9](https://doi.org/10.1007/978-981-15-6292-1-9).
4. K.V. Rajani, **C.L. Ahmed Rizwan** and A.Naveena Kumara . “Phase transition and thermodynamic geometry of regular Bardeen black hole in higher dimensions”. *AIP Conf. Proc.***2220**, 030003, (2020).DOI: [10.1063/5.0001633](https://doi.org/10.1063/5.0001633).
5. **C.L. Ahmed Rizwan**, A. Naveena Kumara and Deepak Vaid. “Thermodynamic Geometry of Regular black hole surrounded by Quintessence”. *Springer Proc.Phys.* **261**, 937-941 (2021). DOI: [10.1007/978-981-33-4408-2\\_134](https://doi.org/10.1007/978-981-33-4408-2_134).
6. A. Naveena Kumara, **C.L. Ahmed Rizwan** and K.M. Ajith. “The Role of Global Monopole in Joule–Thomson Effect of AdS Black Hole ”. *Springer Proc.Phys.* **261**, 415-419 (2021). DOI: [10.1007/978-981-33-4408-2\\_58](https://doi.org/10.1007/978-981-33-4408-2_58).

## 3. International Conferences Presentations:

1. **C.L. Ahmed Rizwan** and A. Naveena Kumara. “Phase transition in AdS black hole via alternate phase space”. *9<sup>th</sup> International Conference on Gravitation & Cosmology (ICGC)* at Indian Institute of Science Education an Research (IISER) Mohali, Punjab, India during 10 -13 August, 2019.
2. **C.L. Ahmed Rizwan**, and A. Naveena Kumara. “Effect of global monopole on the Microscopic Structure of RN-AdS black hole”. *International Workshop on*

*frontiers in high energy physics (FHEP)* at University of Hyderabad, Telagana, India during 14-17 October, 2019.

3. **C.L. Ahmed Rizwan**, and A. Naveena Kumara. “Polarization of Gravitational waves in Modified Gravity using Newmann-Penrose Formulism”. *30th meeting of the Indian Association for General Relativity and Gravitation (IAGR)* at BITS Pilani, Hyderabad, India during 3-5 January, 2019.
4. **C.L. Ahmed Rizwan**, A. Naveena Kumara and Deepak Vaid. “Thermodynamic Geometry of Regular black hole surrounded by Quintessence”. *XXII DAE-BRNS High energy Physics Symposium* at Indian Institute of Technology (IIT) Madras, Chennai, India during 10-14 December, 2018.
5. **C.L. Ahmed Rizwan**, A. Naveena Kumara and Deepak Vaid. “The role of global monopole in Joule Thomson effect of AdS black hole”. *National Conference on Cosmology and particle physics (NC-CAPP)* at Women’s Christian College, Chennai, India, during 1-2 October, 2018.
6. **C.L. Ahmed Rizwan** and Deepak Vaid. “A comparative study: Cosmological BCS mechanism and holographic superconductivity”. *29th meeting of the Indian Association for General Relativity and Gravitation* at Indian Institute of Technology Guwahati, Assam, India during 18-20 May, 2017.

## CURRICULUM VITAE



### **AHMED RIZWAN C.L**

#### **Permanent Address :**

Rahmath Mahal, Lesiyath,  
Chemnad, Kasaragod Dist,  
Kerala, India - 671317

Mobile:(+91)-9497575087

E-mail: ahmedrizwancl@gmail.com,

#### **Academic Qualifications :**

**Master of Science**                      Score : 71.2%

Kannur University,  
Kannur, Kerala, India

**Bachelor of Science**                      Score : 83%

St. Aloysius College,  
Mangalore, Karnataka, India

#### **Research Publications :**

Articles in International Journals : 11

Articles in International Proceedings : 6

Papers presented in International Conferences : 4

Workshops and Schools attended : 20+